



INSTITUTO SUPERIOR TÉCNICO  
Universidade Técnica de Lisboa



## **Analysis of bone remodeling in the tibia after total knee prosthesis**

**Tiago José Fonseca Robalo**

Dissertation for obtaining the Master's Degree in

**Biomedical Engineering**

### **Jury**

<b>President:</b>	Prof. Paulo Freitas
<b>Advisers:</b>	Prof. João Folgado Prof. Paulo Fernandes
<b>External specialist:</b>	Prof. João Gamas
<b>IST specialist:</b>	Prof. Luís Sousa

**November 2011**



## **Acknowledgements**

First of all, I would like to thank my advisors, Prof. João Folgado and Prof. Paulo Fernandes, for all their availability in the clarification of doubts and also for their support through the suggestions to guide my work. I also express my gratitude to Prof. Dr. João Gamelas for all the clinical guidance and for providing me the opportunity to attend a surgical procedure of the knee.

In addition to my advisors, I am also thankful to the entire IDMEC research group for sharing their knowledge and expertise with me. Especially to Carlos Quental, Lina Espinha and Marta Dias that gave me a great assistance throughout this research, and to Paula Fernandes and Ângela Chan that helped me in the preparation of the geometric models.

Finally, I would also like to thank my family for everything they did for me.



## Abstract

Total knee arthroplasty is a surgical treatment with one of the highest usage rate, making it the gold standard treatment for advanced osteoarthritis of the knee. However, knee prosthesis currently used still lack appropriate design solutions. The loss of bone in the tibia due to tibial component is one of the concerns about the success of the knee prosthesis.

The purpose of the present work is to evaluate the bone remodeling that occurs in the tibia after total knee arthroplasty.

A three-dimensional model of the tibia was developed from CT images. The geometric modeling of the tibial components, as well as their discretization in finite elements (FE) were also made.

Bone was modeled as a porous material characterized by its relative density at each point of the domain. The bone remodeling law was derived from a topology optimization problem, in which bone self-adapts in order to achieve the stiffest structure, being the total bone mass regulated by the metabolic cost associated with bone maintenance. By using the FE method together with the bone remodeling model developed in IST it was possible to analyze the physiological situation of bone, and also its behavior in different surgical scenarios.

The results showed that the distribution of bone densities around prosthesis' tibial component depends on the stem configuration and fixation mode. The use of long stems (cemented and uncemented) causes a clear stress shielding of the proximal tibia, leading to a significant reduction of bone density. It was also verified a high stress concentration close to the distal tip of the stem, with consequent hypertrophy of bone at the tip region. For short stems (standard) a tendency for maintaining bone remodeling process of the host bone close to physiological was noticed.

**Key-words:** Biomechanics; Total knee arthroplasty; Bone remodeling; FE method.

## Resumo

A artroplastia total do joelho é uma das cirurgias ortopédicas com maior taxa de utilização, constituindo mesmo o tratamento de eleição para a osteoartrose do joelho em estadio muito avançado. Contudo, as próteses do joelho actualmente utilizadas carecem ainda de soluções de desenho adequadas. A perda de osso na tíbia devido à componente tibial é uma das preocupações em relação ao sucesso da prótese do joelho.

O objectivo deste trabalho é avaliar a remodelação óssea que ocorre na tíbia após uma artroplastia total do joelho.

O modelo tridimensional da tíbia foi desenvolvido a partir de imagens de TC. A modelação geométrica das componentes tibiais, bem como a discretização em elementos finitos (EF) foi também efectuada.

O osso foi modelado como um material poroso caracterizado pela sua densidade relativa em cada ponto do domínio. A lei de remodelação óssea utilizada foi baseada num problema de optimização de topologia, em que o osso se adapta na tentativa de obter a estrutura mais rígida, sendo a massa total de osso regulada pelo custo metabólico associado à manutenção de osso. A utilização do método de EF juntamente com o modelo de remodelação óssea desenvolvido no IST permitiu analisar a situação fisiológica do osso, e também o seu comportamento em diferentes cenários de intervenção cirúrgica.

Os resultados obtidos mostraram que a distribuição de densidades do osso nas zonas adjacentes à componente tibial é dependente da configuração da haste e modo de fixação. O uso de hastas longas (cimentadas e não cimentadas) é acompanhado por um evidente efeito de blindagem de tensões (*stress shielding*) na zona proximal da tíbia, conduzindo a uma redução significativa na densidade do osso. Verificou-se também uma elevada concentração de tensões junto da extremidade distal da haste, com conseqüente hipertrofia do osso na região da ponta. No caso da haste curta (*standard*) houve uma tendência para manter um processo de remodelação óssea próximo do fisiológico.

**Palavras-chave:** Biomecânica; Artroplastia total do joelho; Remodelação óssea; Método de EF.

# Contents

<b>List of Figures .....</b>	<b>VIII</b>
<b>List of Tables .....</b>	<b>XI</b>
<b>List of symbols.....</b>	<b>XII</b>
<b>Abbreviations.....</b>	<b>XIII</b>
<b>I. Resume.....</b>	<b>1</b>
I.1 Motivation and aims .....	1
I.2 Thesis structure .....	3
<b>1. Introduction.....</b>	<b>5</b>
1.1 Anatomy of the knee joint .....	5
1.1.1 Bones of the knee joint .....	6
1.1.2 Menisci .....	9
1.1.3 Ligaments .....	10
1.1.4 Kinematics .....	10
1.2 Bone tissue .....	11
1.3 Bone remodeling .....	13
1.4 Knee arthroplasty.....	17
1.4.1 Pathologic conditions .....	17
1.4.2 Total and partial Knee replacement - TKR and UKR.....	18
1.4.3 Knee prosthesis .....	20
1.4.4 Surgical procedure .....	21
<b>2. Model of Bone remodeling .....</b>	<b>25</b>
2.1. Optimization model.....	25
2.2. Material model for bone .....	26
2.3. Mathematical formulation .....	27
2.4. Computational model .....	29
<b>3. Adopted methodology – computational modeling.....</b>	<b>31</b>
3.1. Geometric modeling.....	31
3.1.1. Geometric modeling of intact bone – tibia .....	31
3.1.2. Geometric modeling of prostheses – tibial components.....	39
3.1.3. Geometric modeling of bone with prostheses – surgical procedure, assembly.....	44
3.2. Finite element method – FEM.....	46
3.2.1. Material properties .....	46
3.2.2. Contact formulation, Boundary conditions and applied loads .....	47

3.2.3. Finite element mesh generation .....	51
3.3 Analysis of the intact bone – Tests for the application of the bone remodeling model...	55
3.3.1. Determination of metabolic cost parameter – uniform density distribution .....	55
3.3.2. Non-homogeneous density distribution .....	58
3.4. Results analysis method .....	60
<b>4. Results and Discussion.....</b>	<b>63</b>
4.1. Standard configuration model .....	63
4.2. Cemented configuration model .....	67
4.3. Press-fit configuration model.....	70
4.4 Stress analysis.....	74
<b>5. Conclusion and future developments.....</b>	<b>81</b>
<b>REFERENCES .....</b>	<b>83</b>
<b>Annex A .....</b>	<b>88</b>

## List of Figures

Figure 1.1 – Anatomy of the knee joint: anterior medial view (UC San Diego School of Medicine). .....	6
Figure 1.2 – Shaft and distal end of femur. A. Lateral view. B. Anterior view. C. Posterior view. D. Cross-section through shaft of femur [29]. .....	7
Figure 1.3 – Proximal extremity of the tibia. A. Superior view – tibial plateau. B. Anterior view. C. Posterior view. D. Cross-section through the shaft of tibia [29]. It is also possible to observe the sites of attachment for menisci, muscles and cruciate ligaments. ....	8
Figure 1.4 – Patella. A. Anterior view. B. Posterior view. C. Superior view [29]. .....	9
Figure 1.5 – Menisci of the knee joint, superior view [29]. .....	9
Figure 1.6 – Types of cells in bone tissue [4]. .....	11
Figure 1.7 – Osteons in compact bone and trabeculae in spongy bone [4]. .....	12
Figure 1.8 – Enlarged aspect of spongy bone, at the left, and the details of a section of a trabecula, at the right [4].	13
Figure 1.9 – Overview of bone remodeling process. Remodeling commences with the initiation of osteoclast formation, osteoclast-mediated bone resorption, a reversal period, and then a long period of bone matrix formation mediated by osteoblasts, followed by mineralization of the matrix [33]. .....	14
Figure 1.10 – Response of bone to the applied loads [42]. .....	16
Figure 1.11 – Knee joint suffering osteoarthritis. ....	17
Figure 1.12 – Total knee arthroplasty adapted from [4]. .....	19
Figure 1.13 – Unicompartmental knee replacement [49]. .....	19
Figure 1.14 – Total Knee prosthesis. A. Sagittal view. B. Frontal view; adapted from [52]. .....	21
Figure 1.15 – Accurate component alignment and resection of the proximal tibia [56]. .....	22
Figure 2.1 – Material model for bone, adapted from [43]. .....	26
Figure 2.2 – Generalized elastic problem with contact, adapted from [58]. .....	27
Figure 2.3 – Flowchart for the computational model procedure, adapted from [58]. .....	29
Figure 3.1 – Diagram of the geometric modeling pipeline that was used to model an anatomical structure – left tibia. The boxes in the left column concern to the software tools and the right column boxes indicate the data file extension [67]. .....	32
Figure 3.2 – Sections of the left tibia. A, B, C – Original CT images: transversal, sagittal and frontal sections, respectively; D, E, F – Respective segmented CT images with global thresholding. ....	34
Figure 3.3 – A, B, C – Iterative process of 2-D deformable surfaces evolution in different time instants (transversal, sagittal and frontal sections of the segmented image data, respectively); D – Iterative process of 3-D deformable surfaces evolution in different time instants. ....	35
Figure 3.4 – A, B, C – Sections of the left tibia, corrected by manual segmentation (transversal, sagittal and frontal sections, respectively); D – 3-D surface model of the tibia. ....	36
Figure 3.5 – Process of 3-D surface mesh adjustments of the left tibia, in which the surface is first smoothed then decimated and smoothed again: A – Segmentation model; B – Smoothed model; C – Smoothed-decimated model; D - Smoothed-decimated-smoothed model of the surface model A (that results from the segmentation stage). .....	37
Figure 3.6 – Smoothed-decimated-smoothed meshes of the surface model that appears in Figure 3.1e A. (final result of the surface mesh adjustments stage): A – Anterior view; B – Posterior view; C – Superior view; D – Inferior view of the surface mesh of the left tibia. ....	38
Figure 3.7 – Solid models of the left tibia generated from the surface mesh in Figure 3.6: A - Without the intramedullary canal – tibia uniform – (the edges represents a superficial mesh automatically generated in SolidWorks®); B - With the modulation of the intramedullary canal – tibia canal. ....	39
Figure 3.8 – P.F.C.® Sigma Stabilized Insert (with a cruciate-substituting design – posterior stabilized): A – Isometric view; B – Top view; C – Lateral view [50]. .....	39
Figure 3.9 – P.F.C.® Modular Tibial Tray (size 2) with the standard configuration: A – Inferior view; B – Posterior view [50]. .....	39
Figure 3.10 – P.F.C.® Sigma Modular Stem Attachment: A – Tibial tray with standard configuration – posterior view; B – Cement stem (13 mm diameter and 30 mm length) - posterior and bottom view; C - Press-fit stem (14 mm diameter and 115 mm length) - posterior and bottom view [50]. .....	40
Figure 3.11 – Stabilized insert: A – Isometric view; B – Sagittal view; C – Anterior view; D – Posterior view [69]. .....	41
Figure 3.12 – Modular Tibial Tray: A - Isometric view; B - Posterior view; C - Anterior view; D - Left sagittal view; E - Right sagittal view [69]. .....	41

Figure 3.13 – Modular Stem Attachment: A - Sagittal view of standard configuration, B and C – Isometric and bottom view of cemented (30 mm length) and press-fit (115 mm length) stems, respectively.....	42
Figure 3.14 – Tibial components of TKA prostheses with the standard configuration (stabilized insert, tibial tray, standard stem and cement in superior third of the tibial tray with about 1 mm thickness): A – Isometric view; B – Anterior view; C – Sagittal view. ....	42
Figure 3.15 – Tibial components of TKA prostheses with the cemented configuration (stabilized insert, tibial tray, cemented stem (with 30 mm) and cement involving the entire tibial tray and stem that will contact with cut bone, with about 1 mm thickness): A – Isometric view; B – Anterior view; C – Sagittal view.....	43
Figure 3.16 – Tibial components of TKA prostheses with the press-fit configuration (stabilized insert, tibial tray, press-fit stem (with 115 mm) and cement in superior third of the tibial tray with about 1 mm thickness): A – Isometric view; B – Anterior view; C – Sagittal view. ....	43
Figure 3.17 – Anterior view of the first stage of surgical procedure: A – Intact bone; B - Resected tibia, with a cut at 90° to its mechanical axis with a level of about 10 mm based on the less involved condyle. ....	44
Figure 3.18 – Final assembly of the standard configuration: A – Isometric view; B – Frontal section, isometric view; C – Frontal section, anterior view; D – Lateral section, right sagittal view. ....	45
Figure 3.19 – Final assembly of the cemented configuration: A – Isometric view; B – Frontal section, isometric view; C – Frontal section, anterior view; D – Lateral section, right sagittal view. ....	45
Figure 3.20 – Final assembly of the press-fit configuration: A – Isometric view; B – Frontal section, isometric view; C – Frontal section, anterior view; D – Lateral section, right sagittal view. ....	46
Figure 3.21 – Load patterns during the investigated activities – Level walking and Knee bend, at left and right, respectively. Upper diagrams = forces, lower diagrams = moments. Vertical orange lines are the selected times that correspond to the load cases considered. HS: heel strike; CTO: contralateral toe off; CHS: contralateral heel strike [79].....	48
Figure 3.22 – Coordinate system for the forces and moments applied adapted from [2]. ....	50
Figure 3.23 – Illustrate the RP and the surfaces where the six load cases are applied: A – Intact bone; B – Implanted bone. ....	51
Figure 3.24 – Process to generate the hexahedral mesh of the tibia uniform solid model: A – Superficial mesh of SolidWorks®; B – Virtual topology; C – Illustrative structure of partition mode of the model, which is drawn on the lower extremity basis of the bone and then is extruded along its longitudinal axis; D – Tibia with partitions; E – Hexahedral FE mesh.....	52
Figure 3.25 – FE mesh of the standard configuration: A – Cut tibia; B – Tibial insert; C – Tibial tray; D - Cement; E – Standard stem; F – Total assembly. ....	53
Figure 3.26 – FE mesh of the cemented configuration: A – Cut tibia; B – Tibial insert; C – Tibial tray and cemented stem; D - Cement; E – Total assembly.....	54
Figure 3.27 – FE mesh of the press-fit configuration: A – Cut tibia; B – Tibial insert C – Tibial tray and press-fit stem; D - Cement; E – Total assembly.....	54
Figure 3.28 – Density distribution resulting from the model of bone remodeling for the intact bone with an initially homogeneous solution $\mu = 0,3$ and, $k=0,001 \text{ N/mm}^2$ , step = 5 and 200 iterations. Relative densities, $\mu$ , are represented in a color scale: red=cortical bone ( $\mu \approx 1$ ) and the remaining=trabecular bone. A – Global view; B – Lateral section, right sagittal view; C – Frontal section, anterior view. ....	56
Figure 3.29 – Density distribution resulting from the model of bone remodeling for the intact bone with an initially homogeneous solution $\mu = 0,3$ and, $k=0,003 \text{ N/mm}^2$ , step = 5 and 200 iterations. Relative densities, $\mu$ , are represented in a color scale: red=cortical bone ( $\mu \approx 1$ ) and the remaining=trabecular bone. A – Global view; B – Lateral section, right sagittal view; C – Frontal section, anterior view. ....	56
Figure 3.30 – Density distribution resulting from the model of bone remodeling for the intact bone with an initially homogeneous solution $\mu = 0,3$ and, $k=0,006 \text{ N/mm}^2$ , step = 5 and 200 iterations. Relative densities, $\mu$ , are represented in a color scale: red=cortical bone ( $\mu \approx 1$ ) and the remaining=trabecular bone. <b>A</b> – Global view; <b>B</b> – Lateral section, right sagittal view; <b>C</b> – Frontal section, anterior view. ....	57
Figure 3.31 – Solid model of the left tibia with the modulation of the intramedullary canal (A and B) and initial distribution of densities for this model (C and D). Relative densities $\mu$ , are represented in a color scale: at red=cortical bone ( $\mu \approx 1$ ), blue=intramedullary canal ( $\mu=0,05$ ) and the remaining=trabecular bone ( $\mu=0,3$ ): A and C – Frontal section, anterior view; B and D – Lateral section, right sagittal view. ....	58
Figure 3.32 – Density distribution resulting from the model of bone remodeling for the initial non-homogeneous input of the Figure 3.31 with $k=0,003 \text{ N/mm}^2$ , step = 5 and 200 iterations. Relative densities, $\mu$ , are represented in a	

color scale: red=cortical bone ( $\mu \approx 1$ ) and the remaining=trabecular bone. A – Global view; B – Lateral section, right sagittal view; C – Frontal section, anterior view. .... 59

Figure 3.33 – Sections of the proximal real tibia showing the distribution of the inner cancellous bone and outer compact bone: A – Lateral section, right sagittal view; B – Frontal section, anterior view..... 59

Figure 3.34 – Implanted bone discretized in the regions (1-6) under study in bone remodeling process: A – Standard; B – Cemented; C – Press-fit configuration. .... 61

Figure 4.1 – Initial and final density distribution resulting from the model of bone remodeling for the implanted bone with standard prosthesis (interface implant-cement bonded). Relative densities,  $\mu$ , are represented in a color scale: red=cortical bone ( $\mu \approx 1$ ) and the remaining=trabecular bone. A – Global view; B – Lateral section, right sagittal view; C – Frontal section, anterior view. .... 64

Figure 4.2 – Initial and final density distribution resulting from the model of bone remodeling for the implanted bone with standard prosthesis (interface implant-cement with friction). Relative densities,  $\mu$ , are represented in a color scale: red=cortical bone ( $\mu \approx 1$ ) and the remaining=trabecular bone. A – Global view; B – Lateral section, right sagittal view; C – Frontal section, anterior view. .... 65

Figure 4.3 – Evolution of the total bone mass (BM) throughout the iterative process of bone remodeling, dimensionless by its initial mass, for the standard configuration considering interface implant-cement bonded (blue) and with friction coefficient of 0,3 (red). .... 66

Figure 4.4 – Initial and final density distribution resulting from the model of bone remodeling for the implanted bone with cemented prosthesis (interface implant-cement bonded). Relative densities,  $\mu$ , are represented in a color scale: red=cortical bone ( $\mu \approx 1$ ) and the remaining=trabecular bone. A – Global view; B – Lateral section, right sagittal view; C – Frontal section, anterior view. .... 67

Figure 4.5 – Initial and final density distribution resulting from the model of bone remodeling for the implanted bone with cemented prosthesis (interface implant-cement with friction). Relative densities,  $\mu$ , are represented in a color scale: red=cortical bone ( $\mu \approx 1$ ) and the remaining=trabecular bone. A – Global view; B – Lateral section, right sagittal view; C – Frontal section, anterior view. .... 68

Figure 4.6 – Evolution of the total bone mass (BM) throughout the iterative process of bone remodeling, dimensionless by its initial mass, for the cemented configuration considering interface implant-cement bonded (blue) and with friction coefficient of 0,3 (red). .... 69

Figure 4.7 – Initial and final density distribution resulting from the model of bone remodeling for the implanted bone with press-fit prosthesis (interface implant-cement bonded). Relative densities,  $\mu$ , are represented in a color scale: red=cortical bone ( $\mu \approx 1$ ) and the remaining=trabecular bone. A – Global view; B – Lateral section, right sagittal view; C – Frontal section, anterior view. .... 71

Figure 4.8 – Initial and final density distribution resulting from the model of bone remodeling for the implanted bone with press-fit prosthesis (interface implant-cement with friction). Relative densities,  $\mu$ , are represented in a color scale: red=cortical bone ( $\mu \approx 1$ ) and the remaining=trabecular bone. A – Global view; B – Lateral section, right sagittal view; C – Frontal section, anterior view. .... 72

Figure 4.9 – Evolution of the total bone mass (BM) throughout the iterative process of bone remodeling, dimensionless by its initial mass, for the press-fit configuration considering interface implant-cement bonded (blue) and with friction coefficient of 0,3 (red). .... 73

Figure 4.10 – Von Mises stresses for sagittal sections of bone and implant models for the cemented configuration, with interface implant-cement: A – bonded; B – with friction. Stresses represented in a color scale: grey=[13,60] MPa and the remaining=[0,13] MPa. .... 74

Figure 4.11 – Von Mises stresses for sagittal sections of bone and implant models with interface implant-cement bonded: A – Intact tibia; B – Standard configuration; C – Cemented configuration; D – Press-fit configuration. Stresses represented in a color scale: grey=[13,60] MPa and the remaining=[0,13] MPa..... 75

Figure 4.12 – Pictures of painful implanted knee prosthesis with a press-fit stem with 115 mm, identical to the model used in this study: scintigraphy (left) and radiography (right) [62]. .... 78

## List of Tables

Table 3.1 – Material stiffness properties used in FE simulations [73].	47
Table 3.2 – Forces and moments from level walking and knee bend applied in FE models [79].	49
Table 3.3– Number of elements and nodes of the FE meshes of the models.	55
Table 4.1– Bone mass variation for the regions 1 to 6 and for the whole bone, result of the bone remodeling process, for the standard prosthesis considering interface implant-cement bonded and with friction coefficient of 0,3.	66
Table 4.2– Bone mass variation for the regions 1 to 6 and for the whole bone, result of the bone remodeling process, for the cemented prosthesis considering interface implant-cement bonded.	70
Table 4.3 – Bone mass variation for the regions 1 to 6 and for the whole bone, result of the bone remodeling process, for the press-fit prosthesis considering interface implant-cement bonded and with friction coefficient of 0,3.	73

## List of symbols

$\mathbf{a}$	microstructure parameters
$e_{ij}$	strain field
$d$	step length of the process
$\mathbf{D}_K$	descent vector
$E$	Young's modulus
$E_{ijkl}^H$	elastic material properties tensor (the superscript $H$ denotes homogenized)
$f$	surface loads
$g$	gap between the two bodies
$n$	normal direction
$NC$	number of considered load cases
$P$	index of load case
$t$	tangential direction
$\mathbf{u}^P$	displacement fields
$\mathbf{v}^P$	virtual displacements
$\alpha^P$	load weight factors
$\Gamma_u$	contact boundary $u$
$k$	biological parameter, metabolic cost for maintaining bone tissue
$\mu$	bone relative density
$\theta$	Euler angles
$\vartheta$	friction coefficient
$\tau^P$	contact loads
$\Omega$	volume of domain

## Abbreviations

ACL	Anterior Cruciate Ligament
BM	Bone Mass
BMU	Basic Multicellular Unit
BMD	Bone Mineral Density
CT	Computed Tomography
FE	Finite Element
FEM	Finite Element Method
LCL	Lateral Collateral Ligament
MCL	Medial collateral ligament
OA	Osteoarthritis
PCL	Posterior Cruciate Ligament
PMMA	Polymethylmethacrylate
RA	Rheumatoid Arthritis
ROI	Region of Interest
TKA	Total Knee Arthroplasty
TKR	Total Knee Replacement
UKR	Unicompartmental Knee Replacement
UHMWPE	Ultra high molecular weight polyethylene

# I. Resume

## I.1 Motivation and aims

The human lower limb is adapted for weight-bearing, locomotion and maintaining the unique, upright, bipedal posture [1]. The knee joint is the middle joint of the lower limb. It works in conjunction with the hip and ankle joint, for supporting and moving the body during a variety of both routine and difficult activities. The weight of the body, inertia forces and muscle forces are transmitted to the ground through the knee, which has to bear compressive forces up to six times body weight during daily life activities [2,3].

The knee is one of the most often injured joints, since it is the most heavily loaded and one of the most mobile joints in the human body and is regularly subjected to great mechanical demands [4, 5]. Because of that, knee is associated with a high incidence of degenerative and inflammatory diseases. The appropriate method of correction differs from case to case and, usually, surgical intervention is considered once exhausted other medical treatment possibilities.

Arthritis is the most common cause of knee joint pathology, which affects about 45 million people in the United States. According to the Arthritis Foundation, arthritis is second only to heart disease as the cause of work disability, and is the leading cause of physical disability among adults over age 65, limiting everyday activities [4, 6]. Its incidence increases with age, and estimates suggest the achievement of 85% of the population up to 64 years, becoming a universal disease at 85 years [7]. For advanced arthritis, the treatment of choice is, generally, the knee replacement surgery, where the joint surface is replaced by an artificial implant [8], allowing the return to activities of daily living.

Although the history of arthroplasty as the creation of an artificial joint with the purpose of restoring motion while relieving pain and maintaining stability had begun early in the nineteenth century, joint replacement took a lot longer to develop [9]. It was not until 1861 that Ferguson [9] reported the first successful knee arthroplasty. This method prevailed for many decades, but there were some problems associated with this attempt at joint reconstruction with the interposition of soft tissues between bone ends. As a result, surgeons began to investigate the use of other materials, including plastic and metal [9].

The first attempt for a knee joint prosthesis was actually a hinge fixed by stems into the femur and tibia marrow cavities, in which damaged articular surface of bone was removed and substituted by hinge prosthesis. These early total knee arthroplasty (TKA) systems were highly constrained causing stress concentrations, loosening and infection. As a consequence, they soon failed, and therefore were abandoned. Since the early 60's, more realistic knee implants have been created and, a new era began in TKA systems, where the incidence of TKA has risen dramatically [10]. Currently, the modern TKA systems contain multiple components made of different materials (metal and polymer) resurfacing femur, tibia and patella that attempt to mimic the natural knee [1]. Therefore, materials and design are important issues in the development biomedical devices.

Nowadays, knee arthroplasty has proven to be a very effective surgical treatment, being one of the most common joint replacement procedures [11]. The results of TKA showed that today most patients can expect a ten-year implant survival rate (without the need for another surgery) in the range of 90% to 95% and a fifteen-year survival rate in the range of 85% - 90% [10, 12-15]. In the USA, statistical studies have estimated that 381.000 TKAs were performed in 2002 [16], but projections for 2030 indicate that 3.482.000 TKAs procedures will be performed [16]. Particularly, in Portugal a study realized between 1997 and 2008 shows that the annual growth in the incidence of TKA was 17% [17]. This rising prevalence of TKA can be explained by a combination of the changing demographics of the general population (older population) and the procedure being offered to an increasingly diverse patient population (younger population) [10, 18-21]. So, the demand for TKA has risen substantially over the past decade in countries around the world. Moreover, despite the excellent clinical results, one can expect that a greater number of primary knee replacements will, in turn, result in a greater number of revisions. Indeed, projections estimate an increase of 601% of revision TKA procedures in the USA from 2005 to 2030, and financial previews shown that the hospital costs might exceed \$2 billion by 2030 [11,16]. Therefore, the survival rates of primary and revision TKA are still an issue and the longevity of the implant should be maximized [18].

The complex nature of the knee brings many problems when designing a suitable prosthesis [1]. The knee implant designs that are being used today have a satisfactory performance, provide a good degree of reconstruction and allow patients to carry on with their lives in a relatively normal manner. However, several studies describe a significant decrease in postoperative bone mineral density (BMD) adjacent to the implant after TKA [22]. At revision TKA, when bone stock is deficient, implanting a long medullary stem is often necessary in order to stabilize the prosthesis while allowing reconstruction of the bone defect [23]. Unfortunately, long stems increase the incidence of stress shielding (shielding of bone from physiologic stress by implant components), causing a reduction in bone density and strength that leads to TKA failure [24, 25]. The need of reoperation after revision TKA is approximately 15%, of which nearly 44% may require two or more additional surgeries [26]. An improvement in the design of the stem and in the means of fixing the stem to bone could minimize this phenomenon.

The finite element (FE) method is a computer based numerical analysis method and has been widely used in orthopedic biomechanics to evaluate the mechanical behavior of biological tissues, particularly bone [27]. This method allows one to determine the stress or strain state of the bone tissue and to link that with biological processes like bone remodeling, through the combination of a mathematical model that simulates this behavior. This way it can be a useful tool to study the changes in bone adaptation due to the insertion of the implant in bone. Moreover, it is possible to estimate the amount of bone resorption related to a specific prosthesis design, such as the tibial component prosthesis used in TKA. On the other hand, computational models of bone adaptation are also useful for testing and optimizing the performance of the orthopedic devices, thus justifying the enormous research effort expended in developing these models. Therefore, a better understanding of the biological and mechanical

changes induced in bone tissue by prosthesis will allow surgeons to adopt the most appropriate solution for each patient.

The purpose of the present study is to better understand the biomechanical influence of the total knee arthroplasty in the process of bone remodeling that occurs in the tibia. It is intended to analyze the influence of the stem configuration (size of the stem) and mode of fixation (cemented/ cementless) in the existing bone loss due to the presence of tibial component implant. To do so the bone remodeling model developed in IST together with the FE method are applied in the implanted tibia model with three different tibial stem configurations (standard, cemented and press-fit) and with two different ways of modeling the contact in the implant-cement interface (bonded and with friction), thus allowing to evaluate the process of bone adaptation. Stress analysis is also presented and, together with bone remodeling results, are compared with experimental and clinical results obtained by other authors. Finally, conclusions about the optimal design of the implant are drawn with respect to the configuration and fixation mode of the stem. The application of computational model for preclinical tests in orthopedic implants is of interest to orthopedic surgeons and implant manufactures.

## **I.2 Thesis structure**

Apart from this resume chapter, this dissertation is structured into five main chapters: 1. Introduction, 2. Model of bone remodeling, 3. Adopted methodology – computational modeling, 4. Results and discussion and 5. Conclusion and future developments.

In chapter 1 a brief introduction of concepts involved in the context of this thesis is done. Firstly, the anatomic features of the knee joint are described. Moreover, bone tissue and bone remodeling process is presented. Finally, pathologic conditions, basic concepts of knee arthroplasty, knee prosthesis and surgical procedure are also discussed.

Chapter 2 describes the basic ideas of the computational model for bone remodeling used in this work. This tool is based on a topology optimization model, and will be utilized to simulate the bone adaptation process due to mechanical loading, i.e., it describes the bone behaviour in response to the mechanical conditions.

Chapter 3 addresses computational modeling, describing and analyzing the steps followed to create geometric models of the tibia, from computed tomography images, and the tibial components of the TKA implant. Then, the methodologies involved in the finite element analysis and in the achievement of bone remodeling results are described.

In chapter 4 bone remodeling analysis results are presented. Moreover, density distribution results induced by different design solutions (standard, cemented and press-fit) are evaluated and discussed. These results are also complemented with stress analysis and compared with experimental results obtained at the University of Aveiro.

In the last chapter, the conclusions of the work are stated and possible future works that may complement this study are also presented.



# 1. Introduction

In this chapter a brief introduction of concepts involved in the context of this thesis is done. Firstly, the anatomic features of the knee joint are described. Moreover, bone tissue and bone remodeling process is presented. Finally, pathologic conditions, basic concepts of knee arthroplasty, knee prosthesis and surgical procedure are also discussed.

## 1.1 Anatomy of the knee joint

The knee is one of the most important and most studied joints in the human body [7]. The myriad of ligamentous attachments, along with numerous muscles crossing the joint, provide insight into the joint's complexity. This anatomic complexity is necessary to allow for the elaborate interplay between the joint's mobility and stability roles. Dynamically, it works in conjunction with the hip joint and ankle to support and move the body during a variety of both routine and difficult activities. It has an important role either in human locomotion as in static erect posture. The knee is composed of two distinct articulations located within a single joint capsule, sharing the same articular cavity: the tibiofemoral joint – the articulation between the distal femur and the proximal tibia –, which is the principal articulation of the knee joint and is weight-bearing; and the patellofemoral joint – the articulation between the posterior patella and the femur [28, 29].

The knee joint is the middle joint of the lower limbs of the human body. It is the largest, most complex and most heavily-loaded joint of the human body and is regularly subjected to stress [4, 5]. As it can be seen in Figure 1.1, it is formed by a combination of hard tissue (bone) and soft tissues (ligaments, muscle, synovial fluid and cartilage). The bone parts that form the knee joint are the distal end of the femur, through the femoral condyles, the proximal end of the tibia, through tibial condyles and the patella. The soft tissue parts that sustain and move the bone structure are: the ligaments, connecting bone to bone (e.g. anterior cruciate and posterior cruciate ligament – ACL and PCL; lateral and medial collateral ligaments – LCL and MCL); the muscles that contribute to the stabilization of the joint and participate in the angular (rotatory) motion (flexion/extension, medial/lateral rotation and abduction/ adduction); and the tendons, which attach muscle to bone (e.g. quadriceps tendon). Other soft tissue parts are: the menisci (lateral and medial) that are interarticular cartilages, act as shock absorbers and improve the congruence between articular surfaces; the articular cartilage that covers the ends of the bones (distal end of the femur, the top of the tibia, and the back of the patella) with a smooth surface that allows easy gliding movement, facilitating motion; and the synovial liquid that have shock absorbing and lubricating functions. The anatomical fitting of the articular surface to the articular capsule, i.e., the topology of articular surfaces, along with the combination of actions from ligaments and cartilages, create the passive stabilizer system of the joint. Various muscles and their tendons form the knee's dynamic stabilizers [5, 28, 30].

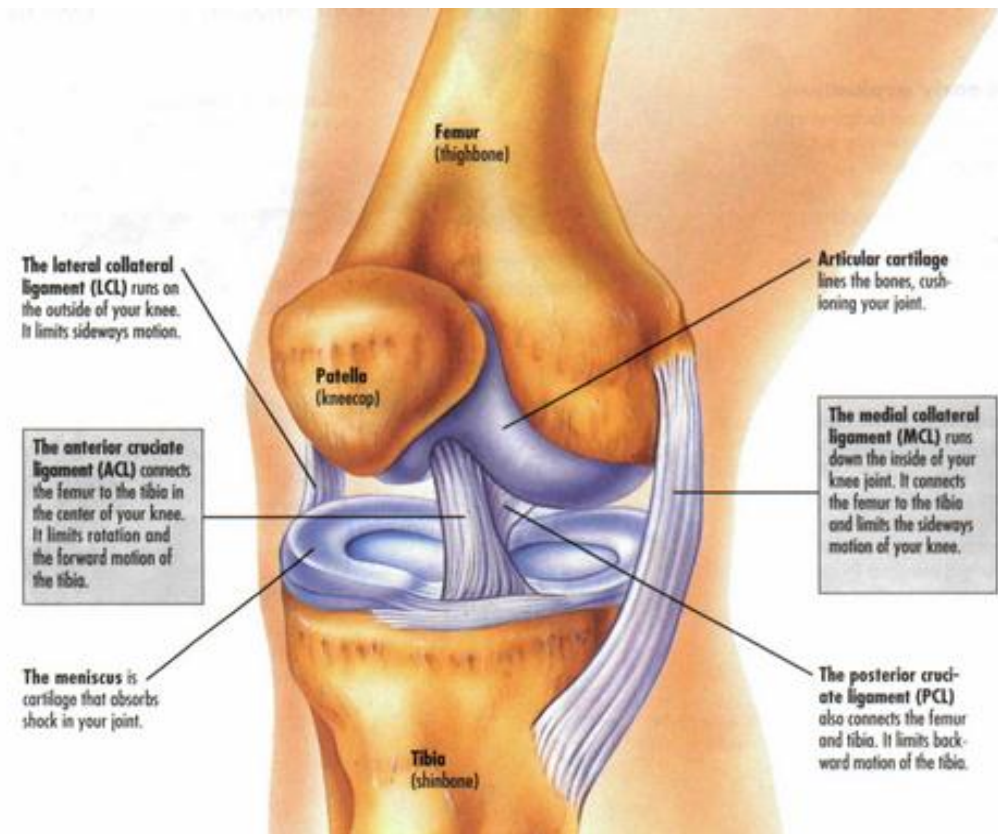


Figure 1.1 – Anatomy of the knee joint: anterior medial view (UC San Diego School of Medicine).

### 1.1.1 Bones of the knee joint

The knee joint is composed of three bones enclosed in a joint capsule: femur, tibia and patella.

#### - The femur

In human anatomy, the femur, or thighbone, is the longest, largest, strongest and heaviest bone [4, 5, 29]. As can be seen in Figure 1.2, the distal extremity of the femur – proximal articular surface of the knee joint –, is composed of two convex protrusions, the medial and the lateral femoral condyles. The condyles are separated posteriorly by an intercondylar fossa and are joined anteriorly by the femoral trochlear groove or surface. At its distal end, its major weight-bearing articulation is with the tibia, at the inferior and posterior surfaces of the femur's condyles (which constitute the surface for articulation with the corresponding condyles of the tibia and menisci). It also articulates anteriorly with the patella, at the trochlear groove [28, 29].

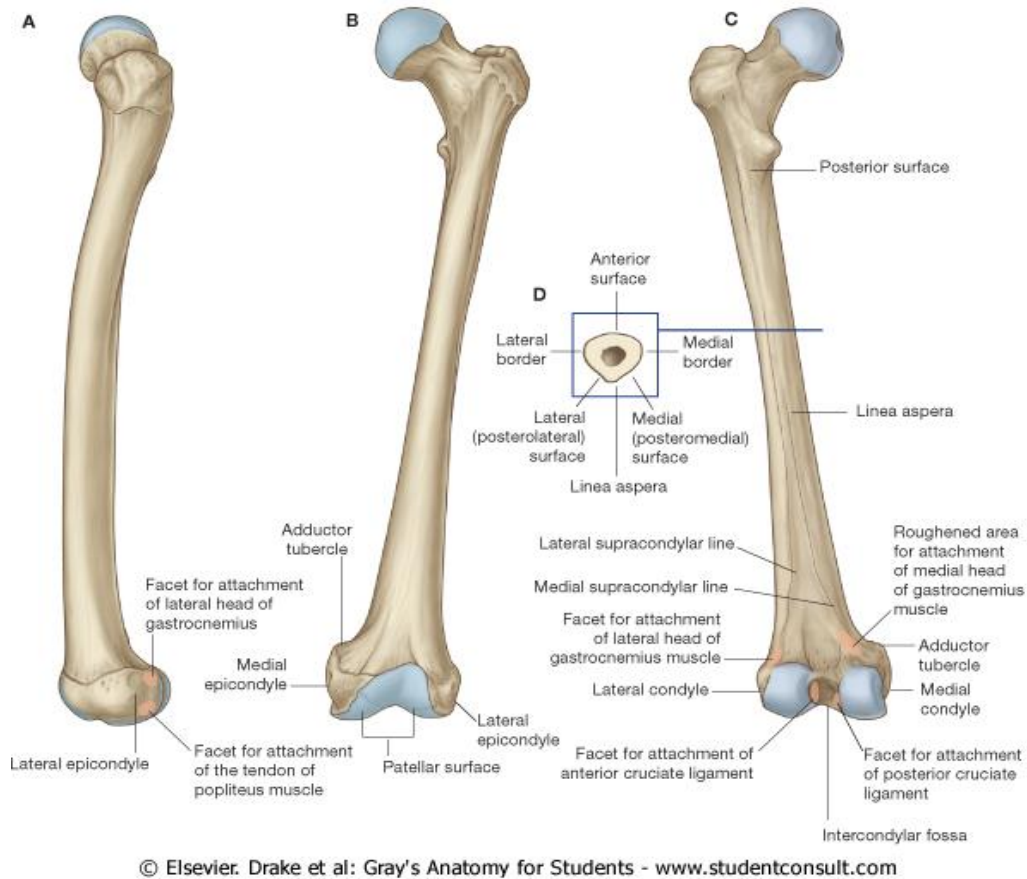
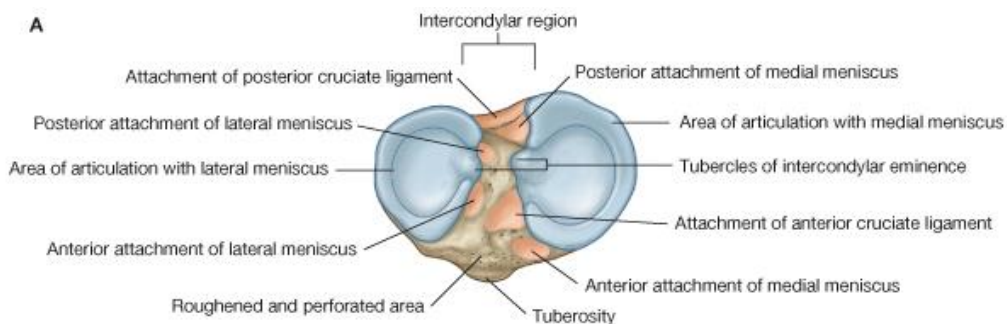
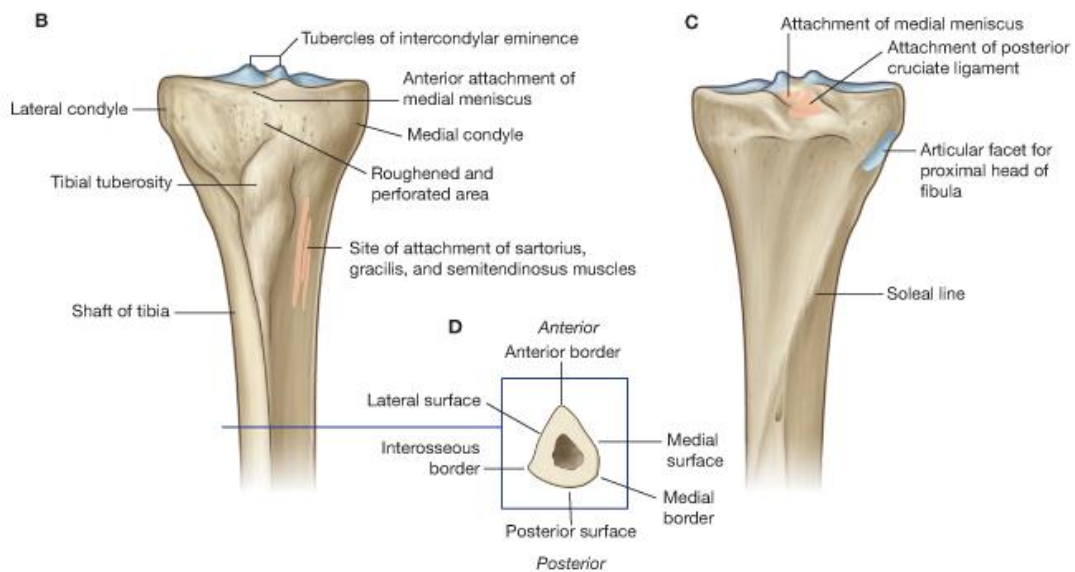


Figure 1.2 – Shaft and distal end of femur. A. Lateral view. B. Anterior view. C. Posterior view. D. Cross-section through shaft of femur [29].

### - The tibia

The tibia is the second largest bone of the human body after the femur. It is the medial one of the two lower leg bones (tibia and fibula), and is the only one that articulates with the femur at the knee joint [4, 29]. The proximal extremity of the tibia is expanded in the transverse plane for weight-bearing reasons, and it is formed by the medial and lateral condyles or plateaus which constitute the distal articular surface of the knee joint. The tibial condyles are separated by an intercondylar region, which is constituted by a roughened area and two bony spines called intercondylar eminence (that serves as attaching points for the cruciate ligaments and for menisci), as it can be visualized in Figure 1.3 [28, 29].





© Elsevier. Drake et al: Gray's Anatomy for Students - www.studentconsult.com

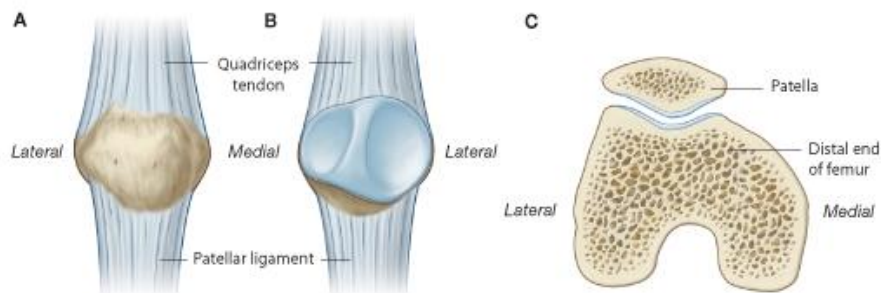
Figure 1.3 – Proximal extremity of the tibia. A. Superior view – tibial plateau. B. Anterior view. C. Posterior view. D. Cross-section through the shaft of tibia [29]. It is also possible to observe the sites of attachment for menisci, muscles and cruciate ligaments.

The central part of the tibial condyles articulates with the corresponding lower and posterior parts of the femur's condyles that constitute the knee articulation. The outer margins of the surfaces are the regions in contact with the interarticular cartilages (menisci). The tibial plateaus are predominantly flat, with a slight convexity at the anterior and posterior margins, suggesting that this bony architecture does not match up well with the convexity of the femoral condyle. Thus, accessory joint structures (menisci) are necessary between articular surfaces to improve joint congruency and bony stability, obliterating the intervals between the tibial and the femoral surfaces in their various motions and compensating for any superficial irregularities [1, 5, 28].

Together the articular surfaces of the tibial condyles and the intercondylar region form a 'tibial plateau', which articulates with and is anchored to the distal end of the femur. During knee extension, the intercondylar eminence of the tibia becomes lodged in the intercondylar fossa of the femur, helping to prevent rotation [4, 28, 29].

#### - The patella

The patella (knee cap) is a flat, triangular bone situated on the front of the knee joint. This bone is the largest sesamoid bone in the body and is embedded in the tendon of the quadriceps femoris muscle – see Figure 1.4. This tendon crosses anterior to the knee joint to insert on the tibia (via patellar ligament, connecting patella to the tibia) [29]. The patella increases the leverage of the tendon, maintains its position when the knee contracts and acts as a shield towards the front of the knee joint, as it is composed mainly of dense cancellous tissue. Protection and muscular attachment are the main functionalities of the patella. During flexion and extension of the knee, the patella slide up and down in the patellar groove or surface [4, 29].



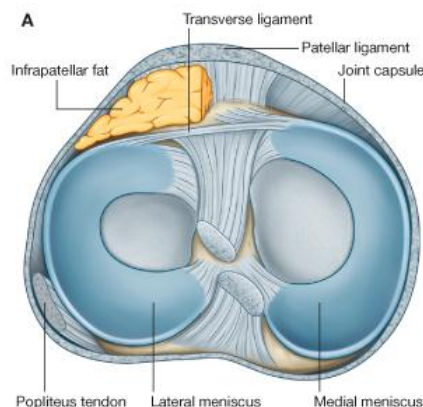
© Elsevier. Drake et al: Gray's Anatomy for Students - www.studentconsult.com

Figure 1.4 – Patella. A. Anterior view. B. Posterior view. C. Superior view [29].

Despite being connected to the tibia (along their lengths by an interosseous membrane and at their distal ends, with little movement occurring between them), the fibula does not form part of the knee joint. So, it does not actively contribute to weight-bearing or to the joint motion and only serves as muscle support [29].

### 1.1.2 Menisci

The menisci are two semicircular shape fibrocartilages that are located on top and circumference of the tibial condyles, covering one half to two thirds of the articular surface of the tibial plateau (see Figure 1.5). They serve to deepen the surfaces of the head of the tibia for articulation with the condyles of the femur (forming concavities into which the femoral condyles sit), improving the congruence and increasing the contact area at the tibiofemoral joint. This way, the menisci distribute the weight-bearing loads from the femur to the tibia more evenly and stabilize the knee joint preventing the translation (sliding) of the femur with respect to the tibia. Additionally, they are a shock absorbing media that protects the joint and serve as lubricant providing for very low friction between the articular surfaces. If the femoral condyles seat directly on the relatively flat tibial plateau, there would be little contact between the bony surfaces [28, 29].



© Elsevier. Drake et al: Gray's Anatomy for Students - www.studentconsult.com

Figure 1.5 – Menisci of the knee joint, superior view [29].

### **1.1.3 Ligaments**

Ligaments connect one bone to another, usually at or near a joint. Ligaments and tendons associated with synovial joints play an important role in keeping joint surfaces together (providing stability for the joint) and guiding motion (allowing and limiting mobility). Excessive separation of joint surfaces is limited by passive tension in ligaments, the fibrous joint capsule, and tendons (passive stability). Active tension in muscles (dynamic stability) also limits the separation of joint surfaces. Given the lack of bony restraint to virtually almost all the knee motions, the knee joint ligaments are variously and have an important role in resisting or controlling the possible movements of the tibia beneath the femur. Ligaments function can change, depending on the position of the knee joint and on what active or passive structures are concomitantly intact [5, 28].

In the knee joint there are two main types of ligaments which assist in tibiofemoral joint stability: the cruciate and the collateral ligaments (see Figure 1.1). The cruciate ligaments are located inside the knee joint, in the intercondylar region, and ensure anterior-posterior stability of the joint. The anterior cruciate ligament (ACL) prevents anterior displacement of the tibia relative to the femur (forward sliding), while the posterior cruciate ligament (PCL) restricts posterior displacement (sliding backwards) [5, 28, 29].

The collateral ligaments are located on the outer surfaces of the knee, one on each side of the joint, and stabilize the hinge-like motion of the knee, providing for varus–valgus stability throughout the range of motion of the joint (impede sideways motion on the frontal plane). The medial collateral ligament (MCL) is placed at the inner part of the joint and is the primary restraint to excessive abduction (valgus - outward angulation of the distal segment) and lateral rotation stresses at the knee, while the lateral collateral ligament (LCL) (connecting the fibula to the femur) is primarily responsible for limiting varus (inward angulation of the distal segment) motion and limit excessive lateral rotation of the tibia [28, 29].

### **1.1.4 Kinematics**

The detailed movements of the knee joint are complex, but basically the knee can be considered as a modified hinge joint that operates mainly in a single plane (sagittal), i.e., the primary angular (or rotatory) motion of the tibiofemoral joint is flexion/extension, although both medial/lateral (internal/external) rotation and varus/valgus (abduction/adduction) motions can also occur to a lesser extent, depending on the flexion/extension position of the knee [1, 5, 28, 29].

Most of the large muscles in the thigh insert into the proximal ends of the two bones of the leg (tibia and fibula) and are mainly responsible for producing movement, flex and extend the leg at the knee joint, beyond their stabilizing function (controlling frontal and transverse plane motions). Therefore, each of the muscles that cross the joint can be grouped as flexors or extensors [1, 28, 29].

## 1.2 Bone tissue

Bone tissue, forming the skeleton, makes up about 18% of the weight of the human body and is the hardest of all the connective tissues. Surrounding its cellular component is an extracellular matrix composed of about 50% inorganic materials (e.g. calcium carbonate and mainly hydroxyapatite), which gives hardness, stiffness and compressive strength; 25% of organic material (primarily type I collagen and minority proteoglycan and glycoprotein) that gives flexibility and resilience; and 25% of water content. The mechanical properties of bone are related with its organic and inorganic material composition [4].

The major cellular components (see Figure 1.6) present in bone tissue are osteogenic cells which are unspecialized stem cells (only bone cells to undergo cell division) that can develop into osteoblasts (bone-building cells), responsible for the synthesis of bone and for its deposition and mineralization. As osteoblasts surround themselves with extracellular matrix, they become trapped in their secretions and become osteocytes (bone-maintaining cells) which are mature and the principal cells of the bone tissue (exchange nutrients and wastes with the blood). From a different origin, osteoclasts (bone-destroying cells) release enzymes and acids which digest the bone matrix in a process designated by bone resorption. This breakdown of bone matrix is part of the normal development, maintenance, and repair of bone [1, 4, 28].

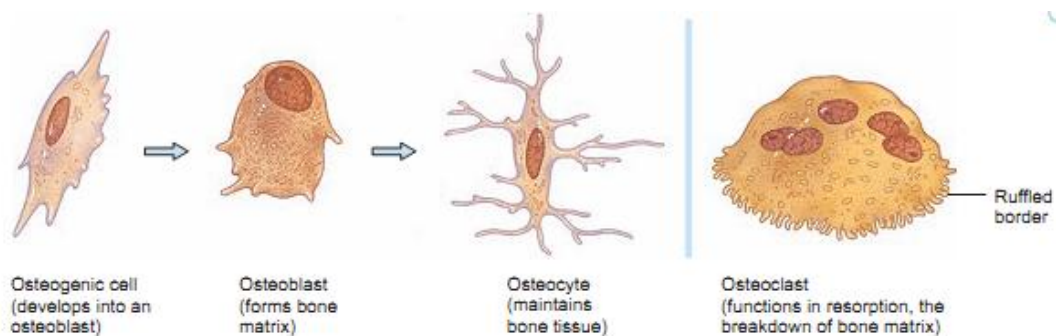


Figure 1.6 – Types of cells in bone tissue [4].

Bone is not completely solid, presenting many small spaces between its cells and matrix components. Some of these spaces serve as channels for blood vessels that supply bone cells with nutrients, while others are storage areas for bone marrow (red and yellow). According to the size and distribution of the spaces (architecture of the bone matrix), and how the cells are arranged, the regions of bone may be classified as cortical (also compact or dense) or trabecular (also cancellous or spongy). From a macroscopic point of view, the main difference between them resides on the density of the bone matrix [4].

As the name suggest, compact bone tissue is extremely hard and dense, representing approximately 80% of the total mass of the human skeleton [31], containing a low porosity (about 5 to 10%) and a high density. These features make the compact bone ideal to form the external layer of all bones and the bulk of the diaphysis of long bones, providing support to the body and protecting the organs. At the microscopic level, it is composed by concentric layers of bone lamellae – rings of calcified extracellular matrix –, which in group form the Havers systems or osteons (see Figure 1.7). The central canal (Havers canal), around which bone lamellae are

arranged, extends longitudinally along the bone and contains a set of blood vessels, responsible for the irrigation of the bone. Osteons are connected to each other and to the periosteum (fibrous layer covering all bones) by oblique channels called Volkmann's canals. Small spaces (or lacunae) are formed between lamellae where the osteocytes are housed [4].

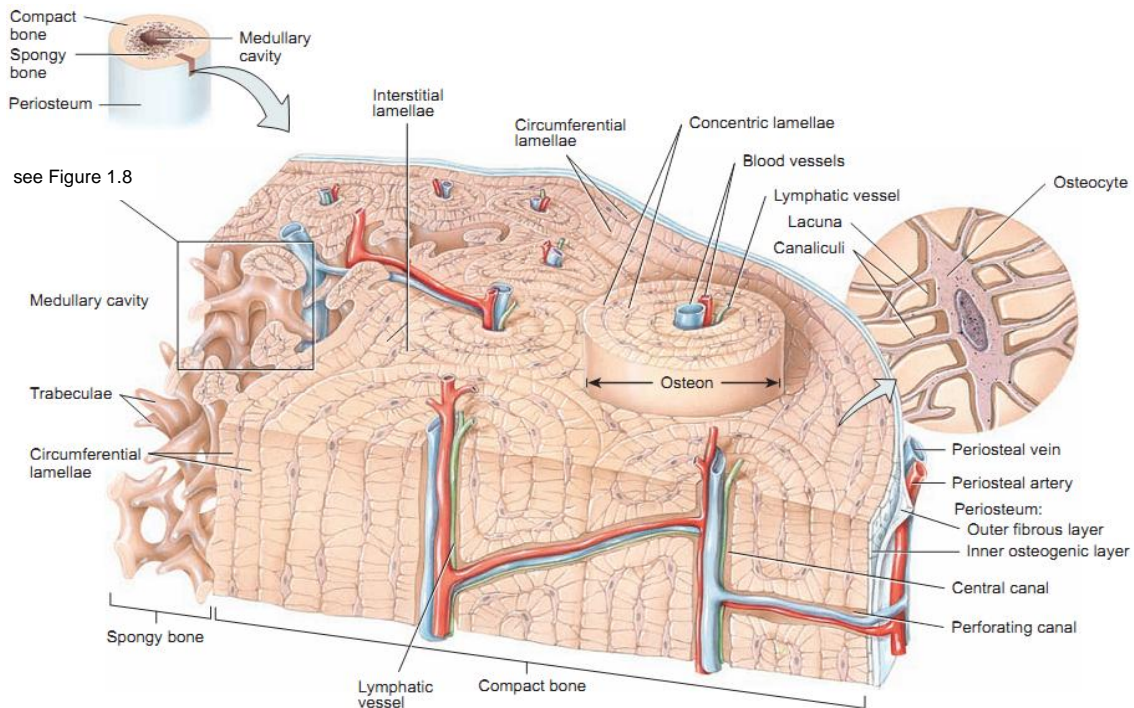


Figure 1.7 – Osteons in compact bone and trabeculae in spongy bone [4].

Spongy bone tissue composes the epiphysis of long bones and of most of the bone tissue of short, flat, and irregularly shaped bones. Instead of osteons, it consists of trabeculae, an irregular latticework of thin columns of bone filled with bone marrow. Within each trabecula are lacunae that contain osteocytes (see Figure 1.8). It presents a high porosity (comprised between 75% and 95%) and low density, which gives to the global bone structure flexibility and resilience. These characteristics reduce the overall weight of a bone and confer support and protection to the bone marrow. Moreover, make its adaptation easier to the mechanical solicitations, due to its capability of energy absorption originated from impacts. The numerous bone trabeculae are oriented according preferred directions, a characteristic that helps bones resist stresses and transfer force without breaking. Spongy bone tissue tends to be located where bones are not heavily stressed or where stresses are applied from many directions [4].

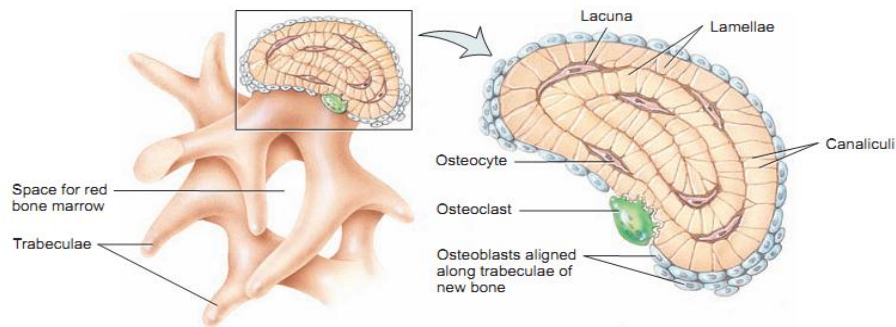


Figure 1.8 – Enlarged aspect of spongy bone, at the left, and the details of a section of a trabecula, at the right [4].

The skeletal system has several functions. It gives mechanical support to the soft parts of the body, protecting the vital organs. It has an important role in the mineral homeostasis, since bone tissue provides a ready store of calcium (about 99% of the body's calcium [32]) and phosphate, and also hosts red bone marrow, that produces blood cells, and yellow bone marrow, that reserves triglycerides (potential chemical energy reserve). Finally, is its concerted action with the tendons, ligaments, joints and skeletal muscle that results in movements, simple and complex, from everyday life [1, 4].

At the macroscopic level, the structure of long bones which are found within the limbs (e.g. tibia), consists of a body or shaft (diaphysis), which has a cylindrical shape and a central cavity termed the medullary canal, and two extremities called epiphyses between which are the metaphysis. The wall of the diaphysis consists of dense, compact tissue of considerable thickness in the middle part of the body, but becoming thinner toward the extremities. Within the medullary canal is some cancellous bone filled with marrow, scanty in the middle of the body but greater in amount toward the ends [1, 4, 29].

### 1.3 Bone remodeling

Bone is a dynamic living tissue (metabolically active organ) that is continuously growing, remodeling and repairing itself, throughout life, in order to maintain stability and integrity [1, 33, 34].

Bone remodeling or bone turnover is the ongoing replacement of damaged or old bone tissue by new bone tissue through all stages of life, allowing the maintenance of bone homeostasis. It has an important role, since about 10% of bone material is being renewed every year [33]. This process involves bone resorption, the removal of minerals and collagen fibers from bone (destruction of bone extracellular matrix) by osteoclasts, followed by bone deposition, the formation of bone matrix by osteoblasts that subsequently become mineralized [4].

At the cellular level, bone remodeling involves the coordinated actions of osteoclasts, osteoblasts and osteocytes within the bone matrix, and osteoblast-derived lining cells that cover the surface of bone [35]. Together, osteoclasts and osteoblasts cells at various stages of maturation, form temporary anatomical structures, called basic multicellular units (BMUs). These units organize themselves in time and space executing the replacement of old bone by

new bone [34–37]. BMUs react very sensitively to any changes of the bone microenvironment. Consequently, modification of any of its components is expected to have significant effects on bone turnover and homeostasis [36].

The bone remodeling cycle involves different sequential steps: activation, resorption, reversal and formation (followed by a quiescent stage). The activation is the first stage of the remodeling process and consists in the activation of cells that are at quiescent stage. This is done with the recruitment and dissemination of osteoclast progenitors, to the surface to be resorbed, which later differentiate into osteoclast. During resorption phase, osteoclasts attach tightly to the bone tissue matrix creating an isolated microenvironment in which it releases enzymes and acids that, respectively, degrade collagen fibers and dissolve mineral salts (digesting the organic and inorganic matrices of the bone). These products of bone resorption (bone proteins and minerals) enter into osteoclast by endocytosis, cross the cell in vesicles, and undergo exocytosis. Finally, once in the interstitial fluid, the products of bone resorption diffuse into nearby blood capillaries providing access to stores of calcium [33, 36, 38].

Once a small area of bone has been resorbed, osteoclasts depart and undergo apoptosis, and osteoblasts move in to rebuild the bone in that area, this is called reversal phase. Thereafter, osteoblasts deposit osteoid (organic portion of the bone matrix that forms prior to the maturation of bone tissue) for a long period and mineralize it, so actually forming new bone until the resorbed bone is completely replaced, this is the formation phase. Finally, in quiescent phase some of the osteoblasts are encapsulated in the osteoid matrix and differentiate to osteocytes. Remaining osteoblasts continue to synthesize bone until they eventually stop and transform to quiescent lining cells that completely cover the newly formed bone surface. These lining cells are highly interconnected with the osteocytes in the bone matrix through a network of canaliculi. The description given for the bone remodeling process is complemented by observation of Figure 1.9 [4, 33, 36, 38, 39].

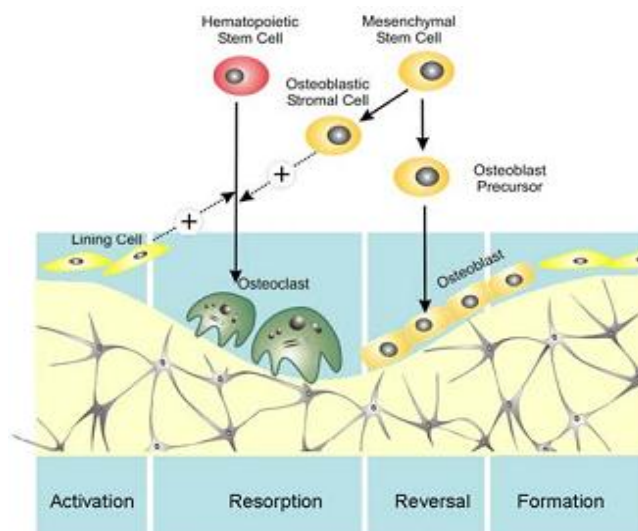


Figure 1.9 – Overview of bone remodeling process. Remodeling commences with the initiation of osteoclast formation, osteoclast-mediated bone resorption, a reversal period, and then a long period of bone matrix formation mediated by osteoblasts, followed by mineralization of the matrix [33].

The remodeling cycle occurs continuously at discrete sites throughout the skeleton in response to mechanical and metabolic influences [35]. In order to have balance in this process it is important that the cellular components of the BMU maintain a well-balanced relationship in spatial and temporal terms, i.e., there must be a coupling mechanism between formation and resorption allowing a wave of bone formation to follow each cycle of bone resorption, thus maintaining skeletal integrity [33, 38]. However, there are several factors that affect bone turnover process and, consequently, the amount and quality of the tissue produced, such as, nutrition, physiologic mechanisms (hormonal, genetic and metabolic factors), aging and local mechanical environment [37, 40].

Historically, since 1638 it has been known that the mechanical loading has profound influences on bone tissue. The current concept is that the bone architecture is controlled by a local regulatory mechanism. This idea originates from Roux (1881) [38], who proposed that bone remodeling is a self-organizing process, which provides the capability of self-repair to bone. The change in form to match function is known as Wolff's law, which appeared in the year 1892. This principle of functional adaptation is based on the observation that trabeculae tend to align with principal stress directions in many bones (e.g. proximal tibia). Wolff described the dependency of bone on applied loads; and proposed that forces are somehow sensed by the bone which adapts its structure and morphology according to mechanical stimuli, acquiring the structure more resistant to this loading, with minimal mass. Within limits, mechanical stress is a particularly potent stimulus for bone cells and, in response to that, bone tissue has the ability to alter its strength [37]. This way, the loading history of trabeculae influences the distribution of bone density and trabecular orientation. Thus, bone is a material with self-optimizing capabilities and able to control its mass and structure in direct relationship to its mechanical demands, ensuring that its mechanical integrity is maintained [33, 37, 38, 40, 41]. The ability of bone to adapt to mechanical loads is brought about by continuous bone resorption and bone formation – bone adaptation – allowing for changes in mechanical properties of the bone [38].

These concepts were captured by Frost (1964-1987) [38], who assumes that local strains regulate bone mass. If strain levels exceed a mechanical 'set-point', new bone is formed (bone deposition), whereas, if strain levels are below this set-point bone is removed (bone resorption). This qualitative theory has motivated many authors and served as theoretical basis for several mathematical and computational theories that were developed to study bone adaptation (Cowan and Hegedus, 1976; Huiskes et al., 1987; Beaupré et al., 1990; Weinans et al., 1992; Mullender and Huiskes, 1995; Adachi et al., 2001) [38, 40]. With the advances in computing and the development of mathematical concepts associated with optimization of structures it is possible to understand better the bone remodeling process, and to develop models that simulate the biomechanical behaviour of the bone, as it will be seen in this work.

The pathway by which mechanical forces are expressed in bone cells is currently one of the main studied issues in bone mechanobiology. Some studies [38] demonstrated that osteocytes

are mechanosensitive cells capable of sending biochemical messengers that influence the response of osteoblasts and osteoclasts. The osteocytes within the bone and lining cells on the bone surface are the most abundant cells in bone. Together, their abundance and connectivity make them a virtual antenna for detecting mechanical strains (deformation), through extracellular fluid flow caused by loading. When osteocytes are subjected to fluid shear stress, they release several messengers, which trigger bone remodeling. Thus, rapidly applied strains in bone tissue promote extracellular fluid flow and the interaction between this moving fluid and bone cells is key to transduce mechanical signals derived from mechanical loading into biochemical signal [37]. This signal will change the cellular activity of osteoblast and osteoclast and, consequently, the coupled apposition and resorption, leading to a change in bone density as an adaptive process (see Figure 1.10) [40, 42]. It is also important to notice that in mechanical stimuli, the magnitude of the stress, the frequency of loadings and the strain rate influence how the bone adaptation is made.

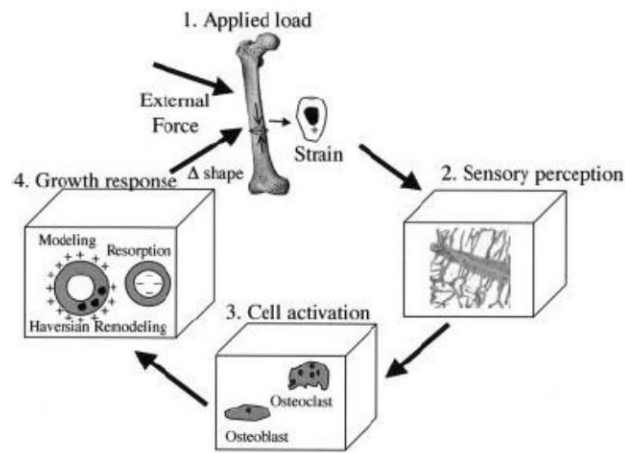


Figure 1.10 – Response of bone to the applied loads [42].

In homeostatic equilibrium resorption and formation are balanced. In that case old bone is continuously replaced by new tissue, ensuring that mechanical integrity of bone is maintained, with no global changes in morphology/architecture and in overall bone quantity [38]. Under adverse conditions, such as implant incorporation in the bone, the different load distribution resulting from the phenomenon of stress shielding (where stress is essentially carried by the implant and, consequently, the stress on bone decreases relative to intact tibia - without prosthesis [43]), can cause an increase in resorption compared to formation, leading to a weakened bone, more prone to the occurrence of fractures [40]. This alteration on the balance between bone formation and resorption, due to the changes in load pattern placed on bone (redistribution of stresses) lead to an increase in bone density in some areas and decreases density in other areas, conducting to a new state of equilibrium. Thus, understanding the bone adaptation process with respect to the mechanical behaviour is a very important issue, especially in the choice of the right orthopaedic implant for a given case [40]. Therefore, the models describing bone behaviour according to the load conditions are of particular value, allowing estimate the amount of bone resorption related to a specific prosthesis design, and are the ones used in this work.

## 1.4 Knee arthroplasty

### 1.4.1 Pathologic conditions

The knee is one of the most often injured joints, since it is the most heavily loaded and one of the most mobile joint in the human body. As we have seen before, this joint is designed to move mostly in one plane like a hinge. This restriction of movement is what makes the knee so vulnerable to traumatic injury [5]. Additionally, the knee is regularly subjected to the stress of both supporting body weight and absorbing shock from activities of daily living. Over time these stresses can cause numerous injuries and degenerative damage of the ligaments, the tendons, and the joint capsule that holds the knee together. So, bone movement may become excessive and may lead to increased articular cartilage degeneration and finally bone-on-bone friction. This leads to pain and dysfunction of bone meeting bone inside the knee joint, i.e., loss of movement and sometimes swelling. At its worst, this condition manifests as arthritis, which is the most common cause of knee joint pathology [5, 28]. Among all types of arthritis, osteoarthritis and rheumatoid arthritis are the ones that mainly affect the knee joint.

Osteoarthritis (OA) is a degenerative disease in which joint cartilage that covers the ends of bones in the joint is gradually lost (see Figure 1.11). As the cartilage degenerates, the bone ends become exposed and small bumps of new osseous tissue are deposited on them in a misguided effort by the body to protect against the friction. These spurs decrease the space of the joint cavity causing pain and limitation of movement as bone begins to rub against bone. OA results from a combination of aging (senescence), obesity, irritation of the joints, muscle weakness, and wear and abrasion. This disease is the most prevalent form of arthritis and the most common reason for hip- and knee-replacement surgery [4, 28, 44]. As the knee is the joint most frequently affected by OA, it is the most common joint replaced [11, 20, 21].



Figure 1.11 – Knee joint suffering osteoarthritis.

Rheumatoid arthritis (RA) is an autoimmune disease in which the immune system of the body for some reason cannot recognize the joint tissues (cartilage and joint linings) as tissues of its own and actually attacks it. The result is the inflammation of the joint and tissue damage (such as cartilage and synovial liquid – natural lubricants), with subsequent joint pain, swelling and loss of function (loss of movement). This is one of the most serious and disabling types, affecting mostly women [4].

Currently, a number of methods have been developed to address knee joint diseases. For arthritis related problems, there are some non-surgical therapeutic interventions available, such as medications and physiotherapy. However, these interventions have been shown to have only small effects on knee pain. When these treatments fail, patients may resort to surgical interventions, such as osteotomy and arthroscopy, although these procedures also have only limited success in pain reduction. So, when the disease develops to a point that most daily routine tasks become practically impossible or suffer constant pain, then a prosthesis needs to be implanted and the joint to be replaced. For each case, there is an appropriate method of correction [10, 11].

#### **1.4.2 Total and partial Knee replacement - TKR and UKR**

Joint arthroplasty is the surgical procedure also known as joint replacement. It is designed to joints that have been severely damaged by diseases, as happens when the disorders mentioned above become severe (e.g. advanced arthritis) [4, 5, 10, 19, 45-47]. Other conditions leading to knee arthroplasty include fracture, dysplasia, malignancy and others [17, 21]. The general goal of the artificial knee replacement is relieve pain and/or restore to the utmost joint motion, improving the functional capabilities and quality of life in patients, although it is not restored to the level of the general population [1, 10, 11, 13, 21, 30, 45]. During knee arthroplasty, damaged parts of the knee joint are removed and artificial components (made of metal, ceramic, or plastic), called prostheses, are fixed in place [4, 30]. Thus, knee replacements are actually a resurfacing of articular surface that may be total or partial.

Total knee arthroplasty (TKA), also referred to as total knee replacement (TKR), is a surgical procedure where worn, diseased, or damaged bone and cartilage, from the surfaces of knee joint, are removed from the distal end of the femur, proximal end of the tibia, and the back surface of the patella (if needed) and replaced with artificial surfaces that try to mimics the natural knee function and motion – see Figure 1.12 [4, 11, 30]. The materials used to resurface the joint are not only strong and durable, but also optimal for joint function as they produce as little friction as possible [30]. According to the situation, the posterior cruciate ligament may either be retained, sacrificed or substituted by a intercondylar polyethylene post.

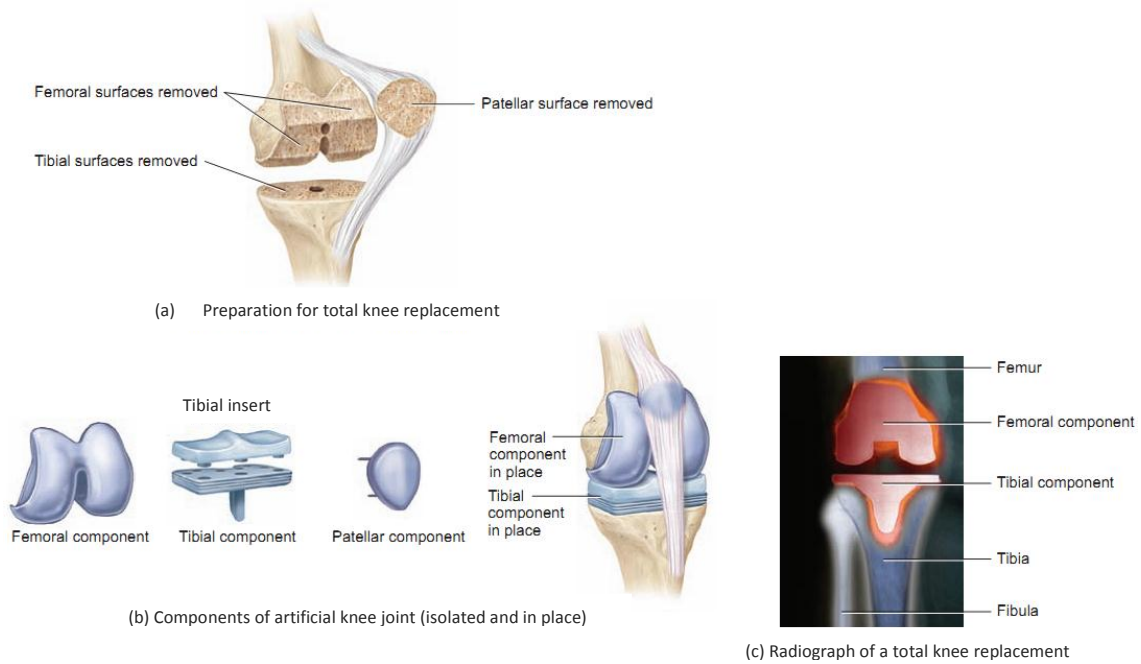


Figure 1.12 – Total knee arthroplasty adapted from [4].

On the other hand, in a partial knee arthroplasty, also called a unicompartmental knee replacement (UKR), only one side of the knee joint is replaced and the cruciate ligaments are preserved (Figure 1.13). This is useful for a particular group of patients, in which the arthritis affects only the medial or the lateral articular surfaces of the knee [4, 48]. It is estimated that only 6 – 10% of patients currently considered candidates for TKA are consider a candidate to UKR [6, 49]. Since only a part of the joint is replaced in the UKR, the surgery can be performed through a smaller incision, with less bone and soft tissue dissection, preserving bone stock and do not violate the non-diseased parts, so it is less invasive and with a more rapid rehabilitation than TKR [48, 49]. However, when comparing UKR with TKR, it can be seen that UKR shows inferior survivorship than TKR, and it requires a technically difficult revision surgery for failed UKR to TKR, because of significant osseous defects. Also, the functional results of revision TKR for failed UKR are inferior to those obtained after primary TKR. So, the role of UKR needs to be more clearly established and should not be used as a temporary procedure to delay TKR [48].



Figure 1.13 – Unicompartmental knee replacement [49].

### 1.4.3 Knee prosthesis

In total knee prosthesis the natural joint is replaced with an artificial joint, which is composed of femoral, tibial and patellar component. Nowadays, several models of knee implants exist with different designs and sizes, appropriate for each patient, depending on bone-implant fixation, joint connection and materials used. A brief description regarding their general characteristics are reported next.

The femoral component serves for attachment to the lower end of a patient's femur to replace the proximal articular surface of the knee joint. As it can be seen in Figure 1.14, this component is similar to the distal end of the femur, as it retains the original sagittal shape and rounded coronal condylar geometry designed to maximize contact area and to minimize average peak stresses on the articulating polyethylene tibial insert (spreading the load more evenly). At the same time, rounded coronal geometry provides the forgiveness needed for a varus or valgus lift-off of the femoral component that may regularly occur in normal gait patterns, while providing the proper level of constraint. Additionally, the femoral component incorporates a single spherical radius patella groove that articulates with the corresponding domed patellar implant, keeping them in constant contact and promoting the normal cinematic of the patellofemoral joint [50].

The tibial component serves for attachment to the upper end of a patient's tibia. The tibial tray or plateau is designed to provide optimal tibial coverage and consistent femoral load transfer to the resected proximal tibia. It has a cross-finned (or cruciform) keel design (see Figure 1.14) that supports the plateau, resists rotational forces, and provides fixation and stability to the tibial component. In addition, it has an important role in load supporting and redistribution [50]. Both the femoral component and the tibial tray are made of metal alloys with excellent corrosion resistance and biocompatibility, without creating a rejection response in the body [50].

The tibial insert are designed to be inserted in the tibial tray, and on the other side it has rounded coronal and sagittal shape which provides stability in this two planes and improves its articulation with femoral component. This way, it serves as artificial cartilage between the femoral component and the tibial base plate, improving shock-capacity of the joint and it is responsible for transferring the loads [1]. As the wear of tibial insert is one of the most important parameters that affect the longevity of the implant and may lead to a revision surgery [18], this is composed of UHMWPE (high density polymer), which has wear resistance and long-term clinical success. In cases where the posterior cruciate ligament is sacrificed, the tibial insert incorporates a central spine that engages in the corresponding intercondylar fossa in the femoral component, compensating for the absence of stabilization by ligament removed (Figure 1.14 B) [50, 51].

The patellar component replaces the surface on bottom of the patella, and as mentioned before, it has a dome geometry that articulates with the femoral component at the patellar groove. It is made of UHMWPE and can be visualized in Figure 1.14.

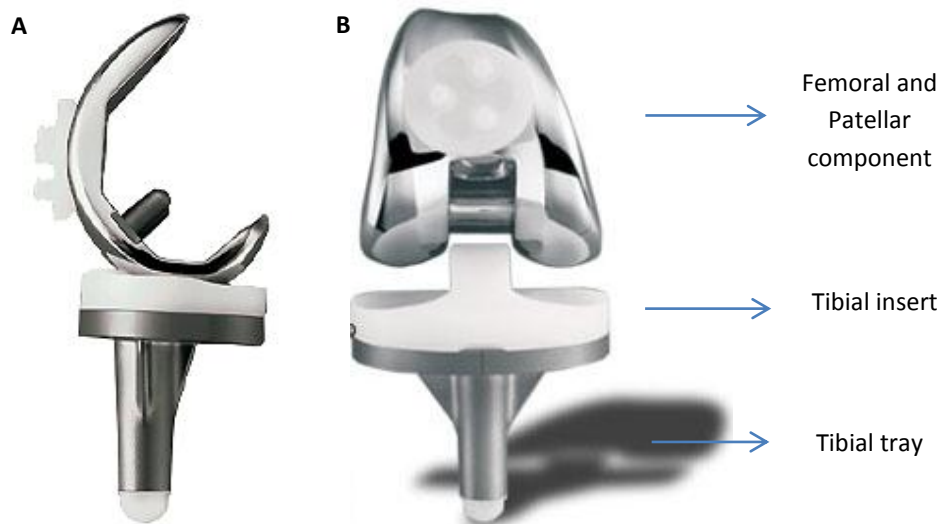


Figure 1.14 – Total Knee prosthesis. A. Sagittal view. B. Frontal view; adapted from [52].

Both tibial and femoral components can include a stem that inserts into the center of the corresponding bone, in order to obtain additional stability and fixation of the components in the bone. These stems are made of metal alloys, are available in a wide range of dimensions (length and diameter combinations), designs and can be implanted in press-fit or cemented fashion. This variety of options maximizes the customizing of the implant to the patient and is essential to the success of the arthroplasty [50]. Shorter stems are used in primary TKA surgery, while revision surgery may require longer stems [53].

The tibial component, object of study of this work, can be implanted by two methods of attachment: cemented and press-fit. The cemented method uses polymethylmethacrylate (PMMA), also known as bone cement, to provide mechanical fixation of the implant components to the bone. As the cement penetrates into spongy bone's porous surface, the small voids and irregularities of the resected bone are readily filled, allowing the stem to perfectly fit into the tibia [14]. The non-cemented method, or press-fit, uses a fluted stem press-fit against the bony surfaces that provide stable fix of the stem directly into the intramedullary canal of the tibia.

Summarizing, the tibial component in TKA can have three different constructs: standard (without stem extension), cemented stem and press-fit stem, which are the most common ones clinically utilized by surgeons in primary or revision TKA [54]. The decision on which method to use depends on the bone quality and strength, on the patient's condition (age, weight and lifestyle), and surgeon's experience [14]. A correct choice of the stem geometry can improve the stem stability and, consequently, increase the life time of the tibial component.

#### 1.4.4 Surgical procedure

As seen previously, implants currently available have a design very close to the normal anatomy of the knee, allowing a good clinical outcome achievement, with a low frequency of complications. In addition, it is crucial that the surgeon follows a series of directives to ensure the quality of the surgical technique [47]. To begin the surgery, the surgeon makes an incision in

the front of the knee and the patella is put aside so as to expose the local where the implant is placed. The ends of femur and tibia are then accurately cut into a shape that matches the corresponding surface of femoral and tibial component, respectively, using instruments to measure and make the precise cuts of the bone. In most cases, the proximal tibia is resected at 90° to its mechanical axis (center of the knee – center of the ankle) with a level of about 10 mm based on the less involved condyle (the exact level of resection vary according to the patient anatomy) – see Figure 1.15. Then trial implants are inserted, and is choose the size that gives the greatest stability and overall alignment. Finally, metal femoral and tibial components are implanted into the respective bones, and tibial insert is snapped into the tibial component. If needed, the patella is resurfaced with patellar component. In the end, the patella is put back in place and is carried out the closure phase [51, 55].

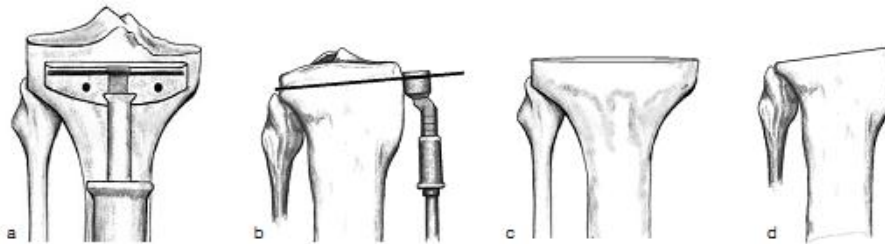


Figure 1.15 – Accurate component alignment and resection of the proximal tibia [56].

It is the surgeon who decides, especially in revision TKA, which type of stem to use to help fix the implant into the bone. In case of a fragile bone is recommended the cemented stem [57], with a smaller dimension than the reamer used, thus resulting a space for a cement mantle with approximately 1 mm between prosthesis and bone. On the other hand, if bone has a good stability a press-fit technique can be used, where the stem has the same dimension of the reamer and is impacted onto the bone, to ensure a good fit between them [51]. After implantation, the bone starts to attach to the cementless stem and the prosthesis can maintain stability, due to this biological fixation by bone/metal interaction [58].

The success of joint replacement depends on many factors, including patient selection, prosthetic design and appropriate sizing (tests are done during the surgery with trial implants), accurate component alignment (extramedullary and intramedullary guidance systems are used to improve the accuracy of the alignment of implants), soft-tissue balancing and accurate patellar tracking (this is done through accurate positioning of the femoral and tibial components and precise resurfacing of the patella) [51, 59, 60].

Actually, the fulfillment of previous criteria leads to a successful and well-proven TKA, providing pain relief and the restoration of the function. Nevertheless, excellent short and medium-term results achieved do not resist over time [47, 59]. Similarly to what happens with every other arthroplasty joint replacements, TKA is associated with several potential complications and failure mechanisms, such as: loosening, wear or dislocation of the replacement components, tibiofemoral instability, infection or fracture of the femur or tibia and pain experienced by patient [4, 13, 22, 47, 51, 59]. In 60.355 procedures of revision TKA performed in the USA, between 2005 and 2006, the most common causes of revision were

infection (25.2%) and mechanical loosening (16.1%). And also, the most common type of revision TKA procedure reported was all component revision (35.2%) and in the third place was tibial component revision (9.5%) [61].

One of the major reasons why artificial joints may eventually fail is because of loosening [30]. Loosening is a fairly common problem, particularly of the tibial component [1], which is the component studied in this work. The loosening of the prosthesis occurs when the stability of the bone-implant interface is compromised and, the prosthesis becomes loose inside the tibia, so it may move and lead to the failure of the joint replacement. The stability of the implant-bone interface depends directly on the bone remodeling process, since bone surrounding the TKA adjusts its mineral density and structure to meet the new mechanical demands [47, 54]. This happens because TKA alters mechanical loading of the knee joint, leading to abnormal distribution of stresses. This redistribution of stresses and strains in the bone after surgery can lead to bone fragility and, consequently, affects the implant-bone interface [47, 54].

Another factor that can cause loosening of implant are the particles that come from the tribological wear of the biomaterials included in prosthesis composition, which are the cause of biological intolerance reactions – particularly the particles of polyethylene wear, that can provoke inflammation of the surrounding tissues – which, in turn, leads to the bone osteolysis, thus comprising the mechanical stability of the prosthesis, and thereby leading to loosening of the knee replacement [47].

In conclusion, several studies describe a significant decrease in postoperative bone mineral density (BMD), adjacent to the implant, after TKA [22]. The prosthesis related bone loss is a concern about the success of the knee prosthesis, as it can lead to bone fracture and reduces the amount of bone available for the future revision surgery. This bone loss is considered to occur mainly as a result of the phenomena of stress shielding, wear and implant loosening [54]. These events cause at long-term, a mechanical failure of the arthroplasty, with detachment of implants from bone support, thereby requiring the implantation of a new prosthesis [47]. To accomplish a stable fixation and ensure better alignment of new prosthetic implants with a good load sharing (bypass load), the revision TKA components are commonly stemmed with metallic augments, thus protecting the limited bone stock remaining [54, 62]. Understanding the effect of TKA design in failure mechanisms is essential to improve implant performance and long-term patient outcomes.



## 2. Model of Bone remodeling

At the end of the nineteenth century, Wolff proposed that bone morphology depends on applied loads and that the adaptation of trabecular bone to its mechanical environment could be described by mathematical rules, as it was seen in the previous chapter. As a consequence, researchers developed progressively more sophisticated and complete mathematical and computational models to predict this behaviour.

This chapter describes the basic concepts of the computational model for bone remodeling used in this work. This model is based on structural topology optimization and simulates the bone adaptation process due to mechanical loading, i.e., it describes the bone behaviour in response to the mechanical environment.

In this formulation, bone is assumed as a porous material with variable relative density and periodic microstructure. Such material is obtained by the repetition of cubic cells with prismatic holes. The equivalent elastic properties of bone are obtained by a homogenization method. The changes on bone relative density are obtained by the minimization of a cost function, which considers both mechanical and the biological cost associated with maintenance of bone tissue. The necessary conditions for optimum are solved numerically through a suitable finite element discretization [58, 63]. Bone density is a physical parameter that reflects the changes in the bone structure and is closely correlated with the mechanical properties of bone.

### 2.1. Optimization model

Considering that bone adapts to the applied mechanical loading stiffening its structure, a model for bone remodeling can be derived from a topology optimization problem. A typical topology optimization model for elasticity problems consists in the process of distributing material by different regions, identifying solid or void regions (filled or without material, respectively), in order to obtain the stiffest structure within a given domain. In this model, the structure is identified by an optimal distribution of material with variable relative density. The introduction of a material with variable relative density permits the formulation as a continuous material optimization problem. In other words, the design variable (the relative density of a porous material) is a continuous function defined on the design domain and with values in the interval  $[0,1]$ . This allows not only the representation of limiting cases, 1 and 0, that correspond respectively to full material and void, but also all the intermediate states [40, 43, 63].

This type of material model is suitable for modeling trabecular bone, since this is a naturally porous material with variable density. Assuming trabecular bone tissue has the same material properties as cortical bone, maximum relative density values correspond to dense cortical bone, while intermediate values correspond to trabecular bone [40, 43, 63].

## 2.2. Material model for bone

In this model, bone is modeled as a porous material with periodic microstructure, which is obtained by the periodic repetition of unit cubic cells with small prismatic holes, with dimension  $a_1, a_2, a_3$ . This cell and its periodic repetition characterizes the material microstructure, as shown in Figure 2.1. Note that the periodicity assumption is only local and thus the density can change through the structure. The relative density,  $\mu$ , at each point depends on local hole dimensions, and is calculated by  $\mu = 1 - a_1 \times a_2 \times a_3$ , with  $a_i \in [0,1]$ . Thus, the hole dimension defines the bone relative density, with values from  $a_i = 0$  (full material/compact bone) to  $a_i = 1$  (void/ without bone). For intermediate values, it corresponds to trabecular bone with variable porosity, as mentioned above [40, 43, 58, 63].

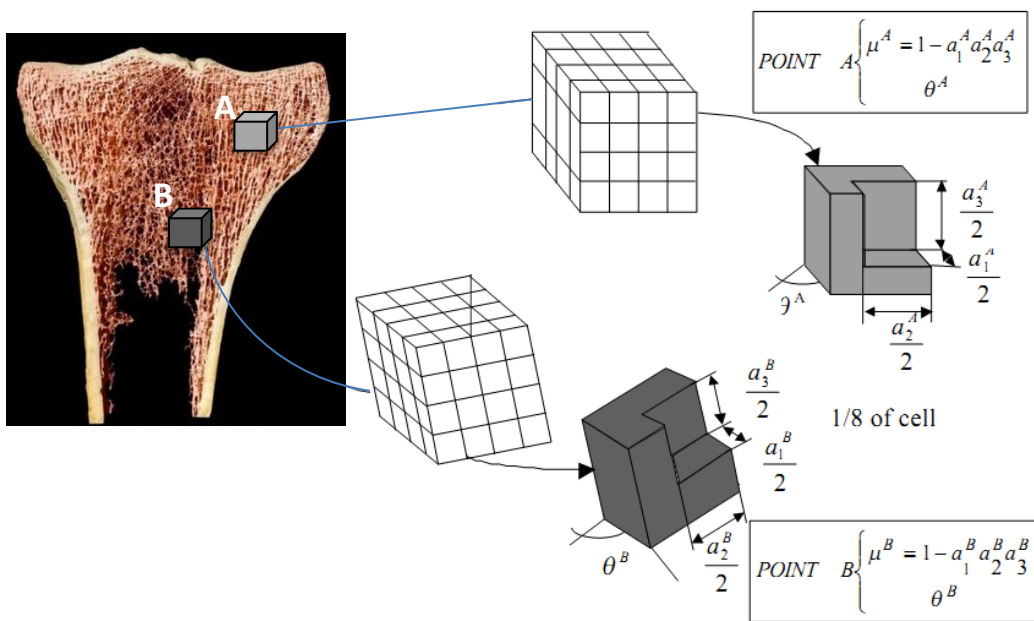


Figure 2.1 – Material model for bone, adapted from [43].

Furthermore, this cellular material definition leads to an orthotropic material, which allows the consideration of an optimal orientation of unit cells and, consequently, simulation of bone as an oriented material, i.e., it is possible to estimate the orientation of trabeculae. Thus, at each point, bone is characterized by the microstructure parameters  $a_1, a_2, a_3$ , which define the local relative density,  $\mu$ , and by cellular orientation that is given by the Euler angles,  $\theta = \{\theta_1, \theta_2, \theta_3\}^T$  [43]. Note however, that since the objective of this study focus on an analysis of densities, it will only take into account the parameters  $a_i$ .

The elastic properties of this material are calculated using asymptotic homogenization methods. In this case, the purpose of homogenization is to find for a porous or heterogeneous material, a homogeneous material with equivalent macroscopic properties without needing to represent each individual microstructure [64, 65]. This way, it can reflect the microscopic structure without looking at details of all the material points of the body, whenever the focus is the mechanical behavior of the macroscopic body. The homogenized properties, functions of

relative density, are obtained by a polynomial interpolation on the interval  $a_i \in [0, 1], i = 1, 2, 3$ . For a more detailed description of this method see e.g. Guedes, Kikuchi [65].

### 2.3. Mathematical formulation

The bone remodeling model consists in the computation of bone relative density (design variable), at each point of the domain, by solving an optimization problem, formulated in the continuum mechanics context. The optimization goal is to minimize, with respect to relative density, a linear combination of structural compliance (inverse of structural stiffness) and the metabolic cost to the organism of maintaining bone tissue [43, 58]. The solution for this problem yields the stiffest bone structure for the applied loads, as the bone adapts to the mechanical environment, with the total bone mass regulated by a parameter that quantifies the biological factors. Thus, the optimization problem reflects both mechanical advantage and metabolic cost [43, 58].

The bone remodeling problem considers bone (or implanted bone) as a structure occupying a volume  $\Omega$ , with fixed boundary  $\Gamma_u$  and subjected to a set of surface loads,  $f$  in the boundary  $\Gamma_f$ . The bone/stem and bone/cement interface are denoted by  $\Gamma_c$  (see Figure 2.2) [58].

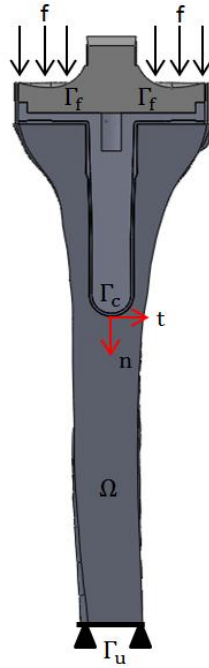


Figure 2.2 – Generalized elastic problem with contact, adapted from [58].

Defining the design variables  $\mathbf{a} = \{a_1, a_2, a_3\}^T$ , for each point as mentioned above and using a multiple load optimization criterion, the problem can be stated as:

$$\min_{\mathbf{a}} \left\{ \sum_{P=1}^{NC} \alpha^P \left( \int_{\Gamma_f} f_i^P u_i^P d\Gamma \right) + k \int_{\Omega} \mu(\mathbf{a}) d\Omega \right\} \quad (1)$$

subjected to

$$0 \leq a_i \leq 1, \quad i = 1, 2, 3$$

$$\int_{\Omega} E_{ijkl}^H(\mathbf{a}) e_{ij}(\mathbf{u}^P) e_{kl}(\mathbf{v}^P) d\Omega - \int_{\Gamma_f} f_i^P v_i^P d\Gamma + \int_{\Gamma_c} \tau_n^P (v_n^{rel})^P + \tau_t^P (v_t^{rel})^P d\Gamma = 0 \quad (2)$$

$$\forall \mathbf{v}^P = 0 \text{ and } \mathbf{u}^P = 0 \text{ on } \Gamma_u$$

$$\left\{ \begin{array}{l} (u_n^{rel})^P - g \leq 0, \tau_n^P \geq 0, \tau_n^P ((u_n^{rel})^P - g) = 0 \text{ on } \Gamma_c \\ |\tau_t^P| \leq \vartheta |\tau_n^P| \rightarrow \left\{ \begin{array}{l} |\tau_t^P| < \vartheta |\tau_n^P| \Rightarrow u_t^{rel} = 0 \\ |\tau_t^P| = \vartheta |\tau_n^P| \Rightarrow \exists \Lambda \geq 0 : u_t^{rel} = -\Lambda \tau_t^P \end{array} \right. \text{ with } P = 1, \dots, NC \end{array} \right. \quad (3)$$

where  $NC$  is the number of considered load cases with the, respectively, load weight factors  $\alpha^P$  satisfying  $\sum_{P=1}^{NC} \alpha^P = 1$ . The multiple load formulation allows considering different load cases corresponding to various types of daily life activities that body structures are often exposed to [58].

In the previous problem statement, Eqs. (2) and (3) corresponds to the set of equilibrium equations for two bodies in contact, in the form of a virtual displacement principle. In these equations,  $E_{ijkl}^H$  is the homogenized material properties of bone (the superscript  $H$  denotes homogenized),  $e_{ij}$  is the strain field,  $v_i^P$  the set of virtual displacements and the last term of Eq. (2) is the contribution of contact loads  $\tau^P$ , where the subscripts  $n$  and  $t$  denotes normal and tangential directions, respectively. In Eq. (3)  $g$  is the gap between the two bodies and  $\vartheta$  is the friction coefficient [58].

The objective function in Eq. (1) is based on the balance of two terms: the first term concerns to the weighted average of the work of applied forces, whereas the second term represents the metabolic cost of maintaining bone. The cost parameter,  $k$ , plays an important role, since the resulting optimal bone mass, not only depends on load values, but also depends strongly on cost parameter values, as demonstrated in [40]. For higher values of  $k$ , the resulting optimal structure presents a lower mass, since there is a higher metabolic cost to the organism for maintaining bone tissue. This is because bone tissue must receive a constant vascular supply to keep its cells viable. So, as a result, the existence of bone mass represents an energy drain to the organism [40].

It is known that bone remodeling is a complex process and its response is different for each individual, even in the presence of identical loading conditions. Therefore, the parameter  $k$  includes biological factors, such as age, hormonal status, disease, and so on. As such, determination of precise values of  $k$  for a given individual is quite difficult [43, 63]. To determine  $k$  in a specific instance is necessary the simultaneous knowledge of equilibrium bone mass and mechanical loading. However, the extreme variability in the biological factors known to influence bone remodeling equilibrium turns this approach beyond the current state of knowledge [40, 63].

For the resolution of the optimization problem formulated by equations (1-3) is used a Lagrangian method. The law of bone remodeling results from the stationarity condition of the Lagrangian method with respect to the design variable  $\mathbf{a}$ , and is stated by the optimal condition:

$$\sum_{P=1}^{NC} (-\alpha^P) \frac{\partial E_{ijkl}^H}{\partial \mathbf{a}} e_{kl}(\mathbf{u}^P) e_{ij}(\mathbf{v}^P) + k \frac{\partial \mu}{\partial \mathbf{a}} = 0 \quad (4)$$

where  $\mathbf{u}^P$  is the displacement field at equilibrium [43].

The law of bone remodeling expressed by Eq. (4) is solved by a suitable numerical procedure, that will be presented next, giving as a result the distribution of bone density. It would be convenient to remark that, although the bone remodeling model assumes a global optimization criterion, the optimal conditions leads to a local remodeling rule [43].

## 2.4. Computational model

Computationally, the model is described by the following steps: initially, the homogenized elastic properties are computed for an initial solution ( $\mathbf{a}_0$ ). Then, the set of displacement field,  $\mathbf{u}^P$ , are calculated by finite element method using software ABAQUS®, according to the mechanical solicitation, solution of equilibrium equations (2) and (3). Based on the displacement field finite element approximation, the necessary optimality condition, i.e., the stationary condition presented in Eq. (4), is checked. If satisfied (equal to zero) the process stops which means that no remodeling will occur (remodeling equilibrium – resorption and formation are balanced). This corresponds to the solution of the problem, which is the optimal distribution of bone density. In other words, this is the stiffest bone relative density distribution for the given loads, taking into account the cost parameter  $k$  [58, 63]. If the stationary condition is not satisfied, improved values of the design variables  $\mathbf{a}$  are computed (as described below Eq. (5)) and the process restarts. So, the iterative process continues and the model will evolve in order to find the solution of the problem [43, 58]. This process ends only when the condition presented in Eq. (4) is satisfied. The flowchart of the process is shown in Figure 2.3.

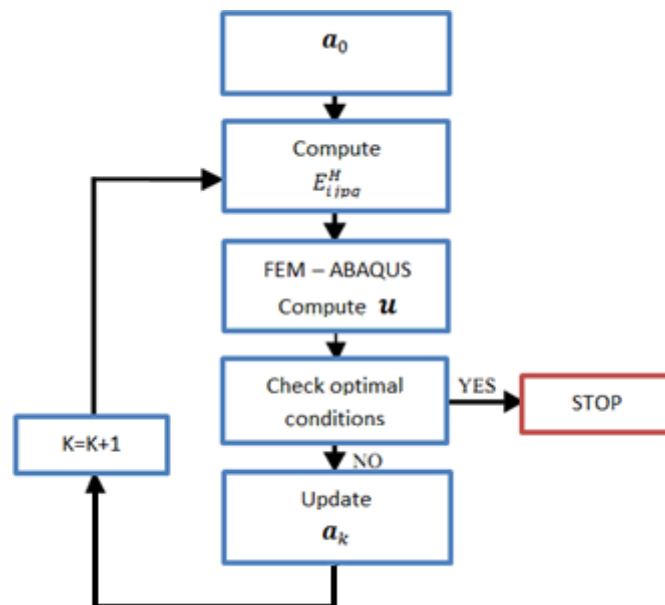


Figure 2.3 – Flowchart for the computational model procedure, adapted from [58].

This procedure assumes that the design variables  $a_i$  are interpolated at the nodes. Thus, the iterative process updates the values of relative density on each node, in other words, it updates the cell design variables at the  $K^{\text{th}}$  iteration by using the following formula:

$$(a_i)_{K+1} = \begin{cases} \max[(1 - \zeta)(a_i)_K, 0] , & \text{if } (a_i)_K + d(D_i)_K \leq \max[(1 - \zeta)(a_i)_K, 0] \\ (a_i)_K + d(D_i)_K & , \text{if } \max[(1 - \zeta)(a_i)_K, 0] \leq (a_i)_K + d(D_i)_K \leq \min[(1 + \zeta)(a_i)_K, 1] \\ \min[(1 + \zeta)(a_i)_K, 1] , & \text{if } \min[(1 + \zeta)(a_i)_K, 1] \leq (a_i)_K + d(D_i)_K \end{cases} \quad (5)$$

where the new value of  $a_i$ , is updated based on the previous value  $(a_i)_K$  and a step of length ' $d$ ' and direction  $D_K$ . This descent direction is given by the negative of the Lagrangian gradient with respect to the design variables  $a_i$ :

$$D_i = \sum_{P=1}^{NC} \alpha^P \frac{\partial E_{ijmn}^H}{\partial a_i} e_{mn}(\mathbf{u}^P) e_{ij}(\mathbf{v}^P) - k \frac{\partial \mu}{\partial a_i} \quad (6)$$

i.e.,  $D_i$  represents the component of the direction vector  $\mathbf{D}$  for the design variable  $a_i$  (component of hole dimension  $i$  for each node) [43, 58, 66]. The parameter  $\zeta > 0$  constrains the changes in density to small transitions between iterations, allowing a smoother iterative process.

In summary, this chapter explained a model based on optimization strategies to computationally simulate the bone adaptation process modulated by mechanical forces, that was motivated by the original ideas of Wolff and others. In practical terms, this model takes into account the relationship between mechanical loads and metabolic activities that is directly related to bone architecture and, consequently, to the process of bone remodeling. To do so, it was necessary the integrated knowledge of different fields of research, such as mechanical engineering, orthopedics and cell biology.

The computational model utilized in this work has been quite successful in predicting naturally occurring bone morphologies (density distribution profiles), enhancing our understanding of the characteristics of the underlying biological mechanisms. This model is also important to predict bone adaptation resulting from orthopedic interventions and to predict the phenomena associated with the implantation of prosthesis, such as stress-shielding [63]. In other words, it enables to investigate the morphological consequences of alternative loading conditions. Therefore, it is a very useful tool to understand the biomechanical processes in human body, in particular bone mechanics (bone behaviour as an adaptive structure) and prosthesis design. Furthermore, this model not only permits the development of consistent mechanical and mathematical model for bone remodeling, but it also gives an important contribution in the identification of the respective stimulus [63]. Hence, it has the potential to become a viable tool for pre-clinical testing of prostheses, with the advantage of a limited amount of *in vivo* experiments [38].

### **3. Adopted methodology – computational modeling**

In this chapter the steps followed to create a three-dimensional solid model of the tibia and the tibial components of the TKA implant are described and analyzed. These models then allowed the simulation of orthopedic surgeries with the incorporation of three different TKA constructs (standard, cemented and press-fit) into the bone. Then, these models undergo to a sequential set of steps with different techniques and objectives, in order to build and discretize these models into finite elements. Thereafter, integrating the finite element (FE) method with a numerical simulation of the process of bone adaptation is possible to obtain the distribution of the bone density in the modeled tibia that is the solution of the process of bone remodeling.

The 3-D anatomical model of intact bone (tibia) was generated by a geometric modeling pipeline that receives as input medical images and gives as output 3-D geometric models, such as solid models that are suitable to generate finite element meshes and, consequently, FE analysis (see Figure 3.1). This pipeline is constituted by several image and geometric processing blocks connected in a sequential manner, such as: image acquisition, image segmentation, surface mesh adjustments and solid model generation. For that, it utilizes the ITK-SNAP (version 2.1, 2010), ParaView (version 3.10.0) and SolidWorks® (version SP0, 2010) software. All the other geometric modeling work (three dimensional models of the prostheses and their assembly) were also obtained by using SolidWorks®, a 3D CAD program. After the geometric modeling part, it was used a program for finite element analysis – ABAQUS® (version 6.10-1, 2010) – that allowed for: the assignment of mechanical properties to the materials, contact formulation, application of loads and boundary conditions and mesh generation. The final step was the submission of the job of FE software to the iterative program of bone remodeling that will interact with ABAQUS®. Moreover, it was also necessary to determine the biological cost parameter,  $k$ , as it will be explained later. All these steps mentioned above are required to obtain the solution of the process of bone remodeling.

Throughout this chapter, the steps involved and all the choices made in the processes of geometric modeling, finite element analysis and bone remodeling, are thoroughly explained. At the end, the result analysis method is also presented.

#### **3.1. Geometric modeling**

##### **3.1.1. Geometric modeling of intact bone – tibia**

In this section, the blocks that constitute the geometric modeling software pipeline are described (see Figure 3.1). This consists on a cascade of computational and digital image operations that using as input an ordered stack of medical images, gives as output the solid model of the left tibia (digital equivalent to the real human tibia). This way, it enables the construction of accurate 3-D anatomical model of tibial bone, which is suitable to generate the FE mesh, required for the study of several bioengineering problems, such as bone remodeling and stress analysis. The list of software employed is also illustrated; the majority of them is non-

commercial (open source freeware, easily accessible on the internet) – ITK-SNAP and ParaView –, and commercial software, commonly available in most academic communities – SolidWorks®.

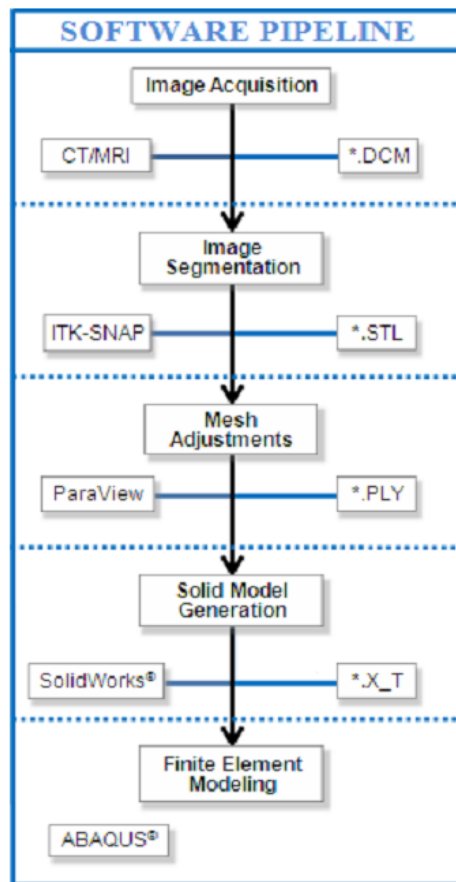


Figure 3.1 – Diagram of the geometric modeling pipeline that was used to model an anatomical structure – left tibia. The boxes in the left column concern to the software tools and the right column boxes indicate the data file extension [67].

### Image Acquisition

First of all, to generate the solid model of intact tibia it was necessary to acquire medical images that reveal the inner parts of the human body, containing the geometrical information of the biological tissue of interest. For bone modeling it was selected the CT imaging method which is more suitable for orthopaedic applications, since hard tissue has a high contrast signal relative to soft tissue.

The CT images (from 2004) of a whole body of a 43-year-old male subject, without any local degeneration (healthy), were acquired from Osirix database<sup>1</sup>. From this data were selected only the slices that represent the lower limbs, between the distal part of the femur and the middle of tibia diaphysis. After, the medical images were imported to the ITK-SNAP software, where a ROI (region of interest) that includes only the region that corresponds to the left limb was defined. Thus, it works with less information, but the necessary one for modeling the

<sup>1</sup> <http://pubimage.hcuge.ch:8080/>

proximal left tibia, without great computational cost. Note that these medical images have high spatial resolution and tissue contrast allowing building accurate 3-D anatomical model of the left tibia.

## **Image Segmentation**

The next step of the geometric modeling pipeline is called image segmentation, which can be defined as a partition of an image into non-overlapping regions, in which each region is the locus of an object. In medical imaging applications, segmentation facilitates the delineation of anatomical structures, i.e., it allows the delimitation of a certain region of interest based on a specific image feature, like intensity (that is homogeneous within this region), allowing the identification of the tissues and their boundaries [67].

Segmentation plays a crucial role in the designed pipeline as it establishes the transition between image data and 3-D mesh data, i.e., its goal is the determination of (x,y,z) volume coordinates where tissue of interest is presented. To solve the bone segmentation problem three techniques were used in conjunction [67, 68]:

- global thresholding;
- active contour method;
- manual segmentation.

Global thresholding consists of selecting the intensities that identify a tissue (foreground – pixels of interest) and cancel all the other values (background – non-interesting pixels), estimating this way the region occupied by the anatomical structure. This technique can be performed as a point processing operation changing each voxel value according to a function that maps the original intensities (Hounsfield values) to new values, i.e., reallocates the original gray levels to new gray intervals. This mapping is also called intensity region filter and transforms the histogram domain to the -1 to 1 interval values of the thresholded image (where the background and foreground pixels correspond, respectively, to the lower and upper extremities), enhancing the contrast. Thus, by partitioning an image into regions according to the voxel intensity value, it usually results into a coarse but overall segmented object (as it can be seen in Figure 3.2). This happens because an anatomical structure is practically characterized by its CT number (gray level). Global thresholding constitutes a necessary pre-processing stage for the application of active contour method [67, 68].

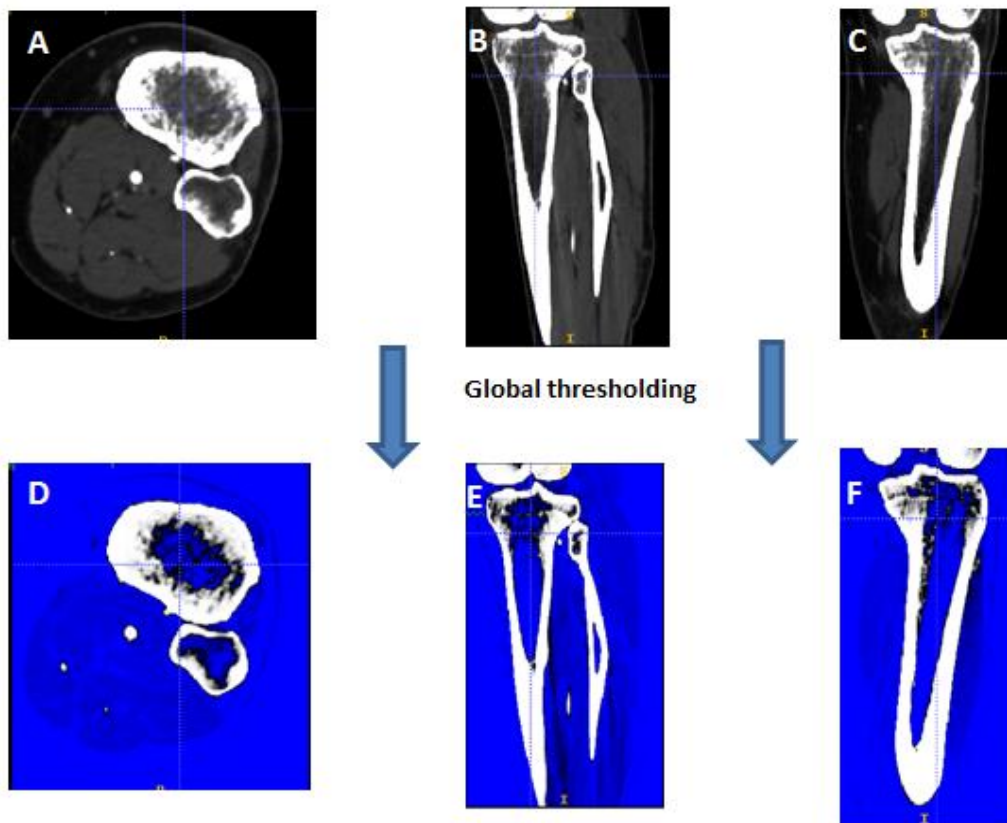
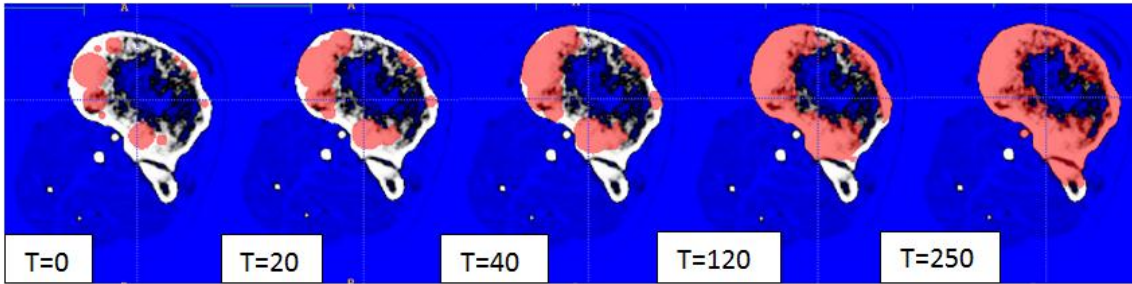


Figure 3.2 – Sections of the left tibia. A, B, C – Original CT images: transversal, sagittal and frontal sections, respectively; D, E, F – Respective segmented CT images with global thresholding.

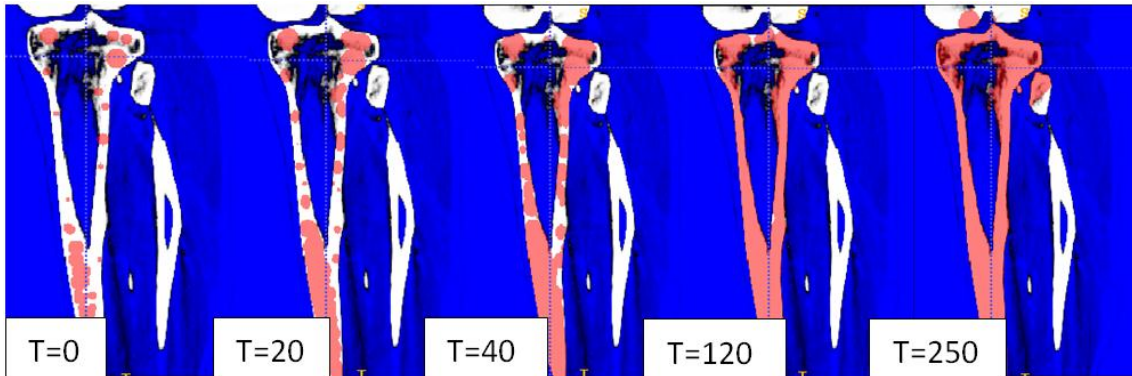
The active contour method is a semi-automatic approach based on deformable surfaces with physical properties that, under the influence of internal and external mechanical forces, deforms adapting to image features (e.g. contours), leading the model to adjust to the object boundaries. At an initial stage the tissue to be modeled can be outlined by placing an initial set of closed surfaces, such as spherical surfaces, in the proximity of the region of interest. Thus, the contour initialization is nothing but a rough estimate of the anatomical structure of interest (see Figure 3.3 for  $T=0$ ). The deformation process evolves as an iterative process where it is calculated, for every point of the image at each iteration  $T$ , the internal force and the external force based on the difference between the probability of a voxel belonging to the foreground or to the background. The voxel probability maps derive from the previously described intensity region filter. The process stops when the deformable surfaces enclosure all the voxels with greater probability value or until the user finds a suitable solution [67, 68].

The iterative process of deformable surfaces evolution is represented in Figure 3.3, where  $T=0$  shows a very rough estimate of the left tibia (contour initialization) and  $T = 120$  represents a very close approximation to the anatomical structure. For  $T = 250$  the process outpaced the contour limits of the tibia and already encompasses regions, such as distal femur and proximal fibula, which are not intended. As it can be seen, the iteration that corresponds to the closest approximation of the intact tibia is for  $T=120$ . So, this was the one selected to continue the rest of the process.

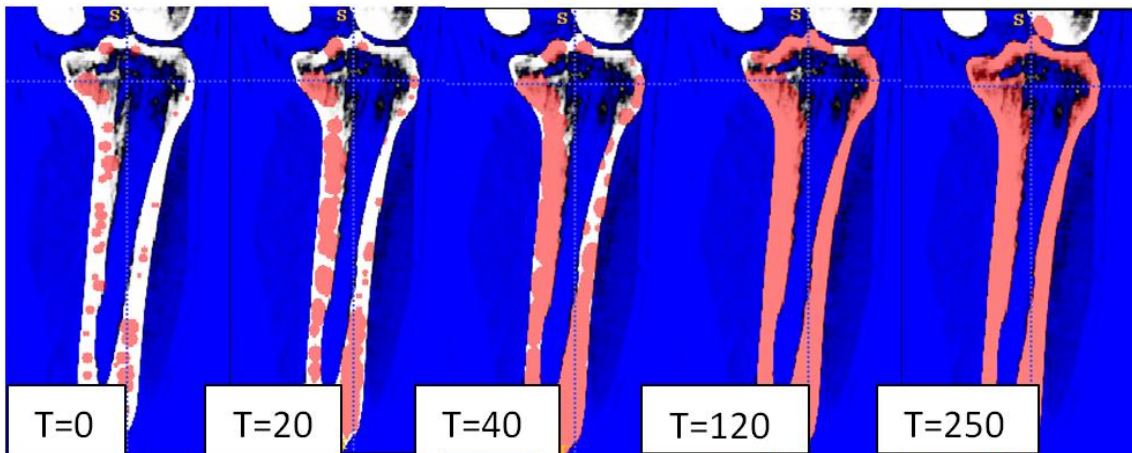
**A. Transversal section**



**B. Sagittal section**



**C. Frontal section**



**D. 3-D evolution**

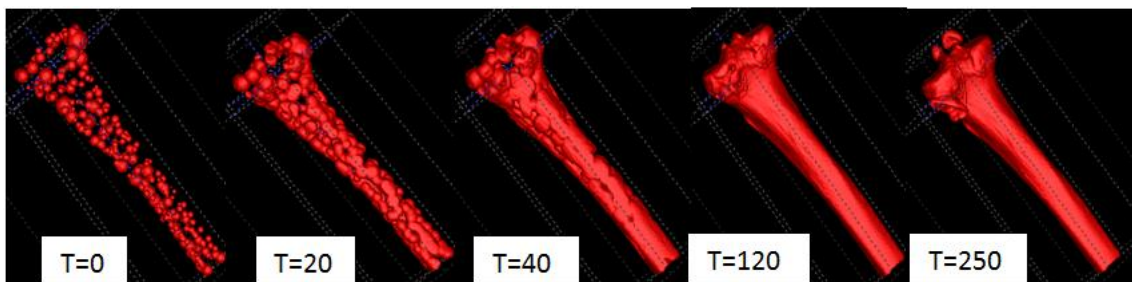


Figure 3.3 – A, B, C – Iterative process of 2-D deformable surfaces evolution in different time instants (transversal, sagittal and frontal sections of the segmented image data, respectively); D – Iterative process of 3-D deformable surfaces evolution in different time instants.

The obtained result by the active contour method (for  $T=120$ ) is not totally accurate due to segmentation errors, since you can see certain regions of the bone that are not selected as such, for e.g. at the epiphysis of the tibia, where cortical bone is thin, so the intensity signal is poorer and closer to soft tissue values, consisting in a boundary discontinuity. Another example of this type of error is in the proximal region of the intramedullary canal (region filled by trabecular bone with low density of trabeculae and other tissues, which is situated in the middle of the diaphysis of the long bones). In order to correct such errors and to improve the accuracy of this process, it was necessary to proceed to manual segmentation.

In manual segmentation procedure, the user must have a priori anatomical knowledge of the structure to be modeled to perceive the acquired data (see in chapter 1 the anatomical structure of the tibia) and keen visual capabilities, selecting manually the points of interest and rejecting those which are non-interesting points (see Figure 3.4). Therefore, segmentation operation is the most time consuming stage of the pipeline and demands cooperation with a physician. Through this process, it was also identified a region of low density in the center of tibia diaphysis that corresponds to the intramedullary canal, so it was modeled too.

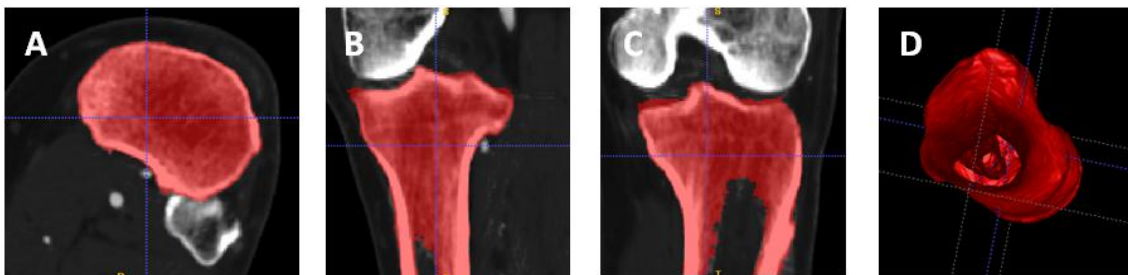


Figure 3.4 – A, B, C – Sections of the left tibia, corrected by manual segmentation (transversal, sagittal and frontal sections, respectively); D – 3-D surface model of the tibia.

The output of the segmentation stage is a binary volume, i.e., each voxel is either 0 or 1, containing the anatomical structure of interest in a voxelized format. ITK-SNAP automatically generates a 3-D surface mesh of the segmented data using the marching cubes algorithm, a technique that creates a triangular surface mesh from a volume scalar field. Figure 3.5 A. presents the 3-D surface mesh of the left tibia that is the output of the segmented data (final result of the segmentation stage).

The surface model generated by the segmentation stage is then exported to the next block of the pipeline that is assured by another open source freeware (ParaView) which is responsible for the surface mesh adjustments.

### Surface Mesh Adjustments

The model created by the output of the segmentation stage (Figure 3.5 A.) presents two characteristics that require careful consideration: a stair-step shape surface, which does not correspond to the natural surface curvature and an excess of nodes and facets that expresses irrelevant information for the future computational processes or numerical simulations,

enhancing the computational cost. In order to surpass these undesired features, it was used the smoothing and decimation techniques, allowing the respective mesh adjustments.

Firstly, the surface model of the tibia, which is strongly corrupted by jagged or step-like artifacts, produced by the reconstruction algorithm, is smoothed by a low-pass filter, called Laplacian filter. This filter changes the node's positions relatively to each other without modifying the mesh topology, thus improving the surface mesh appearance and attenuating the unwanted geometric features (see Figure 3.5 B.).

Then, as this model exhibited excess of nodes and facets, it was submitted to a decimation operation. This mesh simplification technique is an iterative process that reduces the total number of nodes at each step, until the reduction percentage of nodes is reached. The percentage of nodes to be eliminated is user specified; usually it is very high, in between 50-90% [67]. In this case, the node removal percentage was of 75% (see Figure 3.5 C.). The resulting mesh is a good approximation to the original tibia geometry, although it has a lower surface resolution.

Finally, to remove decimation artifacts the smoothed-decimated mesh was smoothed again – Figure 3.5 D.

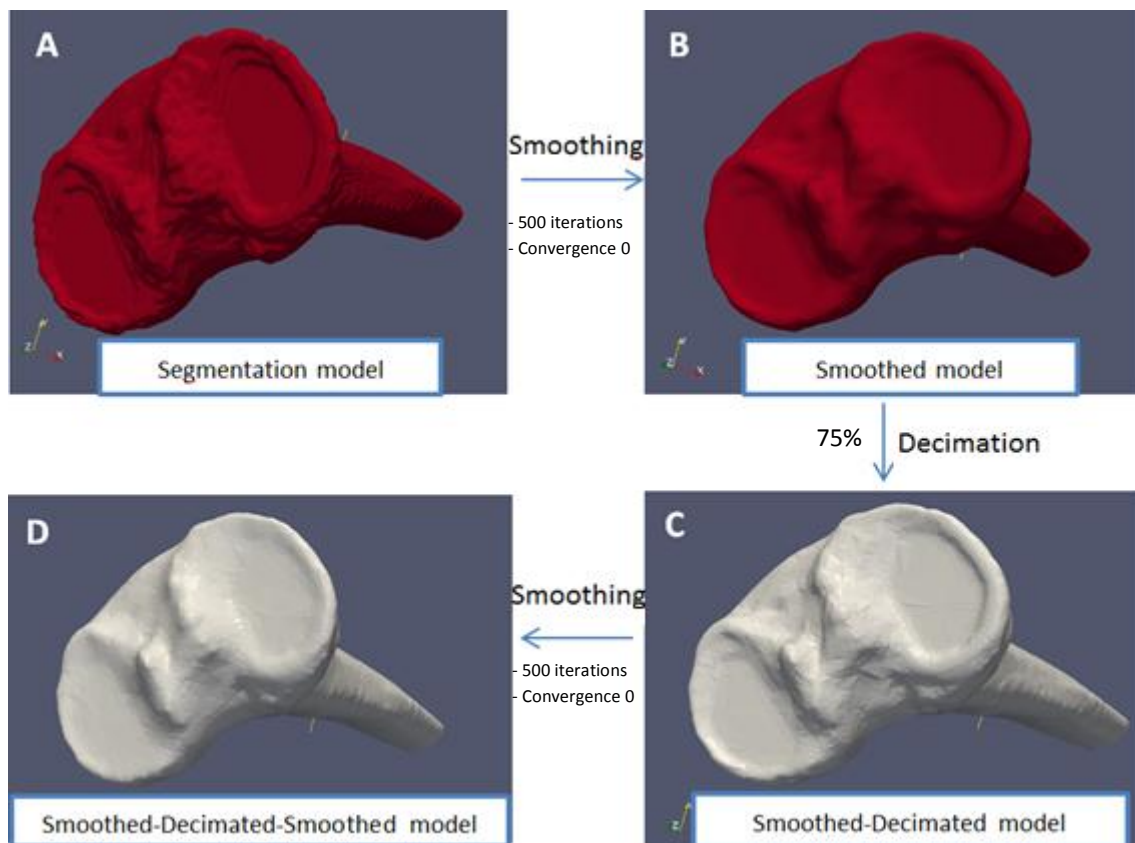


Figure 3.5 – Process of 3-D surface mesh adjustments of the left tibia, in which the surface is first smoothed then decimated and smoothed again: A – Segmentation model; B – Smoothed model; C – Smoothed-decimated model; D - Smoothed-decimated-smoothed model of the surface model A (that results from the segmentation stage).

The surface meshes that result from this surface mesh adjustments techniques (smooth and decimate procedures), are represented in Figure 3.5 D. and Figure 3.6. This model is suitable to generate solid models of the anatomical geometry of the proximal tibia.

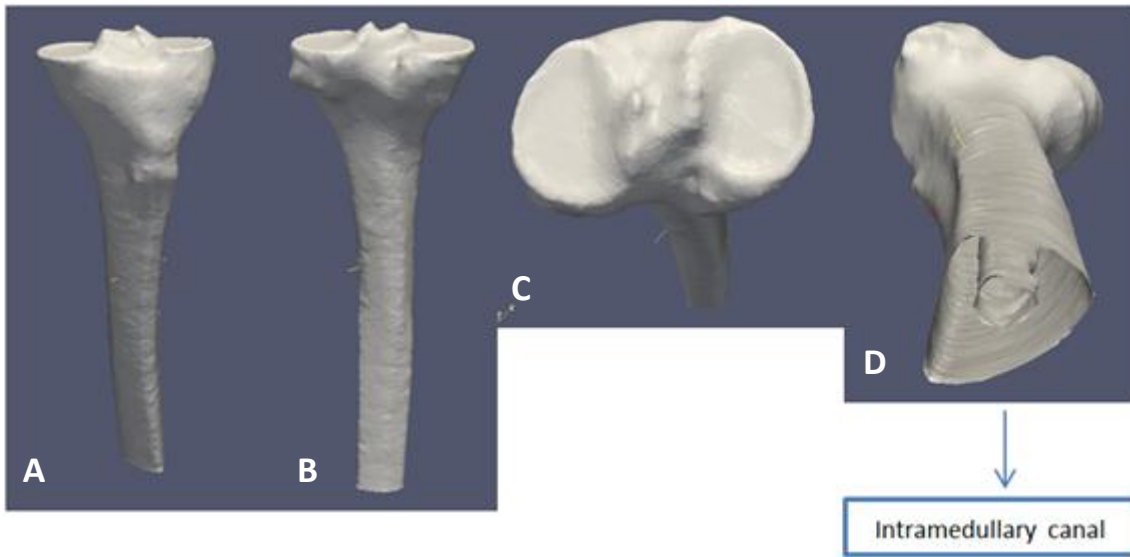


Figure 3.6 – Smoothed-decimated-smoothed meshes of the surface model that appears in Figure 3.1e A. (final result of the surface mesh adjustments stage): A – Anterior view; B – Posterior view; C – Superior view; D – Inferior view of the surface mesh of the left tibia.

### Solid Model Generation

In this step of the pipeline, it was used the commercial software SolidWorks® that includes the ScanTo3D® toolbox which automatically creates the solid model based on the user-defined amount of patch detail, i.e., based on the number of superficial mesh elements defined.

Figure 3.7 presents the two solid models of the proximal left tibia (intact bone) generated from the surface mesh presented in Figure 3.6. The first, on the left (A), without the intramedullary canal – designated by tibia uniform – and the second, on the right (B), with the approximated modulation of the intramedullary canal, which was modeled during the segmentation stage of the pipeline, as stated above – called tibia canal.

The obtained solid models based on a real bone are easily imported to a FE software, e.g. ABAQUS®, and readily prompt for FE tetrahedral or hexahedral mesh generation, which can be used for further computer simulations, especially in the field of biomechanics, as will be seen in next sub-chapter (3.2). For future simulations it will be utilized the “tibia uniform” model.

It should be noted that the reasons to modeling only half of the tibia, i.e., not modeling the distal end of the bone, are: to facilitate the movement constraint at the numerical simulation stage, take less time to model than the complete bone (easier) and generate a lower number of FE (for a particular level of discretization) and, so less computational cost. Furthermore, the changes on bone adaptation due to the placement of prostheses occur mainly in bone areas adjacent to the implant.

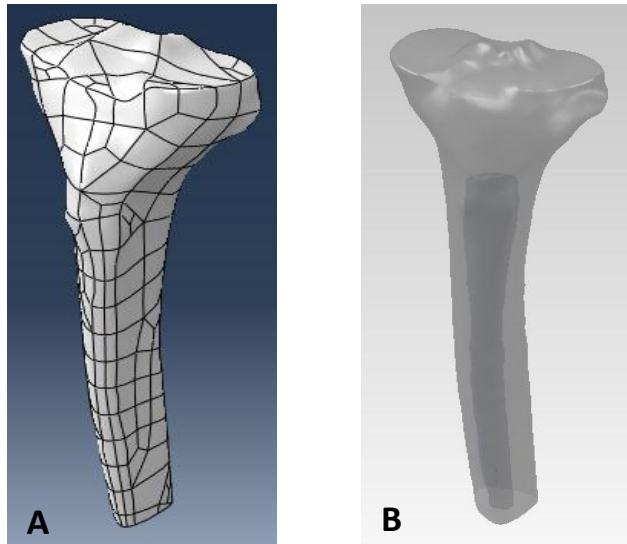


Figure 3.7 – Solid models of the left tibia generated from the surface mesh in Figure 3.6: A - Without the intramedullary canal – tibia uniform – (the edges represent a superficial mesh automatically generated in SolidWorks®); B - With the modulation of the intramedullary canal – tibia canal.

### 3.1.2. Geometric modeling of prostheses – tibial components

After the modeling of the proximal left tibia, the solid models of the tibial components of TKA prostheses were developed, based on real models and with the support of the P.F.C.® Sigma Knee System: Technical Monograph [50]. This modeling work was done using SolidWorks® software.

These are the tibial components that are intended to model and study:

- P.F.C.® Sigma Stabilized Insert – Figure 3.8;
- P.F.C.® Modular Tibial Tray (size 2) – Figure 3.9;
- P.F.C.® Sigma Modular Stem Attachment (standard, cemented and press-fit)–Figure 3.10;

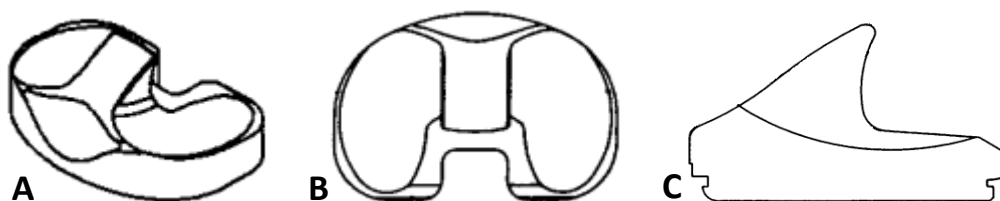


Figure 3.8 – P.F.C.® Sigma Stabilized Insert (with a cruciate-substituting design – posterior stabilized): A – Isometric view; B – Top view; C – Lateral view [50].

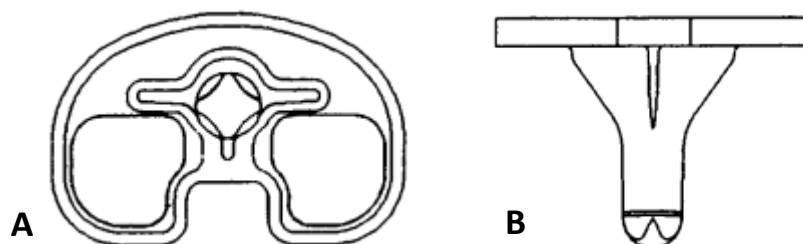


Figure 3.9 – P.F.C.® Modular Tibial Tray (size 2) with the standard configuration: A – Inferior view; B – Posterior view [50].

The P.F.C.<sup>®</sup> Modular Tibial Tray accept various configurations of tibial stems that have different lengths and fixation methods (cemented/ non-cemented). Usually, shorter stems are used in primary TKA surgery (standard configuration – Figure 3.9 and Figure 3.10 A), where a removable distal stem plug is located in the distal tip of the modular tray, while revision surgery may require longer stems [53]. These stem extensions can be coated with a cement mantle – cemented stem – (Figure 3.10 B) or be press-fitted against the bony surfaces – press-fit stem (Figure 3.10 C). These three configurations are given below.

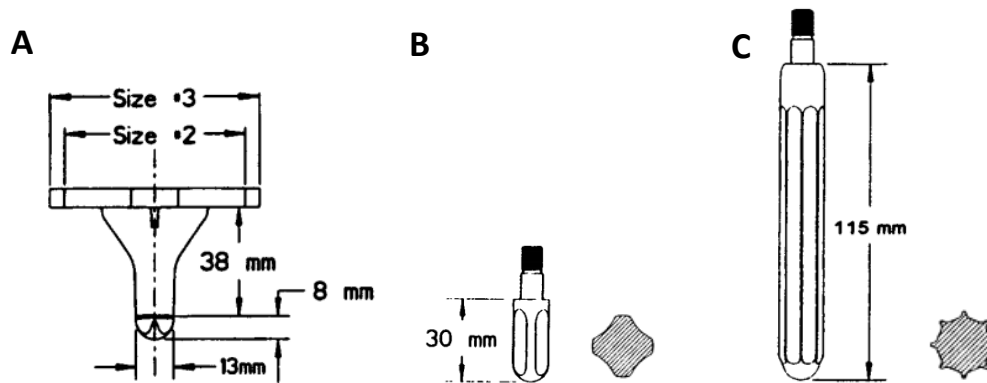


Figure 3.10 – P.F.C.<sup>®</sup> Sigma Modular Stem Attachment: A – Tibial tray with standard configuration – posterior view; B – Cement stem (13 mm diameter and 30 mm length) - posterior and bottom view; C – Press-fit stem (14 mm diameter and 115 mm length) - posterior and bottom view [50].

Each of these tibial components is also offered in a wide range of length and diameter combinations to allow the surgeon to appropriately size the modular component assembly for each patient. These options maximize the customizing of the implant to the patient and are essential to the success of the arthroplasty [50].

The tibial components geometries of the TKA system, specifically the tibial insert, tibial tray and press-fit stem were kindly provided by Ângela Chan, unmeshed. They were modeled according to the P.F.C.<sup>®</sup> Sigma Knee System: Technical Monograph of DePuy [50] and based on real models. This modeling work was done with the appropriate tools of SolidWorks<sup>®</sup>. To know more about how they were modeled, consult [69]. These final solid models are presented next.

The polyethylene tibial insert solid model is shown in Figure 3.11.

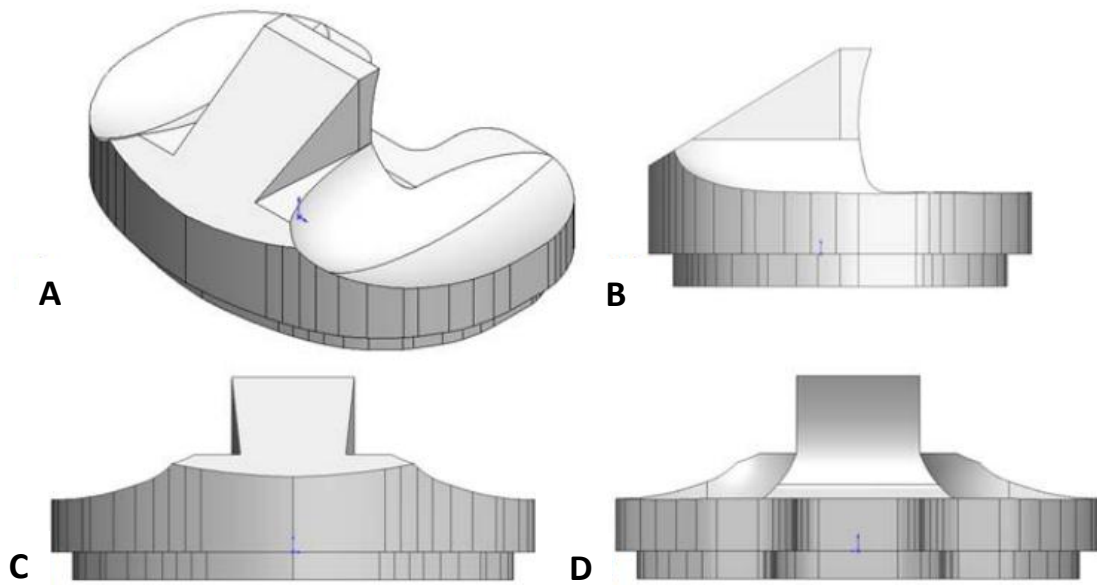


Figure 3.11 – Stabilized insert: A – Isometric view; B – Sagittal view; C – Anterior view; D – Posterior view [69].

The solid model of tibial tray, which is made of metal alloy based on titanium, is presented in Figure 3.12.

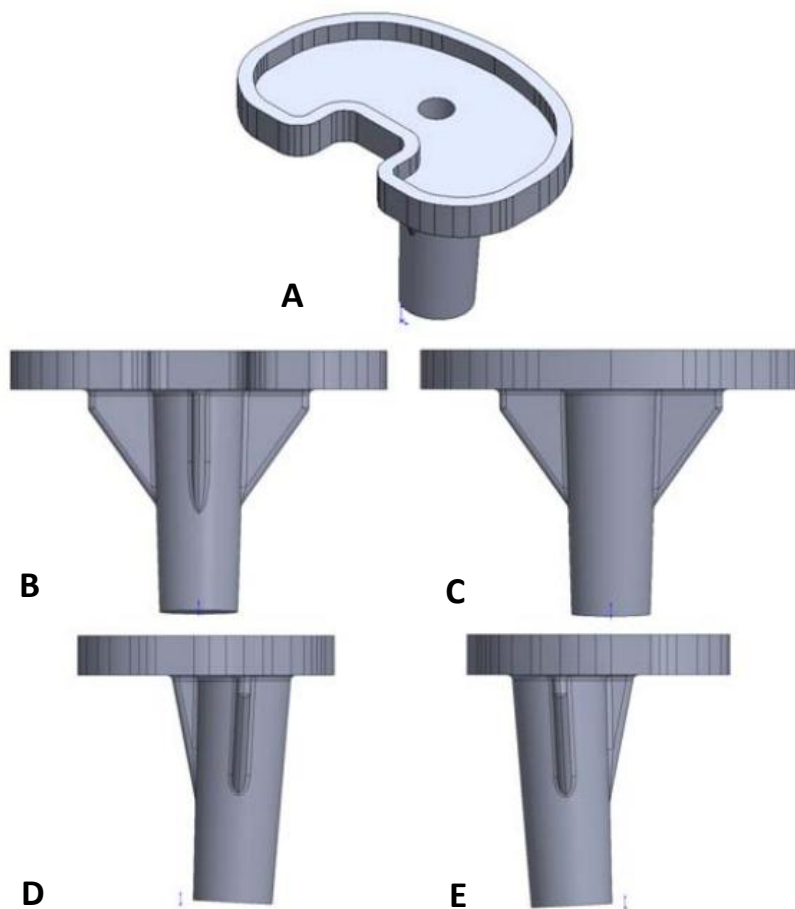


Figure 3.12 – Modular Tibial Tray: A - Isometric view; B - Posterior view; C - Anterior view; D - Left sagittal view; E - Right sagittal view [69].

The solid models of the tibial stems, standard (made of polyethylene), cemented and press-fit (both made of titanium based alloy) are shown in Figure 3.13.

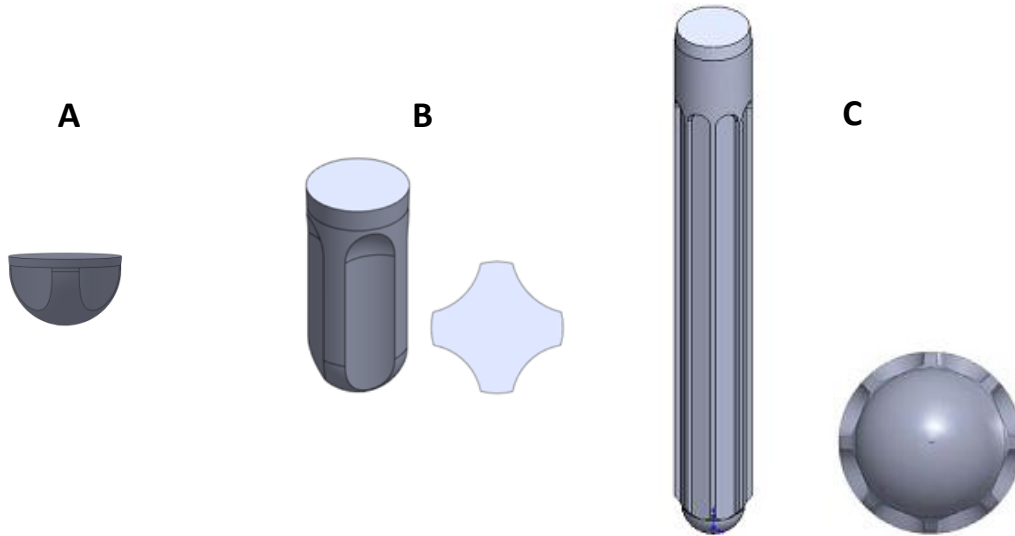


Figure 3.13 – Modular Stem Attachment: A - Sagittal view of standard configuration, B and C – Isometric and bottom view of cemented (30 mm length) and press-fit (115 mm length) stems, respectively.

Once all the tibial components have been modeled, the final step was to assemble them. The assembly final results for: standard, cemented and press-fit configurations are presented next in Figure 3.14, 3.15 and 3.16, respectively. To do so it was used SolidWorks' available tools, such as mate, which allows the optimal adjustment between the components from the definition of the surfaces and edges that will be in contact. To simplify the complexity of the 3D assembled model, the stem attachment and the tibial trays were combined into one unique piece (except for the standard design, in which the stem is made of a different material from the tibial tray).

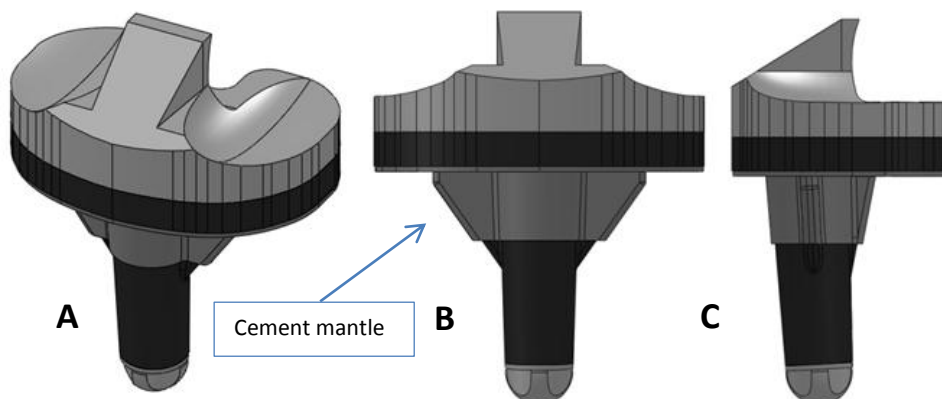


Figure 3.14 – Tibial components of TKA prostheses with the standard configuration (stabilized insert, tibial tray, standard stem and cement in superior third of the tibial tray with about 1 mm thickness): A – Isometric view; B – Anterior view; C – Sagittal view.

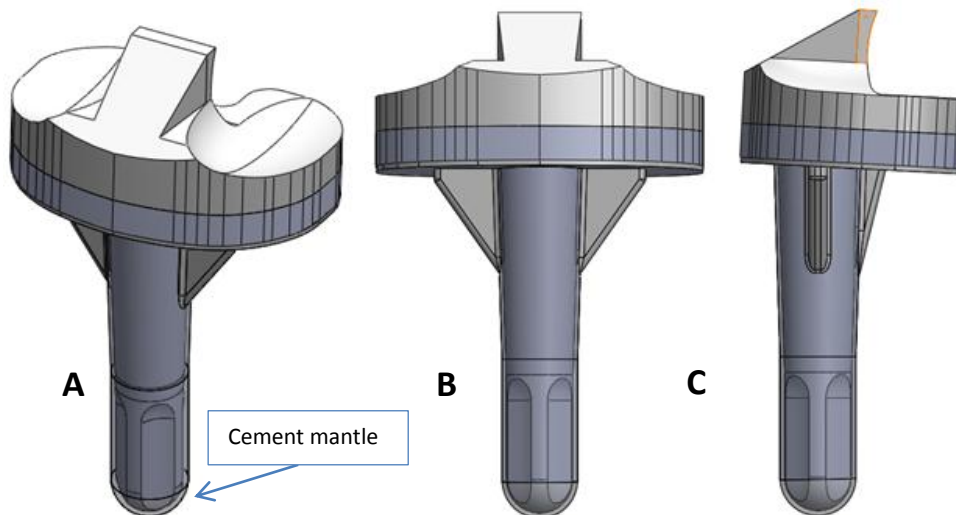


Figure 3.15 – Tibial components of TKA prostheses with the cemented configuration (stabilized insert, tibial tray, cemented stem (with 30 mm) and cement involving the entire tibial tray and stem that will contact with cut bone, with about 1 mm thickness): A – Isometric view; B – Anterior view; C – Sagittal view.

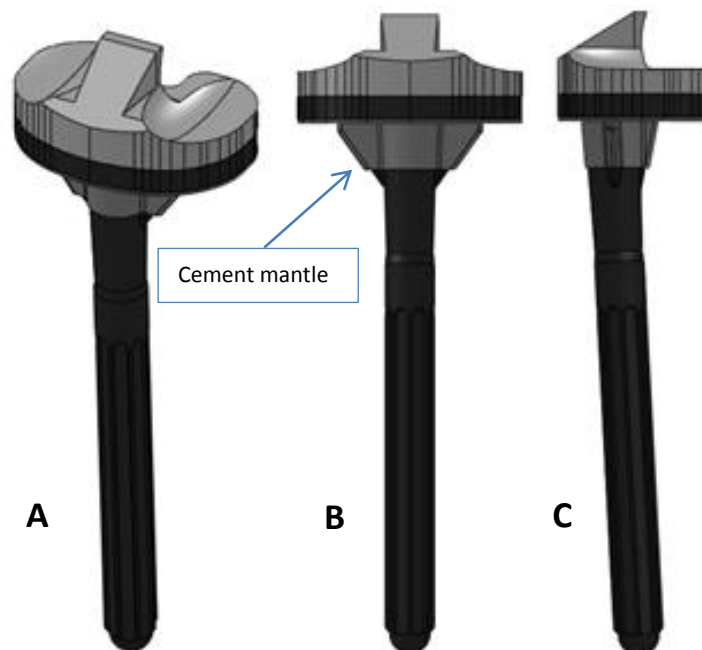


Figure 3.16 – Tibial components of TKA prostheses with the press-fit configuration (stabilized insert, tibial tray, press-fit stem (with 115 mm) and cement in superior third of the tibial tray with about 1 mm thickness): A – Isometric view; B – Anterior view; C – Sagittal view.

To assure an optimal mechanical fixation of the components to the bone, cement was used under the tibial tray. In the case of the standard and the press-fit model, the bone cement involves the superior third of the tibial tray's keel, the undersurface of the tray and the metaphyseal region [70]. Whereas, on the cemented configuration the bone cement involves the entire tray and the stem too. Thus, cement mantles with about 1 mm thickness were modeled for the three cases in study (the standard and press-fit are equal). For reasons of visualization, these cement mantles that are placed in the middle of the cut bone/implant

interface during the surgical process are also illustrated in these models (Figure 3.14, 3.15 and 3.16).

### 3.1.3. Geometric modeling of bone with prostheses – surgical procedure, assembly

At this stage, the intention is to build the models in which the anatomical distal articular surface of the knee joint is substituted by artificial components that are fixed in place. In order to assemble the tibial components of the TKA prostheses into the intact bone, it was necessary to make some changes to the bone. First, considering the prostheses components size, the bone model needed to be rescaled (scale value 0,8). This way, later in the assembly phase it provides an optimal adjustment between the considered structures. Thereafter, changes that were made on bone are only related with the surgical process (presented in chapter 1) and are presented below.

To begin the virtual surgery, the proximal end of tibia was resected at 90° to its mechanical axis with a level of about 10 mm based on the less involved condyle (see Figure 3.17). Then, the bone was accurately cut into a shape that matches the corresponding surface of tibial components, using cutting tools of the SolidWorks®.

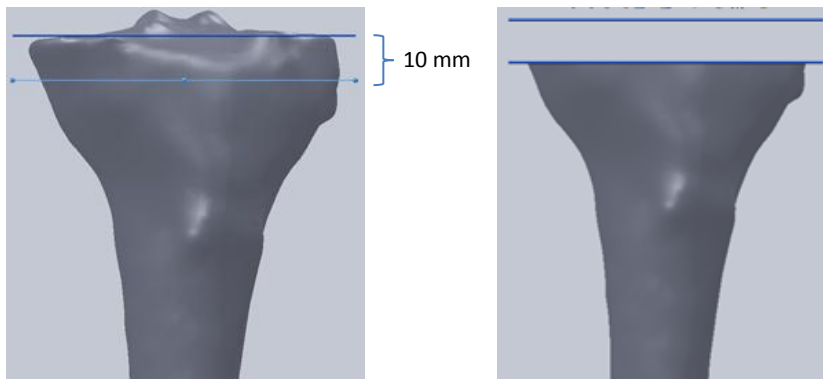


Figure 3.17 – Anterior view of the first stage of surgical procedure: A – Intact bone; B - Resected tibia, with a cut at 90° to its mechanical axis with a level of about 10 mm based on the less involved condyle.

The last stage was to incorporate the assembled tibial components, for standard, cemented and press-fit configurations, into the bone with the accurate component alignment concern. The assembly results of all 3D models are shown in Figure 3.18, 3.19 and 3.20, respectively.

All these procedures were performed according to the clinical protocol, presented in the introduction chapter (1.4.4), which is in consonance with the surgical technique manual [51], and with what was advised by Dr. João Gamelas (experienced orthopedic surgeon, co-adviser of this work).

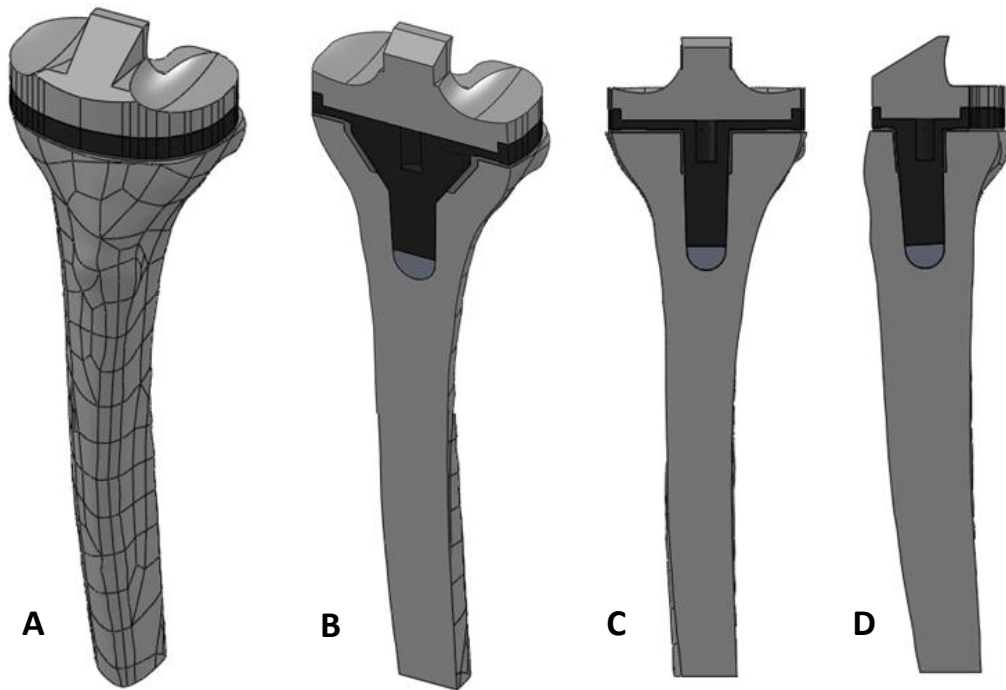


Figure 3.18 – Final assembly of the standard configuration: A – Isometric view; B – Frontal section, isometric view; C – Frontal section, anterior view; D – Lateral section, right sagittal view.

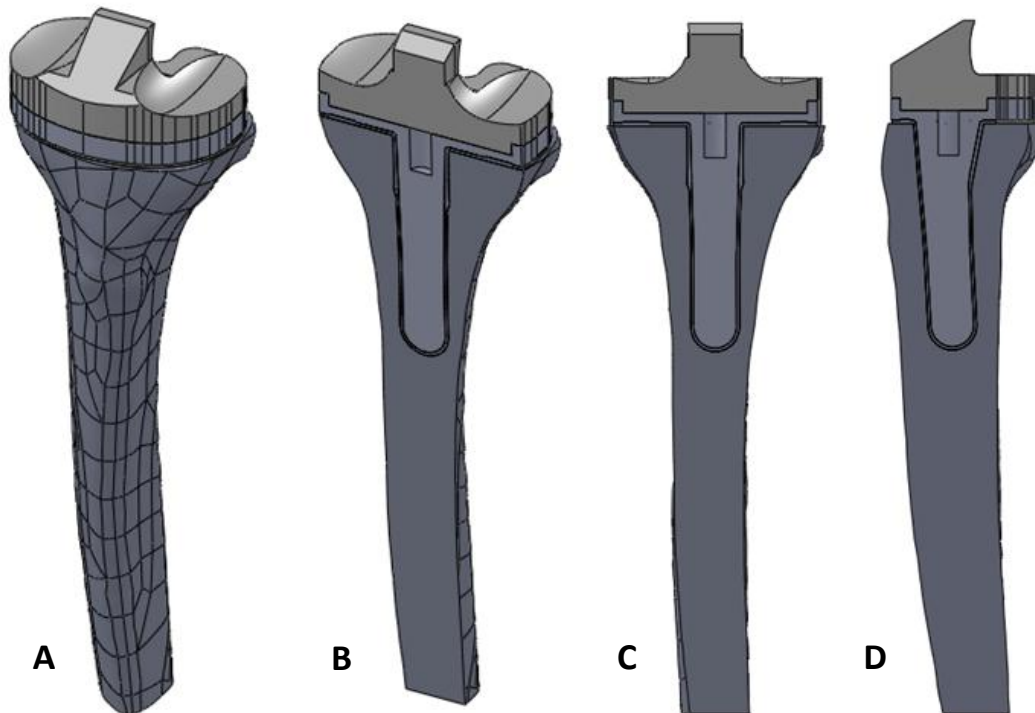


Figure 3.19 – Final assembly of the cemented configuration: A – Isometric view; B – Frontal section, isometric view; C – Frontal section, anterior view; D – Lateral section, right sagittal view.

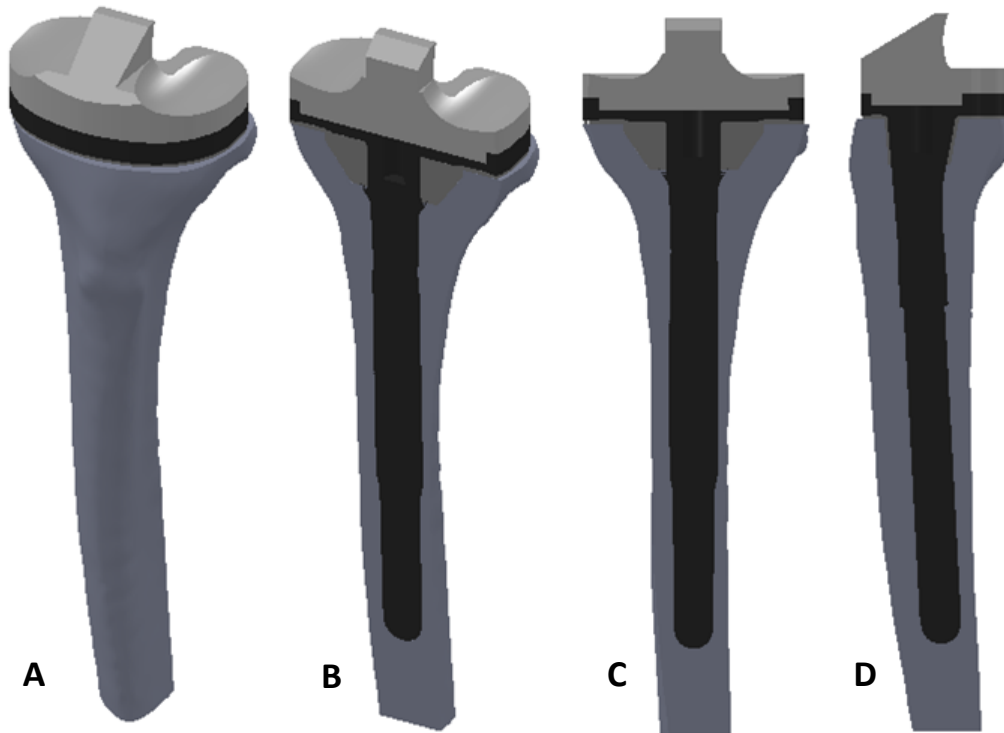


Figure 3.20 – Final assembly of the press-fit configuration: A – Isometric view; B – Frontal section, isometric view; C – Frontal section, anterior view; D – Lateral section, right sagittal view.

### 3.2. Finite element method – FEM

To perform the simulation of bone adaptation in a computational model, it is necessary to have a mathematical description of the process/phenomena (as seen in chapter 2) combined with the finite element method (FEM). The FEM is a powerful numerical technique that is used to solve real problems, e.g. orthopaedic biomechanics, that involve complicated domains (both geometry and material constitution), loads, and which are governed by equations (mathematical models) and a set of boundary conditions that are often difficult to solve and forbid the development of analytical solutions.

The main idea behind this method is the representation of the domain of the problem by smaller and simple subdomains, called finite elements. The collection of finite elements is denominated the finite element mesh and these elements are connected to each other at points called nodes. Following the finite element discretization, over each element, an approximation to the solution is developed. Finally, the assembly of the elements enables to obtain the solution to the whole domain [71].

The fundamental steps involved in the FE analysis, were defined in ABAQUS®, and are presented next.

#### 3.2.1. Material properties

The bone tissue has a combination of properties that are difficult to reproduce in bone numerical models used to study adaptive bone remodeling and mechanobiology. The

mechanical properties of bone are known to be elastic anisotropic (material properties depend on direction) and inhomogeneous in terms of mechanical resistance and densities (depending on the bone region) [63, 72].

In this work, the bone is modeled as a cellular material with an orthotropic microstructure, in which the relative density can vary along the domain and, is given by the material optimization process, i.e., it results from the problem solution. The elastic (equivalent) properties for this material are computed using the homogenization method, as mentioned before in chapter 2. The Young's modulus,  $E$ , for dense compact bone is 17 GPa, in other words, this is the condition that defines what is the maximum  $E$  that may exist, which occurs for  $\mu = 1$  (maximum relative density). All the other intermediate values of density correspond also to other intermediate values of elastic modulus, i.e., the elastic properties are functions of relative density.

Table 3.1 contains the materials properties assigned, which were assumed to be homogeneous, isotropic and with linear elastic behaviour, except for bone [22, 62, 73].

Table 3.1 – Material stiffness properties used in FE simulations [73].

Component	Material	Elastic Modulus /GPa	Poisson's coefficient
<b>Compact bone</b>		17	0,3
<b>Tibial tray and stems</b>	Titanium alloy	110	0,3
<b>Tibial insert</b>	UHMWPE	0,5	0,3
<b>Cement</b>	PMMA	2,28	0,3

The Young's modulus (measure of the stiffness) of the prosthesis (tibial tray, stem and cement layer) is a critical variable, since it largely determines how the load is transferred to the bone. So, it is one of the most important parameters in the control of the life span of artificial knees [30].

### 3.2.2. Contact formulation, Boundary conditions and applied loads

The contact between bone-cement and tibial tray-tibial insert was considered rigidly bonded (tied) for all the three configurations – standard, cemented and press-fit [22, 74]. Also, for the standard design the tibial tray-stem interface was considered tied, because they are made of different materials so, they were not combined before. In the other two models the tibial trays and stems were combined into one unique piece, as stated before.

For the contact between implant-bone, a coefficient of friction of 0,3 was used [75]. For the remaining contact, two different ways of modeling the interface between implant-cement were considered: an interaction in which the implant is bonded to cement [76, 77] – case 1 – and another case with a coefficient of friction of 0,3 [74, 76, 77] – case 2. In some studies the interface implant-cement was assumed to be either completely bonded or unbounded, with a friction coefficient. This happens because, although at an initial stage there is a firm and lasting

bond between the cement and the implant, over time, this effect tends to disappear, leading to the implant-cement debonding [74, 77]. Thus, the friction implant-cement interface is assumed to be more realistic than the bonded interface in the clinical scenario [74]. Summarizing, these two cases are tested in all the three configurations (standard, cemented and press-fit) leading to a six study cases. These two different ways to configure the interface implant-cement also allows to compare the influence that each of connection modes has on bone remodeling.

For the contact modeling the small-sliding option was selected. So, the contacting surfaces can undergo only relatively small sliding relative to each other. The frictional behaviour was modeled with the penalty friction formulation with the specified friction coefficients [78]

The lower extremity of the tibia was fixed with the boundary condition, called “encastre”, and six different load cases were applied, using the multiple load criteria with equal weights (1/6), four correspond to the movement of level walking and, the remaining two load cases concern to the deep knee bend movement. These six load cases were measured by an instrumented prosthesis and were based on the *in vivo* knee joint loading study developed by Kutzner, Heinlein, Bergmann, et al. 2010 [2, 18, 79]. Figure 3.21 illustrates the selected moments of the gait cycle and of the knee bend movement considered for the six load cases. These data were acquired from a free public database – Orthoload – corresponding to the K1L subject with body weight of 1000 N [79].

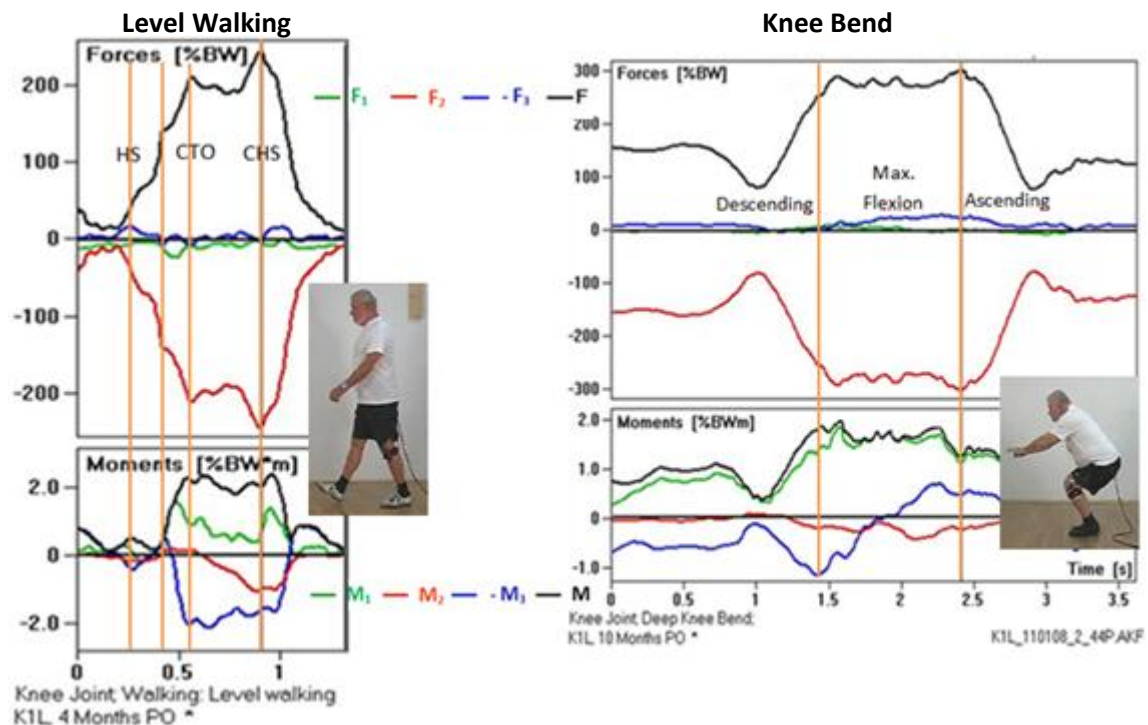


Figure 3.21 – Load patterns during the investigated activities – Level walking and Knee bend, at left and right, respectively. Upper diagrams = forces, lower diagrams = moments (BW=Body weight). Vertical orange lines are the selected times that correspond to the load cases considered. HS: heel strike; CTO: contralateral toe off; CHS: contralateral heel strike [79].

The activities included in this study do not represent the complex spectrum of physiological movements of everyday life. Nevertheless, they correspond to most frequent strenuous activities of daily living, such as walking and sitting [18]. The fact that equal weights are assigned to the six load cases, gives greater weight to the movement of walking (4/6) than to knee bend (2/6), being the first more representative. These selected load cases correspond to discrete times of these activities and are considered representative of the range of loads that exist in these movements. It is assumed that these physiological loading conditions simulate the daily loading history of the tibia and are valuable for FE analysis. This happens because it is computationally very expensive and almost impossible to consider the entire range of loading data associated to the movement. Table 3.2 presents these load cases (3 forces and 3 moments for each load case), which were applied in FE analysis, corresponding to the K1L subject – acquired from Orthoload [79].

Table 3.2 – Forces and moments from level walking and knee bend applied in FE models [79].

	Force/ N			Moment/ N.mm		
	F1	F2	F3	M1	M2	M3
<b>Level Walking</b>	-76,05	-318,9	-169,96	2420	-1900	3430
	-144,65	-1442,14	52,79	3760	1090	-4790
	-71,96	-2141,34	61,18	8850	1070	20220
	-20,16	-2476,89	24,11	4760	-10820	16990
<b>Deep Knee bend</b>	75,8	-2537,57	-8,3	13220	-2230	12030
	-26,55	-2801,01	-292,26	17400	-2790	-7230

Forces directions relative to the tibial component:  $F_1$ ,  $F_2$  and  $F_3$  act in medio-lateral, vertical and posterior-anterior, respectively. Moments  $M_1$ ,  $M_2$  and  $M_3$  act in the sagittal, horizontal and frontal plane of the tibial component.

The three components of the spatial knee contact force  $F$  and the three components of the spatial moment  $M$ , which acts on the tibial component, were measured *in vivo*, using instrumented, telemeterized knee implant. The center of the coordinate system is fixed at the tibial component on the extended stem axis at the height of the lowest part of the polyethylene insert (see Figure 3.22). The forces and moments that were given in this study were reported to the right knee, so it was necessary to convert it to the left side – left tibia. The forces components  $F_1$ ,  $F_2$  and  $F_3$  act in medio-lateral, vertical and posterior-anterior direction on the tibial component. Moments  $M_1$ ,  $M_2$  and  $M_3$  act in the sagittal, horizontal and frontal plane of the tibial component and turn right around their respective axis [2, 18].

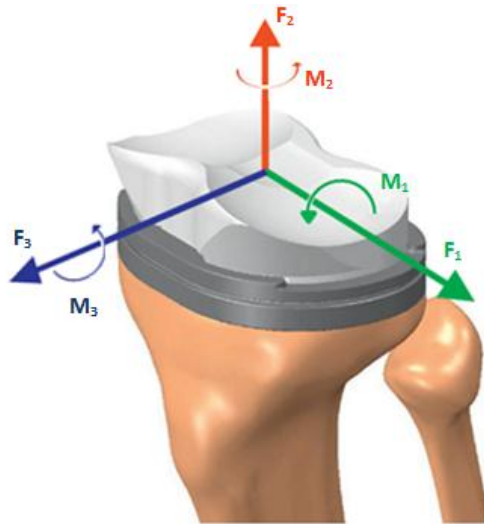


Figure 3.22 – Coordinate system for the forces and moments applied adapted from [2].

The knee joint is loaded by external forces (ground reaction force, masses and acceleration forces of foot and shank). Their sum is counterbalanced by the forces acting across the joint, such as, the tibio-femoral contact forces, muscle forces and forces in soft tissue structures [2]. So, determining the *in vivo* loading environment in the human knee is difficult due to the combination of complex structural anatomy [3].

It must be further mentioned that these knee contact loads, three forces and three moments acting in the implant, are only a fraction of the total knee loads, i.e., the instrumented implant measures only a part of the total load acting in the knee joint. Thus, what is measured are the *in vivo* reaction loads in the knee joint (tibio-femoral contact forces and moments) and not all the loads applied to the tibia. Additional forces and moments transmitted from the femur to the tibia are transferred not only to the prosthesis, but also to tendons, ligaments and other soft tissues. However, as all these structures can only bear tensile forces, particularly the measured force  $F_2$ , which is the axial compressive force (always negative), could be interpreted as the total external axial knee force [18]. So, the loads obtained by the tibial component of the telemeterized implant, and which were applied in the FE analysis, are a good approach of the majority of the mechanical demands of the tibia, and do not constitute a great limitation to this study.

The information about the muscles and soft tissue forces (like, collateral and patellar ligaments responsible to stabilize and move the joint) are obtained from musculoskeletal modeling techniques e.g. inverse dynamics and static optimization [80]. However, they were not included in this work, because large variations of reported loading exist and, also there are great discrepancies between the forces actually measured and those obtained analytically [2, 81]. These discrepancies result most likely from the high degree of mechanical redundancy due to the number of muscles involved in human motion [81]. Moreover, the available data was not compatible to the data of Bergmann et al. work.

It should also be mentioned that the reported data were obtained with a specific implant design. So, they cannot be transferred directly to other implants or to the natural knee.

However, similar values were reported in other *in vivo* studies using other instrumented implants (D’Lima et al., 2007; Munderman et al., 2008; Taylor et al., 1998). In addition, the axial force  $F_2$  and the resultant force  $F$  will most likely not be affected much by the type of TKR [2].

Thus, these realistic *in vivo* data (six load cases with six load components – 3 forces and 3 moments) were utilized in the FE analyses of this work, both in the natural knee as in all the three prostheses configurations (standard, cemented and press-fit), allowing the study of the numerical simulation of the bone remodeling process according to TKR design.

These loads and moments were applied in a reference point (RP) that coincides to the center of the coordinate system (Figure 3.22) and which was constrained (Coupling - continuum distributing) to surfaces of the proximal tibia. This way, the forces and moments are uniformly distributed to these surfaces and actually acting on them. This is so because in reality the forces are not applied only in single points, but in an area of the proximal tibia, giving better physiological representation and avoiding stress concentration artifacts [24]. In the intact bone model the selected surfaces were the articular surface of the tibial plateau (see Figure 3.23 A), since there was no equivalency of the considered loads to the natural bone (equal medial-lateral load split was assumed [82]). Whereas, in all the three cases of the implanted tibia (standard, cemented and press-fit) the surfaces where the loads were applied correspond to the condylar surfaces of tibial insert (see Figure 3.23 B).

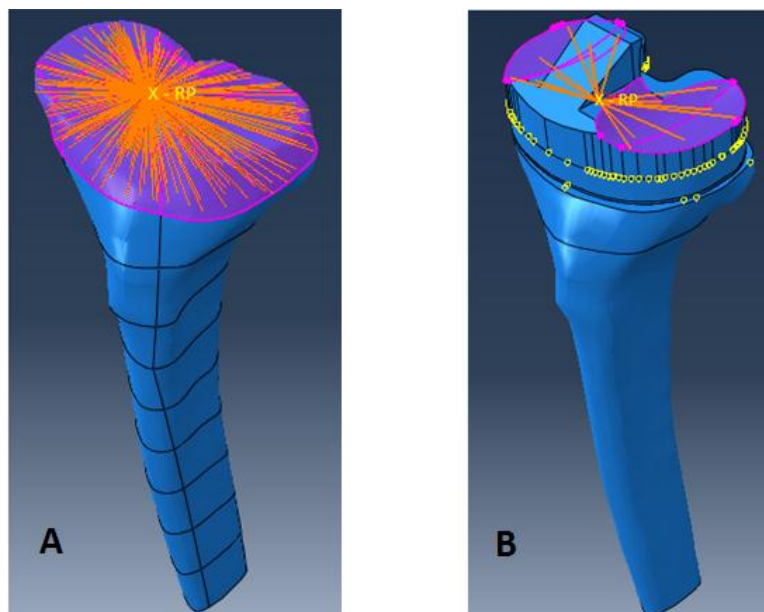


Figure 3.23 – Illustrate the RP and the surfaces where the six load cases are applied: A – Intact bone; B – Implanted bone.

### 3.2.3. Finite element mesh generation

#### FE modeling of intact tibia

At this stage it was generated a volume mesh from the solid model previously described in the sub-chapter 3.1.1. (tibia uniform), using the FE program ABAQUS®. Taking into account the mesh tools supplied by this software, generating a tetrahedral mesh is a simple assignment to

fulfill. However, tetrahedral FE meshes produce slightly less accurate results than the hexahedral FE meshes [83]. So the aim was to make a hexahedral mesh, which involves a process a lot more complicated due to the complex anatomical curvatures of the structure being modeled (condyles, intercondylar region and tuberosity) [67]. To generate the hexahedral mesh with eight-node elements of the tibia uniform solid model, it was necessary some pre-processing of the model, that is explained next.

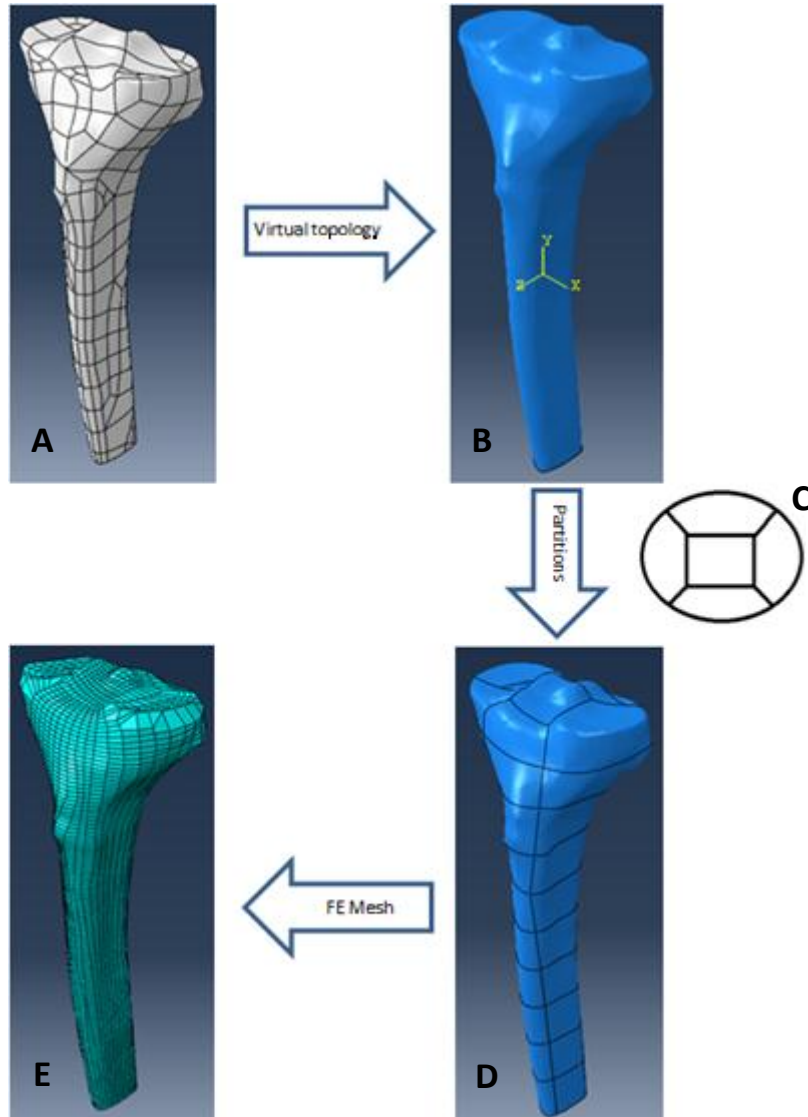


Figure 3.24 – Process to generate the hexahedral mesh of the tibia uniform solid model: A – Superficial mesh of SolidWorks®; B – Virtual topology; C – Illustrative structure of partition mode of the model, which is drawn on the lower extremity basis of the bone and then is extruded along its longitudinal axis; D – Tibia with partitions; E – Hexahedral FE mesh.

Firstly, the tibia uniform solid model was imported to ABAQUS®. The initial superficial mesh automatically generated in SolidWorks® was then eliminated, using the virtual topology tool. Thereafter, the domain to be discretized (tibia) was divided into blocks, i.e., a complex region was subdivided into sub-regions, which are then meshed separately. These partitions were made to generate, over an imaginary longitudinal axis of the bone, parts with divisions that

resembled the structure of the Figure 3.24 C, thereby generating blocs with four lateral faces (similar to a parallelepiped) that are easily meshed. It should be noted that, this process is quite time consuming since each new partition affects the partitions previously made, hence the need to perform an accurate and detailed action. Finally, the hexahedral mesh was generated. Figure 3.24 illustrates the steps followed to successfully obtain the FE mesh of the tibia.

The final model of the tibia presents a total of 31840 eight-node hexahedral element (linear) and 34706 nodes. This resulting FE mesh has a good anatomical detail, which is important to produce accurate and real FE results.

### FE modeling of implanted bone

After obtaining the hexahedral mesh of the tibia uniform model (intact bone), this same strategy was used to generate the different hexahedral FE meshes for each of the models with implant, described at the end of the sub-chapter 3.1. In order to do so, a series of steps, indicated in Figure 3.24, were followed. However, due to the high complexity of these models it was not possible to get a hexahedral mesh, so they were all meshed with tetrahedral FE meshes, which requires less human effort and computational resources than the hexahedral meshing [83].

Below the images of the obtained FE meshes for the three different implant configurations (Figure 3.25, 3.26 and 3.27) are shown. In all of them the four-node tetrahedral elements (linear) were utilized.

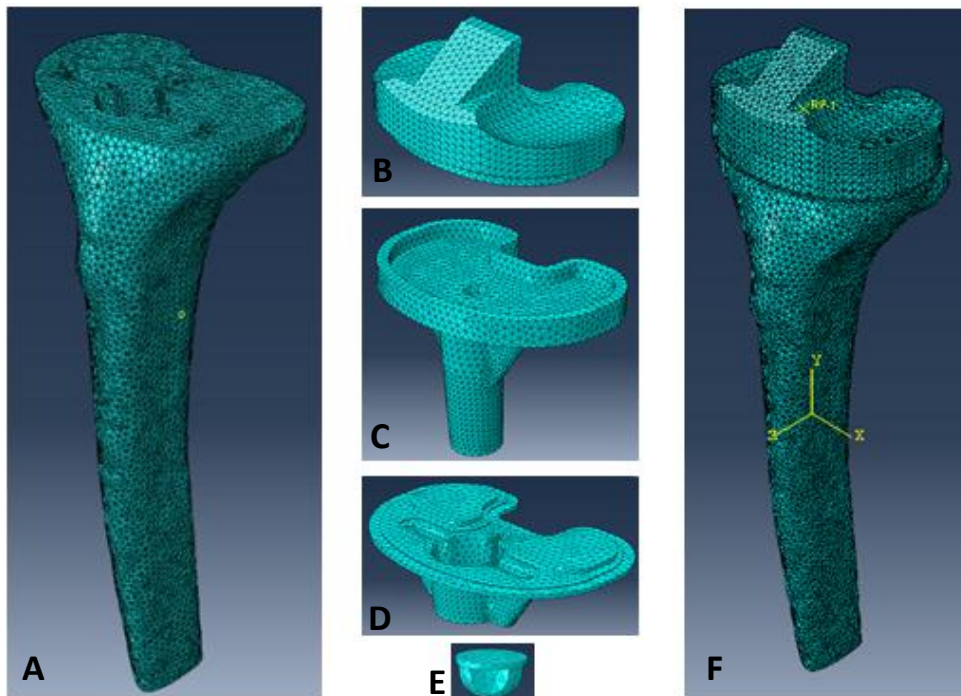


Figure 3.25 – FE mesh of the standard configuration: A – Cut tibia; B – Tibial insert; C – Tibial tray; D - Cement; E – Standard stem; F – Total assembly.

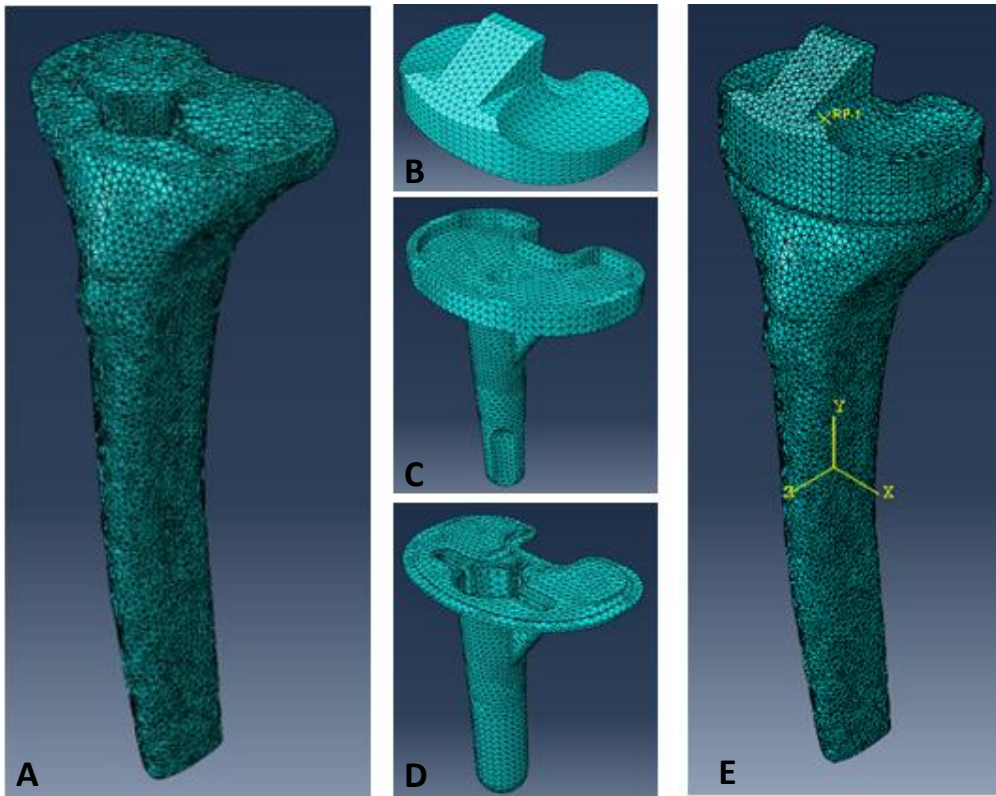


Figure 3.26 – FE mesh of the cemented configuration: A – Cut tibia; B – Tibial insert; C – Tibial tray and cemented stem; D - Cement; E – Total assembly.

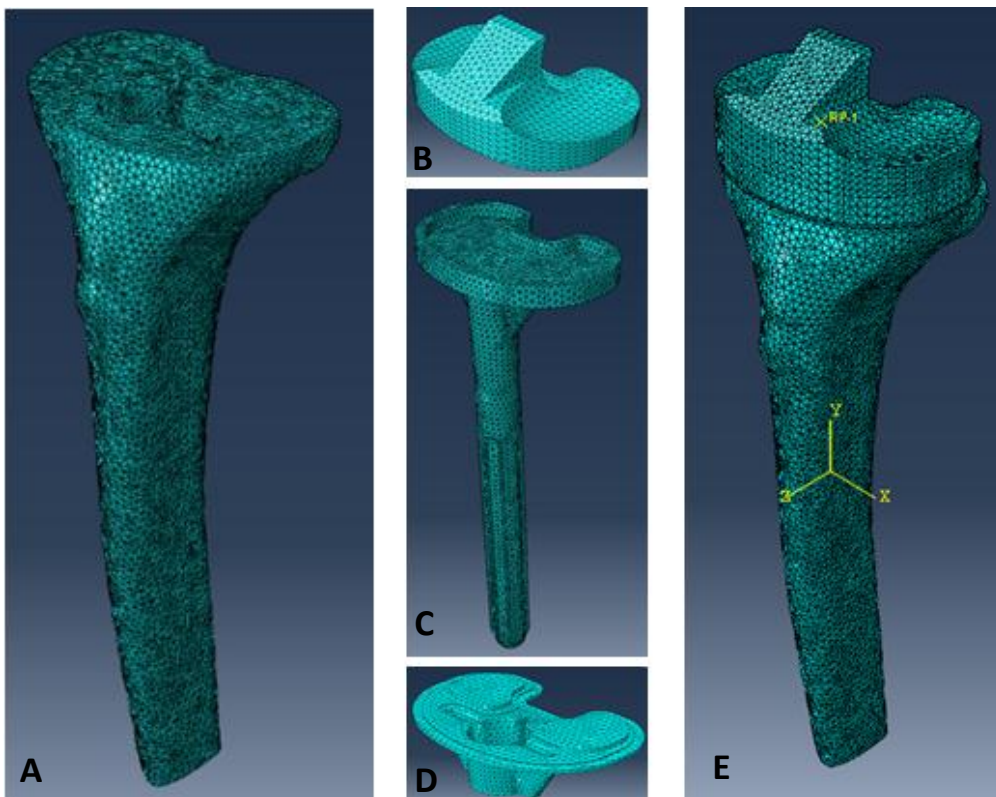


Figure 3.27 – FE mesh of the press-fit configuration: A – Cut tibia; B – Tibial insert C – Tibial tray and press-fit stem; D - Cement; E – Total assembly.

The accuracy of the results derived from the FE analysis depends not only on the type of elements but also on the mesh refinement, which is controlled by indicating the element size [27, 83]. Taking this into consideration it was selected an adequate mesh refinement (number of elements) without compromising too much the computational cost. Table 3.3 presents the number of elements and nodes for each selected meshed model.

Table 3.3– Number of elements and nodes of the FE meshes of the models.

Model	Type of FE	Number of FE elements/nodes of the bone	Number of FE elements/nodes of the total assembly
Intact bone	8-node hexahedral	31840 / 34706	- / -
Standard configuration	4-node tetrahedral	138569 / 26811	201706 / 42032
Cemented configuration		142241 / 27779	214068 / 45483
Press-fit configuration		161923 / 31876	246902 / 52078

Finally, the last step was the submission of the jobs of FE software to the iterative program of bone remodeling. However, it was necessary to determine in advance some parameters of the bone remodeling process, such as cost parameter  $k$  and the step, as shown below. It should also be mentioned that FE calculations are made in the nodes rather than in the elements.

### 3.3 Analysis of the intact bone – Tests for the application of the bone remodeling model

#### 3.3.1. Determination of metabolic cost parameter – uniform density distribution

The most appropriate value of the biological parameter  $k$  was determined from the qualitative analysis of bone remodeling model applied to the intact bone model (without implant). To do so various values were tested, selecting the one that reproduced the morphology most similar to the real bone. For reasons of synthesis only three of the most relevant results obtained are presented in Figure 3.28, 29 and 30, which correspond respectively to the following values of  $k$ : 0,001, 0,003 and 0,006 N/mm<sup>2</sup>. These results were obtained starting with an initially homogeneous solution, with a uniform bone relative density distribution of 0,3.

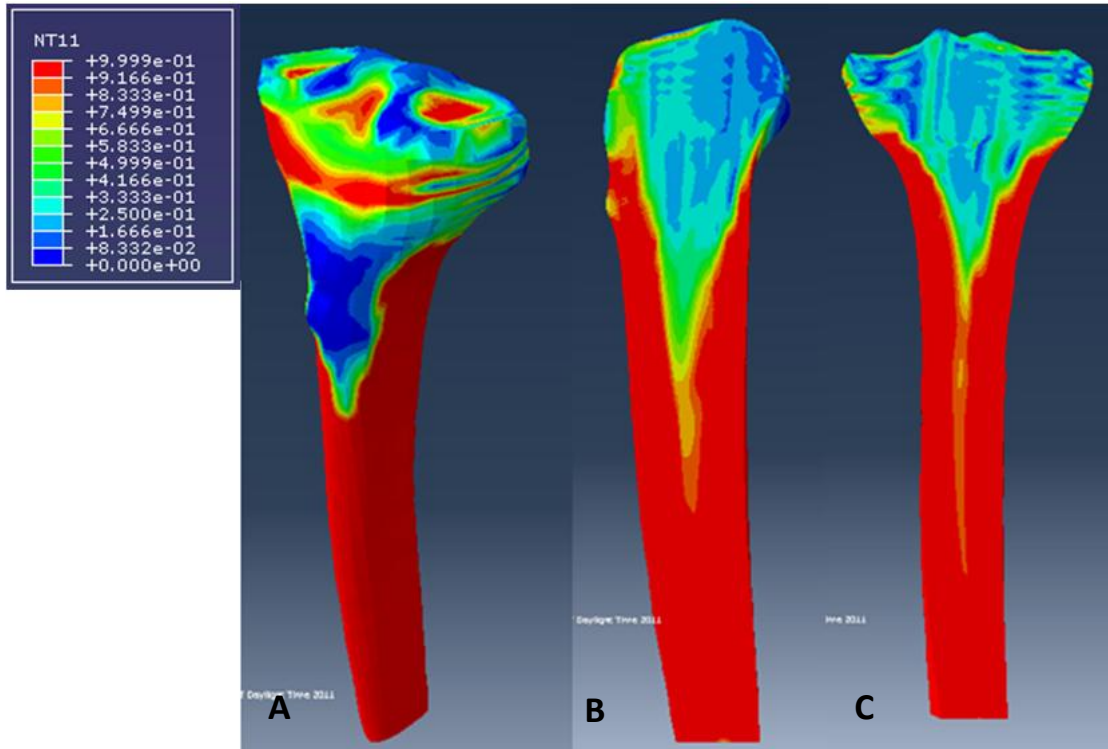


Figure 3.28 – Density distribution resulting from the model of bone remodeling for the intact bone with an initially homogeneous solution  $\mu = 0,3$  and,  $k=0,001 \text{ N/mm}^2$ , step = 5 and 200 iterations. Relative densities,  $\mu$ , are represented in a color scale: red=cortical bone ( $\mu \approx 1$ ) and the remaining=trabecular bone. A – Global view; B – Lateral section, right sagittal view; C – Frontal section, anterior view.

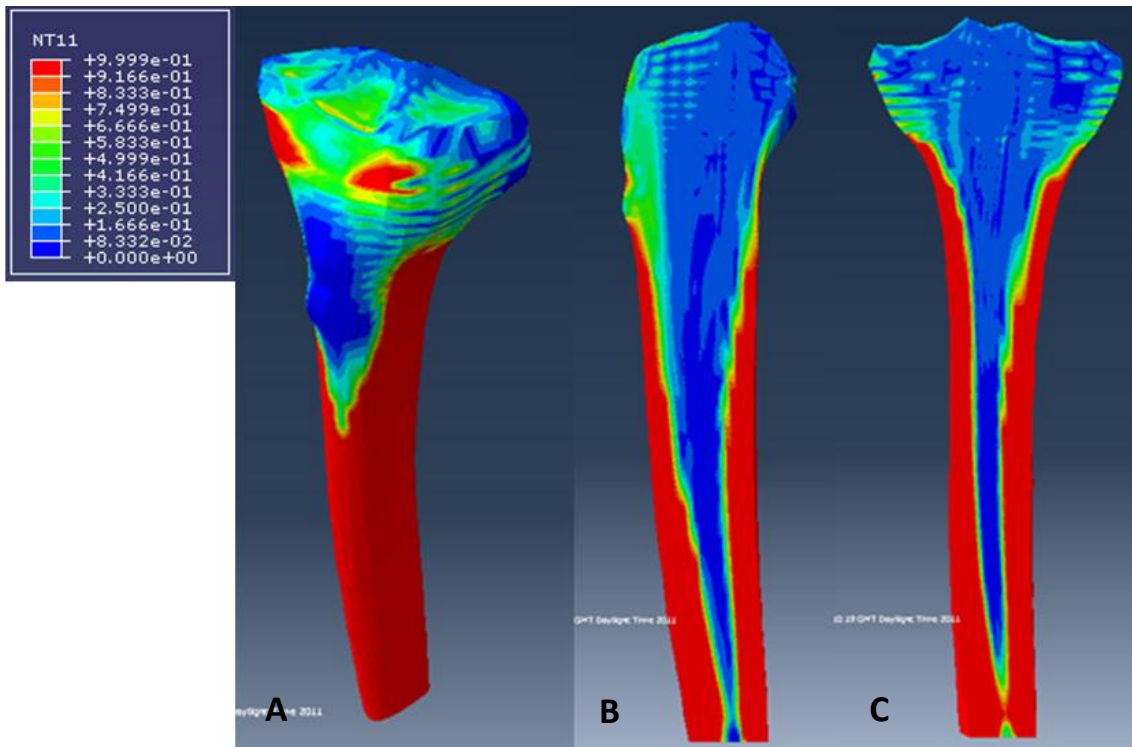


Figure 3.29 – Density distribution resulting from the model of bone remodeling for the intact bone with an initially homogeneous solution  $\mu = 0,3$  and,  $k=0,003 \text{ N/mm}^2$ , step = 5 and 200 iterations. Relative densities,  $\mu$ , are represented in a color scale: red=cortical bone ( $\mu \approx 1$ ) and the remaining=trabecular bone. A – Global view; B – Lateral section, right sagittal view; C – Frontal section, anterior view.

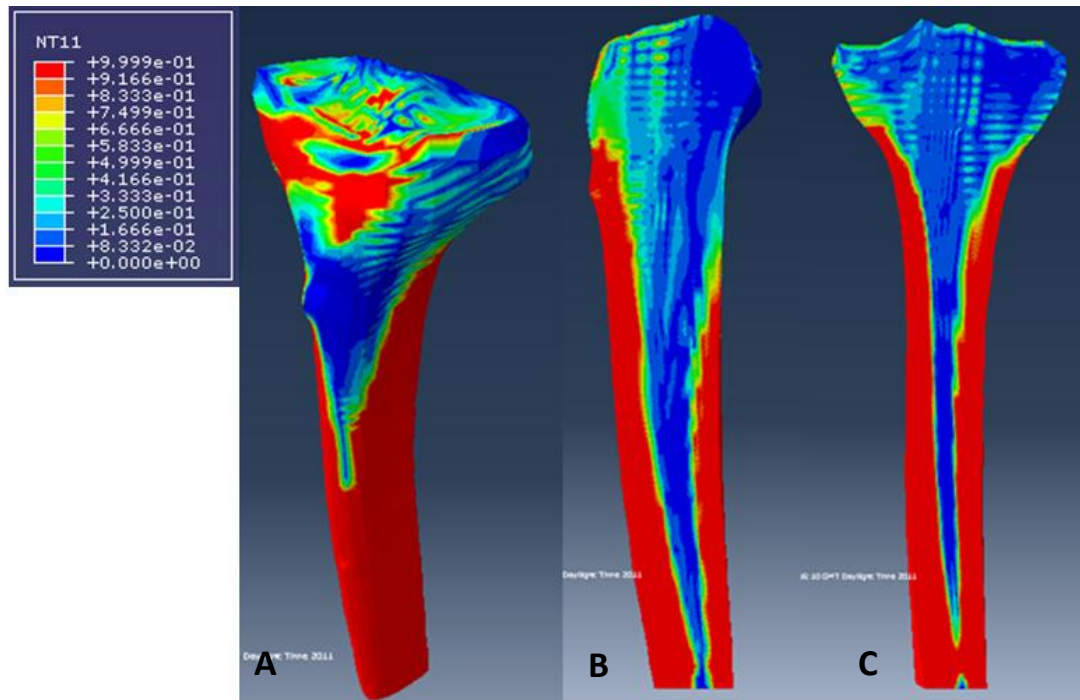


Figure 3.30 – Density distribution resulting from the model of bone remodeling for the intact bone with an initially homogeneous solution  $\mu = 0,3$  and,  $k=0,006 \text{ N/mm}^2$ , step = 5 and 200 iterations. Relative densities,  $\mu$ , are represented in a color scale: red=cortical bone ( $\mu \approx 1$ ) and the remaining=trabecular bone. **A** – Global view; **B** – Lateral section, right sagittal view; **C** – Frontal section, anterior view.

The results obtained for the density distribution of the intact tibia, even starting from a homogenous density distribution and with the given loading conditions, reflected several morphological features observed in actual density patterns of the bone, such as a central canal in the diaphysis – intramedullary canal – surrounded by compact tissue of considerable thickness in the middle part, but becoming thinner toward the extremities; within the medullary canal there is some cancellous tissue, scanty in the middle of the diaphysis (minimum density) but greater in amount toward the ends, i.e., in the metaphysis and epiphysis there are nodes with intermediate densities, between 0,05 and 0,6, that correspond to the trabecular bone of the proximal region of the real tibia. So, from these features, one can conclude that the model converges to a solution with high similarity to the morphology of the real tibia, reproducing the behaviour of the real bone.

To estimate the value of  $k$ , which highly influence the amount of bone mass, it was necessary to compare more rigorously these results of the density distribution with the one of the real bone. For  $k=0,001 \text{ N/mm}^2$  although the proximal region of bone has a good reproduction of trabecular bone, there is virtually no intramedullary canal, i.e., too much cortical bone on the diaphysis. To overcome this problem the metabolic cost of maintaining bone was increased, so that the bone mass decreased, by reducing the relative densities. In the case of  $k=0,006 \text{ N/mm}^2$  the formation of the intramedullary canal is evident, but in the proximal region, particularly in epiphysis, there exists an excessive loss of bone (low density). For the intermediate value of the parameter,  $k=0,003 \text{ N/mm}^2$ , it was obtained the closer result to pattern of density distribution of the real bone. Thus, this was the most appropriate value of the

metabolic cost parameter and was the selected one. However, it should be noted that there are some limitations on the result obtained, such as absence of a thin layer of cortical bone coating the surface of the proximal metaphysis and epiphysis, and there is an exaggerated thickness of cortical bone in the diaphysis (should be 2–3 mm).

### 3.3.2. Non-homogeneous density distribution

To overcome the previous limitations, it was considered a second distribution of initial densities of intact bone, more similar to the reality than the uniform case, for the input of bone remodeling model. Taking advantage of previously performed modeling of the intramedullary canal from CT images (tibia canal model), it was considered an initial solution with all the nodes that are part of the canal with a minimum relative density of 0,05 (low density or very sparse distribution of trabeculae). It was also considered a thin layer of cortical bone coating the tibia, by assigning to all the superficial nodes of the bone a maximum relative density of 1. For the remaining nodes a relative density of 0,3 was attributed (see Figure 3.31). Thus, at an initial stage of the simulation there is a canal with low-density bone material which is important for the bone remodeling process, since having trabeculae in this area may allow to hypothetically gain or lose bone mass in this location without affecting much the stiffness of the bone. And, also cortical bone at the surface of bone, without imposing a certain thickness to the cortical part, which is usually exaggerated in the area of the epiphysis and metaphysis, when it is done in the elements, as it required having a certain thickness.

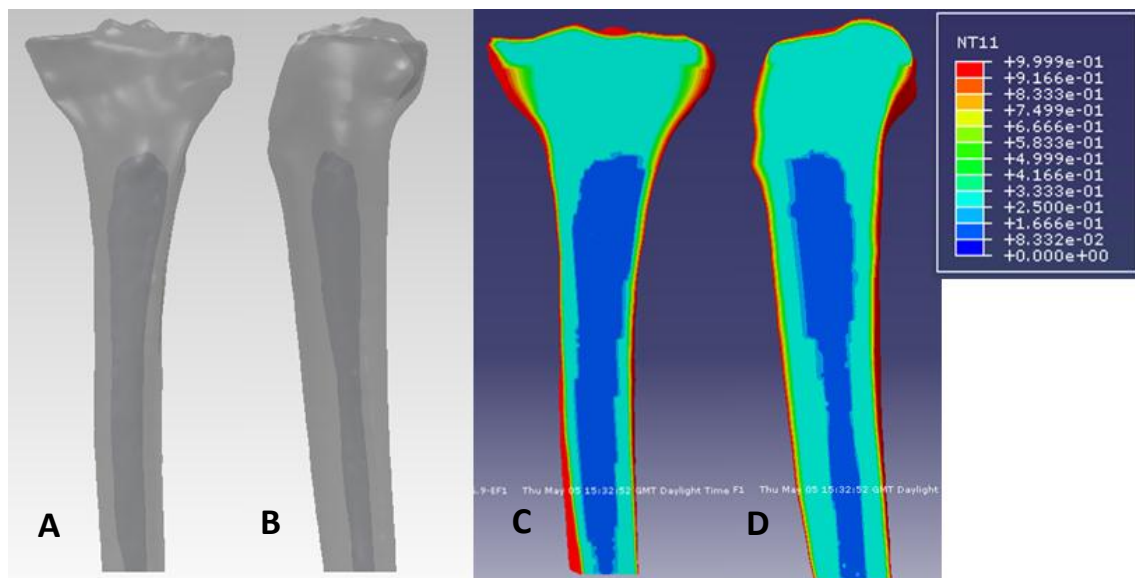


Figure 3.31 – Solid model of the left tibia with the modulation of the intramedullary canal (A and B) and initial distribution of densities for this model (C and D). Relative densities  $\mu$ , are represented in a color scale: at red=cortical bone ( $\mu \approx 1$ ), blue=intramedullary canal ( $\mu=0,05$ ) and the remaining=trabecular bone ( $\mu=0,3$ ): A and C – Frontal section, anterior view; B and D – Lateral section, right sagittal view.

This initial distribution of densities was submitted to the model of bone remodeling with a parameters:  $k=0,003 \text{ N/mm}^2$  and step=5 with a total of 200 iterations. The result is shown below (Figure 3.32), as well as an image of the real bone (Figure 3.33) for a comparative study.

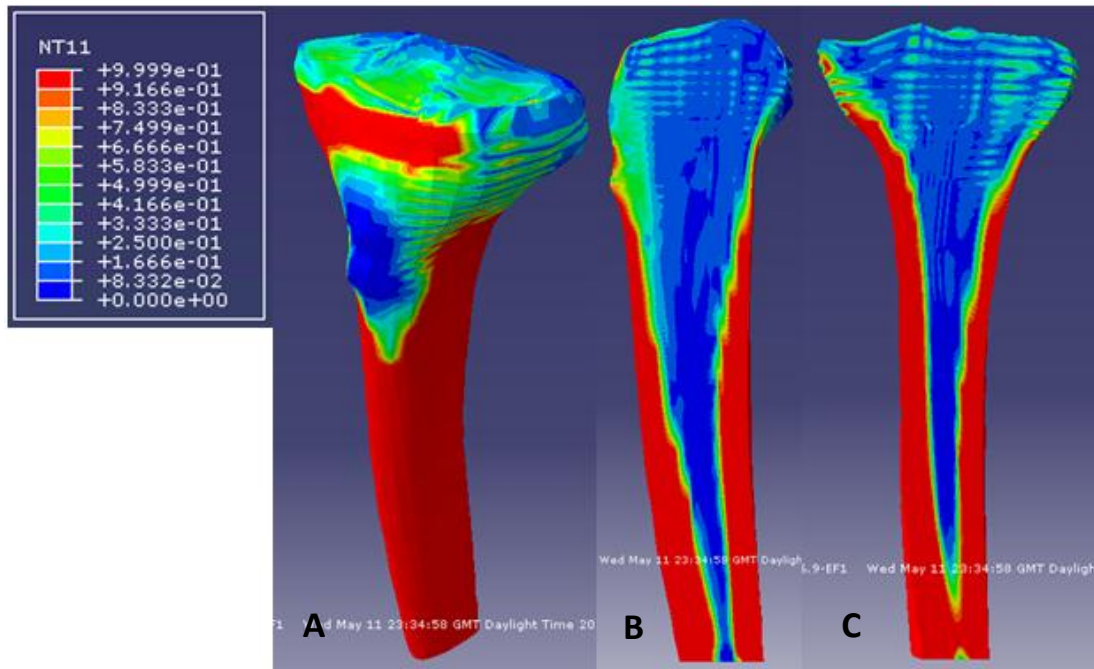


Figure 3.32 – Density distribution resulting from the model of bone remodeling for the initial non-homogeneous input of the Figure 3.31 with  $k=0,003 \text{ N/mm}^2$ , step = 5 and 200 iterations. Relative densities,  $\mu$ , are represented in a color scale: red=cortical bone ( $\mu \approx 1$ ) and the remaining=trabecular bone. A – Global view; B – Lateral section, right sagittal view; C – Frontal section, anterior view.

Comparing this result with the previous one (Figure 3.29) there are slight differences: it now appears that there is a bit wider thin layer of cortical bone coating the surface of the tibia, although it is not perfect; it is also observed a light mass gain in the proximal region of the tibia, as it was intended. Therefore, despite the small differences between these two results of density distribution, the latter (Figure 3.32) is closest to the real bone, as it can be seen in a comparative analysis (see Figure 3.33).

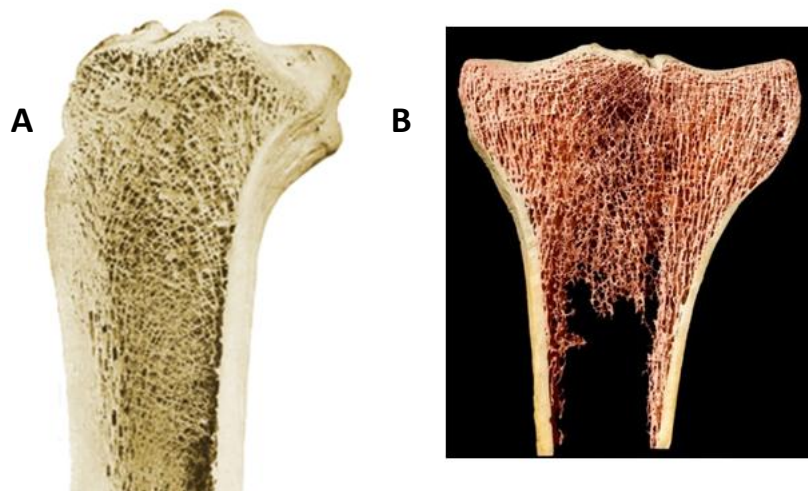


Figure 3.33 – Sections of the proximal real tibia showing the distribution of the inner cancellous bone and outer compact bone: A – Lateral section, right sagittal view; B – Frontal section, anterior view.

After all these tests to determine the value of the biomechanical parameter  $k$ , the evolution process of bone remodeling is applied to models with implant. In the three models tested with

standard, cemented and press-fit prosthesis, only the bone is considered as design area with initial density distribution that correspond to final densities obtained in the model of intact bone with the intramedullary canal (Figure 3.32), i.e., it is considered as starting point the distribution of densities obtained in the previous model, tibia without implant. Since the meshes of the models are different (section 3.2.3.), it was developed an algorithm in Matlab, to transit the densities of the nodes of one mesh to another – described in Annex A. Thus, each bone implanted model starts from an initial situation with greater resemblance to reality and, consequently to the clinical scenario.

Application of this strategy both may allow for more precise analysis of the remodeling process taking place in the bone tissue (facilitating the evaluation of the process), as it makes more real the evolutionary process of bone remodeling.

Analogous to the model of intact bone, in each model with implant the lower extremity of the tibia is fixed and six different load cases are applied, as described in section 3.2.2. in Table 3.2. Thus, integrating the FE method with a numerical simulation of the process of bone adaptation is possible to obtain the distribution of the bone density in the modeled tibia that is the solution of the process of bone remodeling, as it will be seen.

### 3.4. Results analysis method

To achieve the objectives of this work the results analysis will consist essentially of two approaches. The first is a qualitative analysis in which the figures of the initial and final situation of the implanted bone are compared, in other words, the before and after the bone remodeling process, respectively. As this analysis is performed by slices (2-D images) not contemplating the bone in its entirety, it can sometimes lead to a hasty and inappropriate conclusion. Thus, to complement this analysis is also used a quantitative analysis, with two types of approach. Initially, is analyzed the evolution of the total bone mass throughout the iterative process, dimensionless by its initial mass, allowing a general sense of strengthening or weakening of the bone. Since the global behaviour may not translate effectively the local behaviour of bone formation or resorption, the bone was also divided into 6 different regions of interest (ROI), which are separately analyzed, allowing to observe the remodeling process in more detail. The percentage of bone mass variation for a given ROI is given by the following expression:

$$BMvar_{ROI}(\%) = \frac{\sum_{i=1}^N \mu_i^{final} V_i^{node} - \sum_{i=1}^N \mu_i^{initial} V_i^{node}}{\sum_{i=1}^N \mu_i^{initial} V_i^{node}} \times 100 \quad (7)$$

where  $\mu_i$  is the relative density of node  $i$ ,  $V_i^{node}$  the volume associated to node  $i$  (extracted from the computational model of bone remodeling) and  $N$  the total number of nodes that compose the region under study (node  $i \in ROI$ ). So, one obtains the mass evolution for the whole bone and for each of the considered sections, allowing a better sensitivity of the process of bone remodeling for each of the different regions of the bone. The Figure 3.34 illustrates the models

of the implanted bone, with the three prosthesis configurations, and the six regions considered where the results are obtained and compared. All the regions have the same height and are in increasing order from the proximal extremity to the distal one.

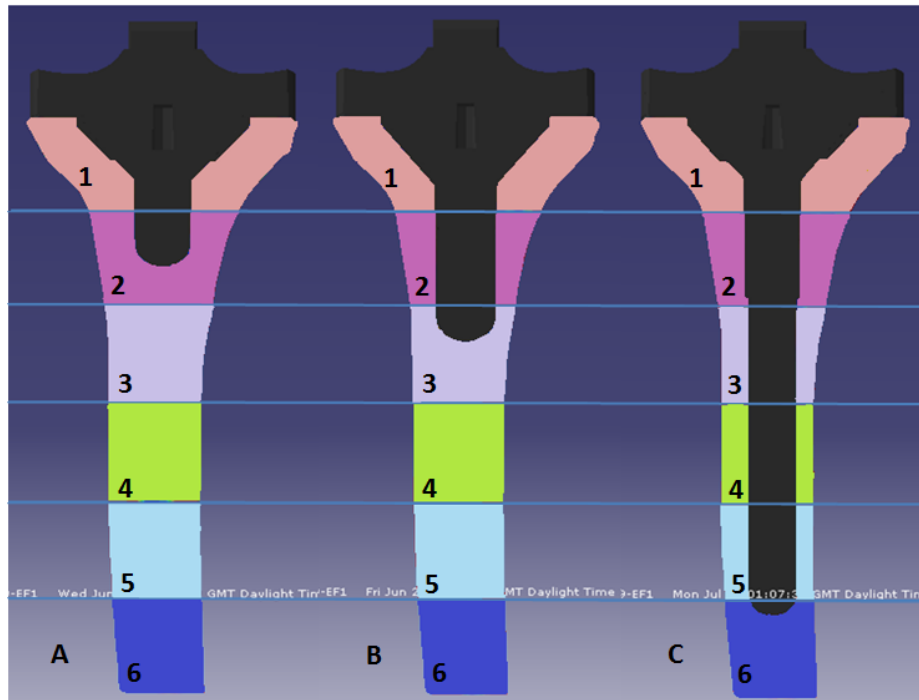


Figure 3.34 – Implanted bone discretized in the regions (1-6) under study in bone remodeling process: A – Standard; B – Cemented; C – Press-fit configuration.



## 4. Results and Discussion

As mentioned previously, bone density measurements have been shown to correlate closely with the mechanical properties of bone, suggesting that the loss of bone in the tibia due to the tibial component is one of the main concerns about the success of the knee prosthesis, since it can be a threat to implant stability [25]. The main goal of this study is to better understand the biomechanical influence of the total knee arthroplasty in the process of bone remodeling that occurs in the tibia.

In this chapter, the results obtained from the bone remodeling analysis are presented, and the density distribution results induced by the different design solutions are compared, using the parameters  $k = 0,003 \text{ N/mm}^2$  and  $\text{step} = 5$ . These results are also complemented with stress analysis and compared with experimental results obtained at the University of Aveiro [54, 62].

### 4.1. Standard configuration model

The results of bone remodeling model for the case of standard stem design, considering interface implant-cement bonded and with friction are presented in Figure 4.1 and Figure 4.2, respectively. In order to analyze the evolution of each of the density distributions, the starting point is also shown, which is equal for both cases.

Through the observation of the Figure 4.1 is possible to identify a small decrease of bone mass (BM) in the proximal region (region 1), especially in the thin surface layer of cortical bone that surrounds the bone and in the proximal posterior area. However, is also observed a modest densification of bone (increase in bone density) near the interface with prosthesis. The same is noticed for the friction interface case (Figure 4.2), but with a much more evident BM gain in the region that interacts with the prosthesis (regions 1 and 2). In both cases, all the other regions (regions 3 to 6) show no significant alterations of density distribution.

In Figure 4.3 is shown the process of bone adaptation in global terms, i.e., the evolution of total BM throughout the iterative process, dimensionless by its initial mass. It should be noted that the process has reached the desired convergence – the change in BM stabilized – within the number of iterations considered for the two cases of contact implant-cement definition. This means the solution of the model converge towards endpoint condition representing an equilibrium state between successive bone formation and bone resorption events. As it can be seen, in both cases there is a slight increase in total BM, most notorious in the case with friction interface, in which the final total BM gain is of 5,97% and 0,4% for the bonded interface, which is almost negligible. So, it can be said in general terms, that there is a slight strengthening of bone, consequence of a greater bone formation than absorption. This happens essentially due to an increase in the densities of bone nodes that are near and at the interface with the prosthesis.

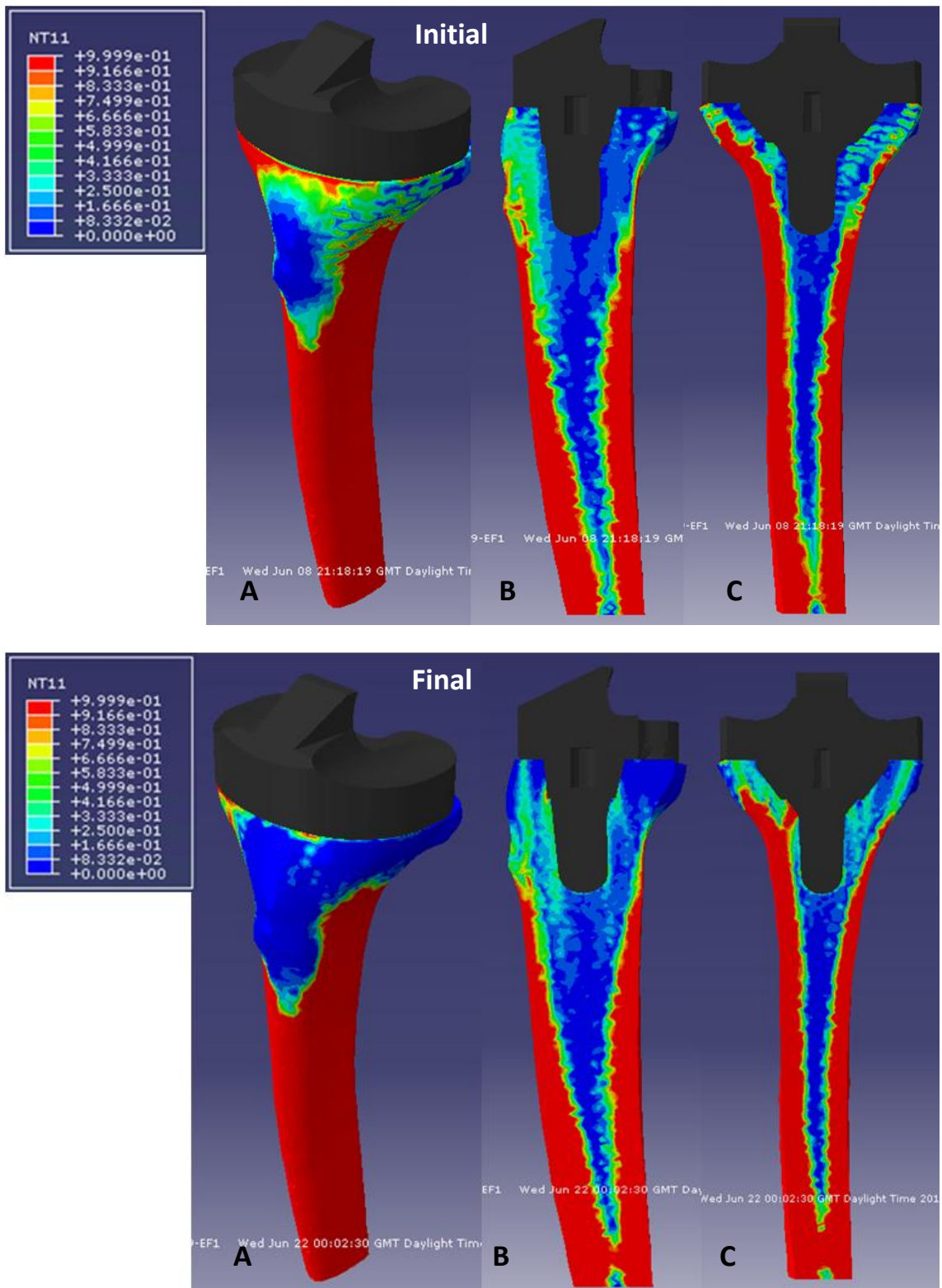


Figure 4.1 – Initial and final density distribution resulting from the model of bone remodeling for the implanted bone with standard prosthesis (interface implant-cement bonded). Relative densities,  $\mu$ , are represented in a color scale: red=cortical bone ( $\mu \approx 1$ ) and the remaining=trabecular bone. A – Global view; B – Lateral section, right sagittal view; C – Frontal section, anterior view.

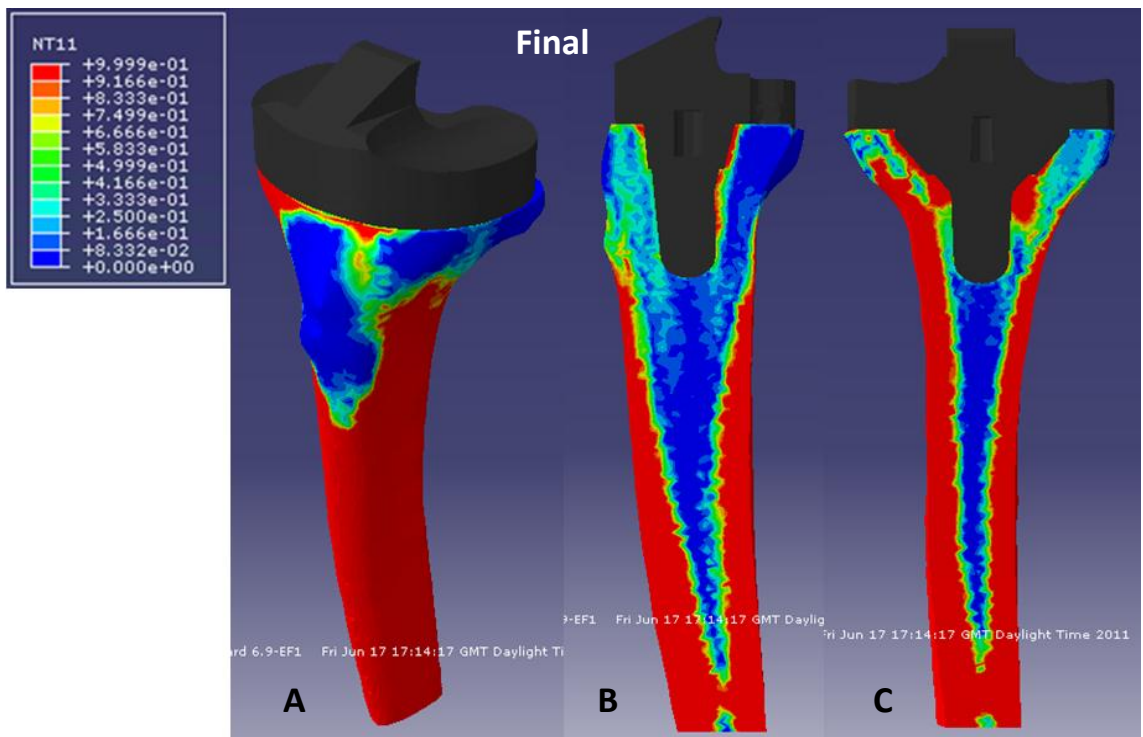
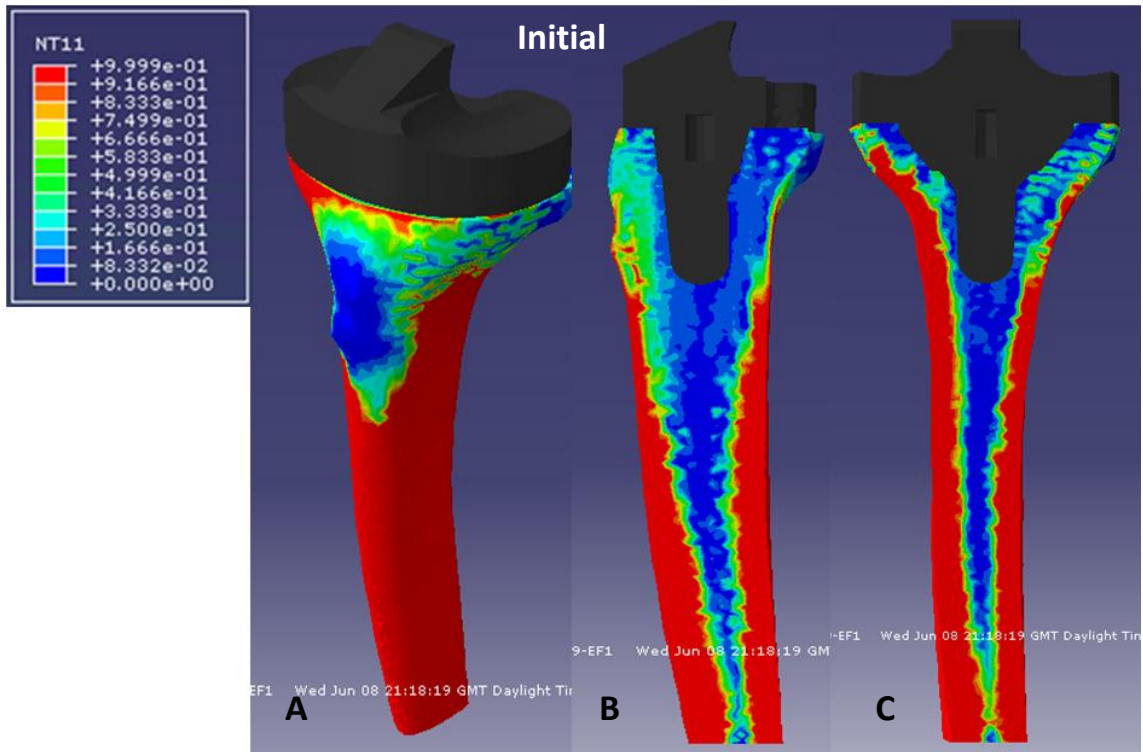


Figure 4.2 – Initial and final density distribution resulting from the model of bone remodeling for the implanted bone with standard prosthesis (interface implant-cement with friction). Relative densities,  $\mu$ , are represented in a color scale: red=cortical bone ( $\mu \approx 1$ ) and the remaining=trabecular bone. A – Global view; B – Lateral section, right sagittal view; C – Frontal section, anterior view.

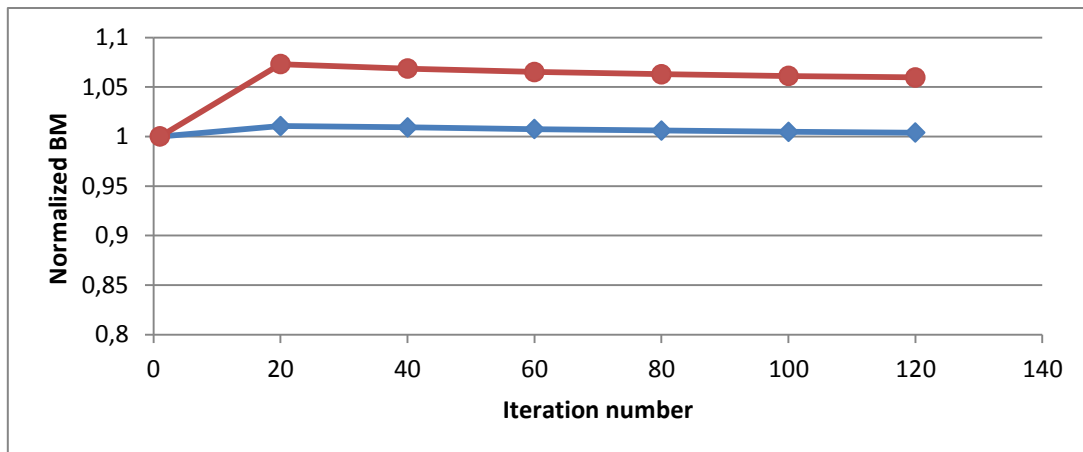


Figure 4.3 – Evolution of the total bone mass (BM) throughout the iterative process of bone remodeling, dimensionless by its initial mass, for the standard configuration considering interface implant-cement bonded (blue) and with friction coefficient of 0,3 (red).

Table 4.1 presents the percentage of BM variation for each of the regions in which the implanted bone was discretized. Through its analysis is verified a slight increase in BM in all the regions, except in the region 1 of the bonded interface case, where the BM decreases (-8,74%). For the case of implant-cement interface with friction the most significant increase in BM are recorded in regions 1 and 2, i.e., the regions that include the interface bone-implant. All the other regions of both cases have a bone mass gain between 1 and 3% which is not quite significant. These results are in agreement with those described previously.

Table 4.1– Bone mass variation for the regions 1 to 6 and for the whole bone, result of the bone remodeling process, for the standard prosthesis considering interface implant-cement bonded and with friction coefficient of 0,3.

	Bone mass variation (%)	
	Interface implant-cement Bonded	Interface implant-cement With friction
<b>Region 1</b>	-8,7379	19,0707
<b>Region 2</b>	3,0165	8,1572
<b>Region 3</b>	1,4059	1,4581
<b>Region 4</b>	1,6676	1,6724
<b>Region 5</b>	2,4695	2,4688
<b>Region 6</b>	2,8552	2,8548
<b>Global</b>	0,4	5,97

## 4.2. Cemented configuration model

The Figure 4.4 and Figure 4.5 show the density distribution that results from the bone remodeling model for the case of cemented stem design, considering interface implant-cement bonded and with friction, respectively. The initial density distribution is also shown, which is equal for both cases, allowing analyze the evolution of each of the density distributions.

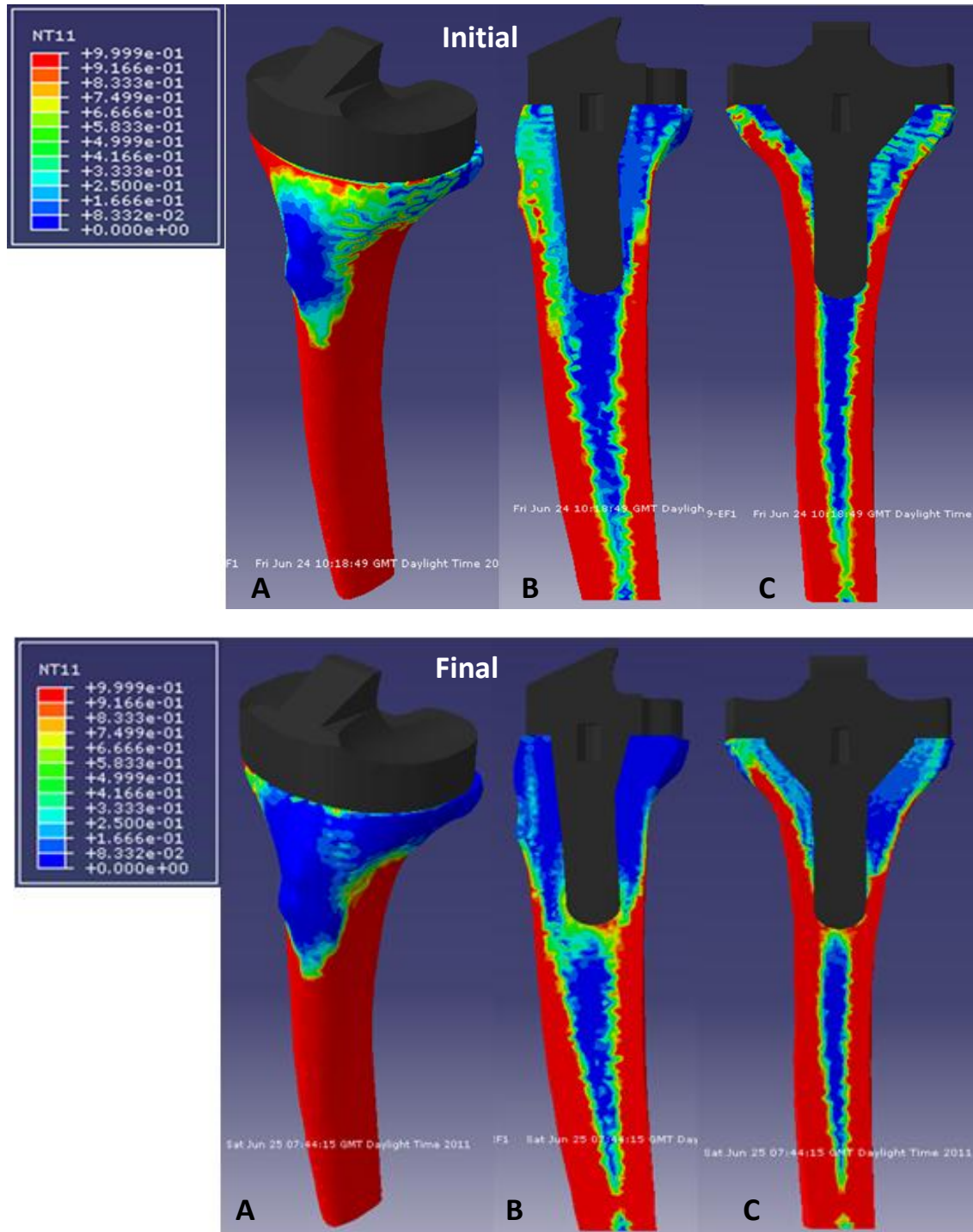


Figure 4.4 – Initial and final density distribution resulting from the model of bone remodeling for the implanted bone with cemented prosthesis (interface implant-cement bonded). Relative densities,  $\mu$ , are represented in a color scale: red=cortical bone ( $\mu \approx 1$ ) and the remaining=trabecular bone. A – Global view; B – Lateral section, right sagittal view; C – Frontal section, anterior view.

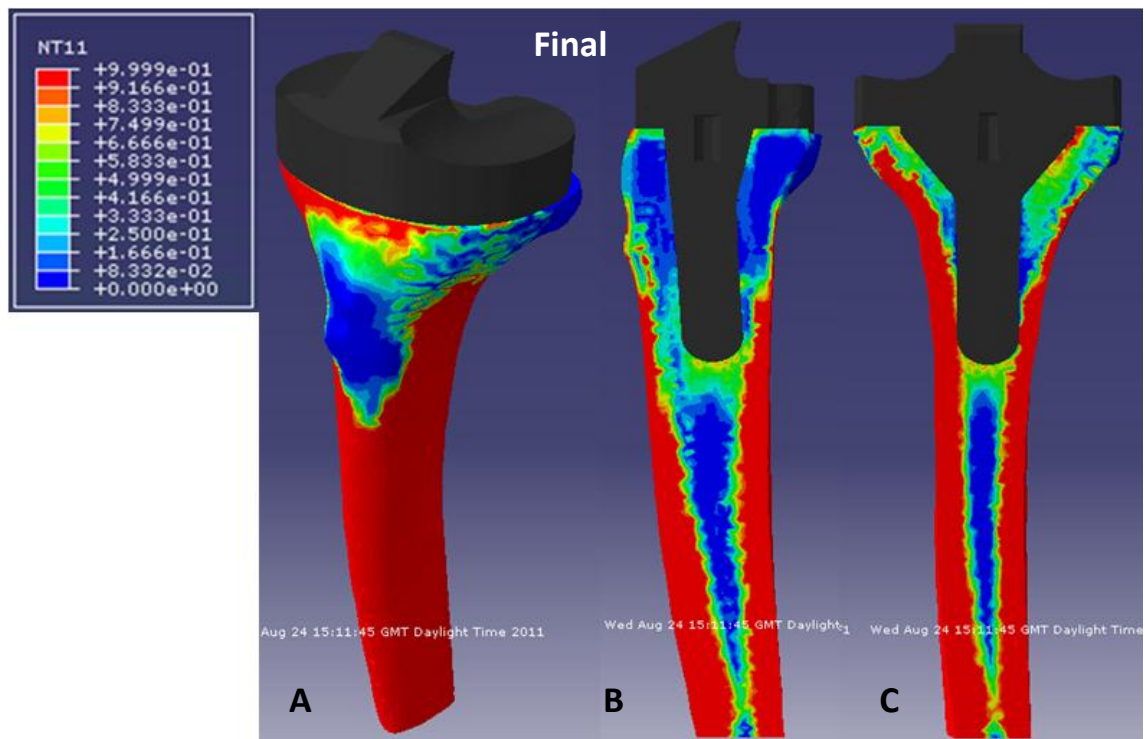
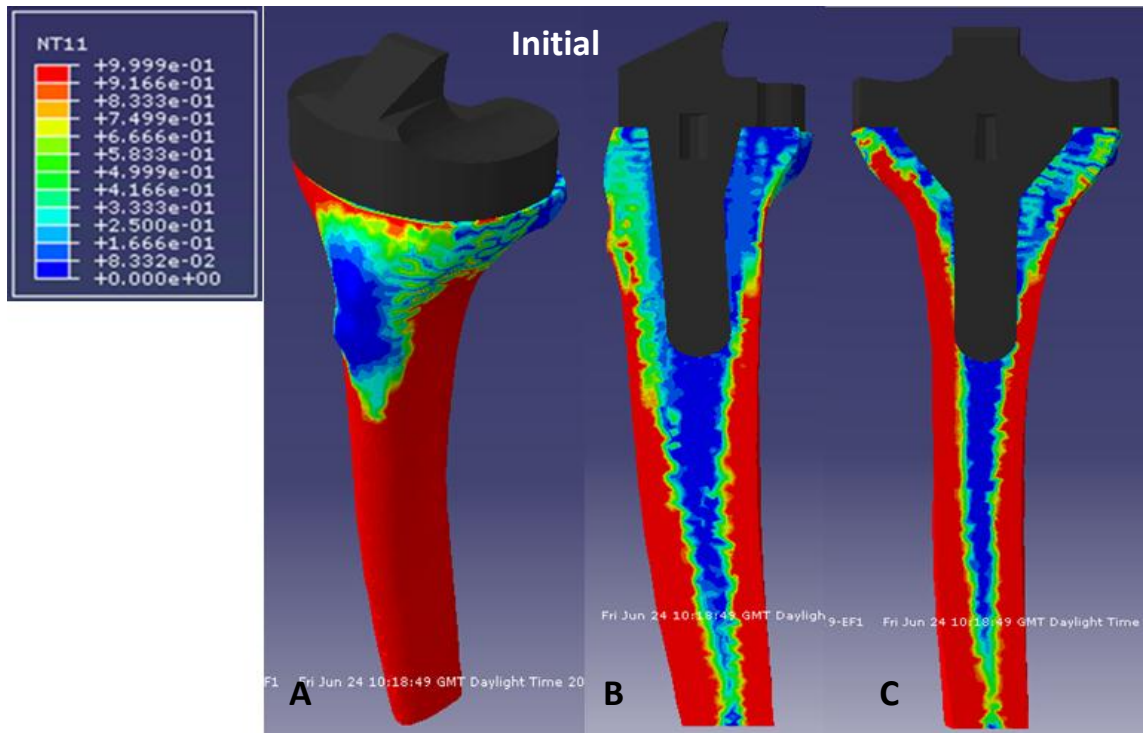


Figure 4.5 – Initial and final density distribution resulting from the model of bone remodeling for the implanted bone with cemented prosthesis (interface implant-cement with friction). Relative densities,  $\mu$ , are represented in a color scale: red=cortical bone ( $\mu \approx 1$ ) and the remaining=trabecular bone. A – Global view; B – Lateral section, right sagittal view; C – Frontal section, anterior view.

By analyzing the Figure 4.4 it is verified an elevated and generalized decrease of bone densities in the proximal regions adjacent to the prosthesis, namely regions 1 and 2. Nevertheless, in region 3 an increase of BM is shown in the area near the tip of the stem. In the

case of Figure 4.5 the same alterations are observed but with a notorious difference in the proximal bone area that surrounds the cement of the implant, in which the bone densities are increased compared with the first case. For the remaining regions (4-6) there are no observable changes for both considered cases.

The evolution of total BM of the two cases of cemented configuration, presented in Figure 4.6, reveal slightly disparate evolutions. In the case of interface implant-cement bonded there is a decrease of -9,78% in total BM, due to the contribution of bone areas adjacent to the implant, more precisely in regions 1 and 2 (see

Table 4.2), whereas the friction case exhibits a slight increase of 1,78%. The latter can be explained as a consequence of a greater bone formation than absorption near the interface with prosthesis and in the region 3 (around the tip of the stem), leading to an increase in bone density and subsequently in BM. It should also be mentioned that the process has reached the desired convergence within the number of iterations considered for both cases of interface implant-cement.

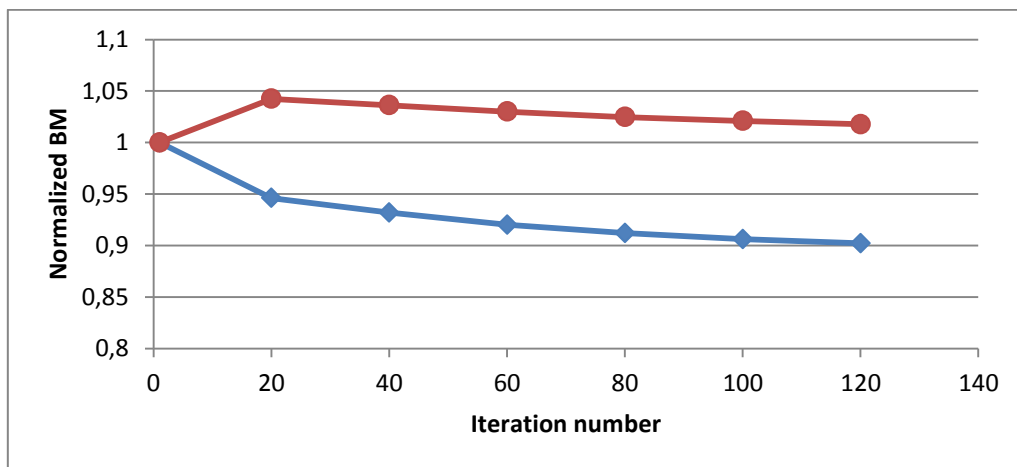


Figure 4.6 – Evolution of the total bone mass (BM) throughout the iterative process of bone remodeling, dimensionless by its initial mass, for the cemented configuration considering interface implant-cement bonded (blue) and with friction coefficient of 0,3 (red).

Table 4.2 shows an accentuated loss of BM for the proximal region underneath the tibial tray until the proximal diaphysis (region 1 and 2), from about -40% to -30%, for the case of bonded interface and, of about -10% in region 2 for the case with friction. Furthermore, as seen previously, there is a significant BM gain around the tip of the stem (region 3) of about 5% and 8% for the bonded and friction case, respectively. In all the other regions a slight and mostly not significant increase in BM is observed, for both cases. So, these results are consistent with those described above and allow inferring a possible existence of stress shielding effect in the bone for the cemented configuration, since this effect is strongly correlated with the loss of bone density.

Table 4.2– Bone mass variation for the regions 1 to 6 and for the whole bone, result of the bone remodeling process, for the cemented prosthesis considering interface implant-cement bonded.

	Bone mass variation (%)	
	Interface implant-cement Bonded	Interface implant-cement With friction
<b>Region 1</b>	-41,6776	3,9503
<b>Region 2</b>	-30,7143	-10,3232
<b>Region 3</b>	4,8321	8,4769
<b>Region 4</b>	1,8224	1,8319
<b>Region 5</b>	2,8889	2,8805
<b>Region 6</b>	3,2284	3,2188
<b>Global</b>	-9,78	1,78

### 4.3. Press-fit configuration model

The results of bone remodeling model for the case of press-fit stem design are presented in Figure 4.7 and Figure 4.8, considering interface implant-cement bonded and with friction, respectively. As in previous prosthesis cases the starting point is also shown, which is equal for the both cases, allowing analyze the evolution of each of the density distributions.

From Figure 4.7 it is possible to identify a severe and widespread loss of BM in the regions 1 to 4. However, in region 6 in the area which contacts with the tip of the stem it seems to exist a significant increase of densities of the nodes of the intramedullary canal. In region 5 there are no observable alterations. The same changes can be observed in Figure 4.8, but with a difference in regions 1 and 2, where is verified a small increase in densities in the area around the prosthesis, which is especially noticeable in the transition zone between tibial tray and stem, due to a small difference between their diameters.

The evolution of total BM for the implanted tibia, with a press-fit design, throughout the iterative process is shown in Figure 4.9. Through its observation it can be said that in both cases there is a clear decrease in total BM, which suggests that exists a generalized weakening of the bone, a consequence of increased bone resorption over formation. This happens essentially because of a decrease in the densities of bone nodes that are in areas adjacent to the prosthesis. For the case of the bonded interface the final total bone mass loss value converges to -19,39%, whereas for the case with friction interface it converges to -18,35%, i.e., the overall decline is quite similar and elevated too. It can also be considered that for both cases the convergence of the process occurs within the number of iterations used, since in the

last iterations the objective function of the process of bone remodeling presented variations in the order of  $10^{-2}$ .

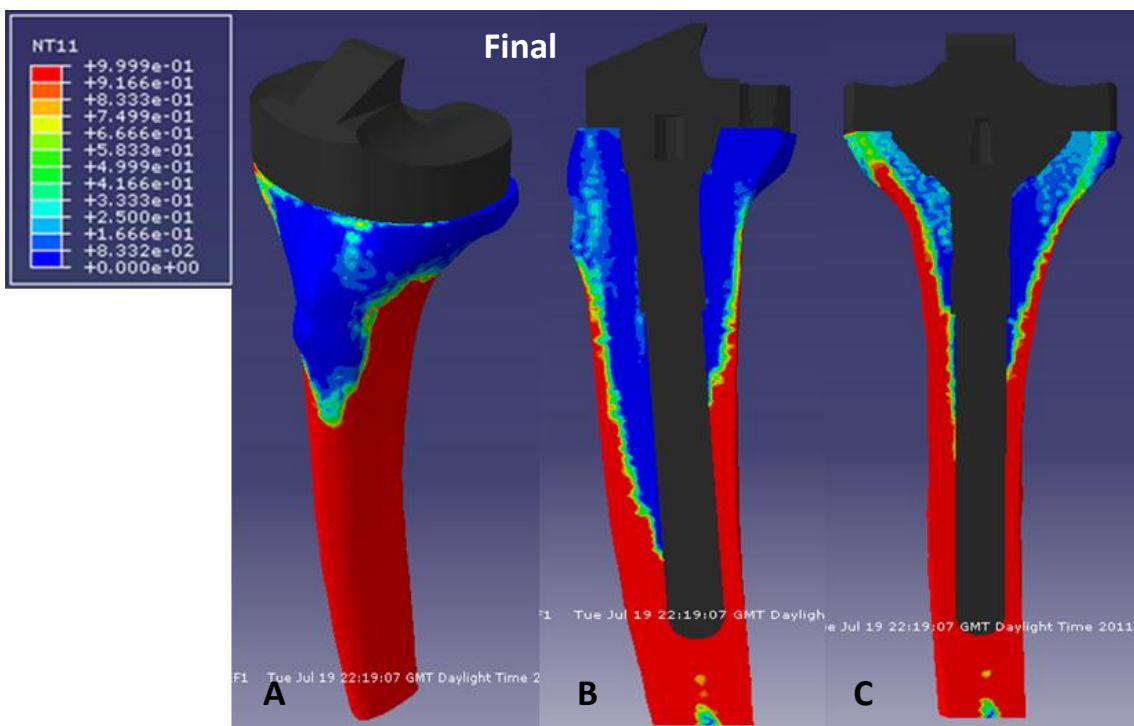
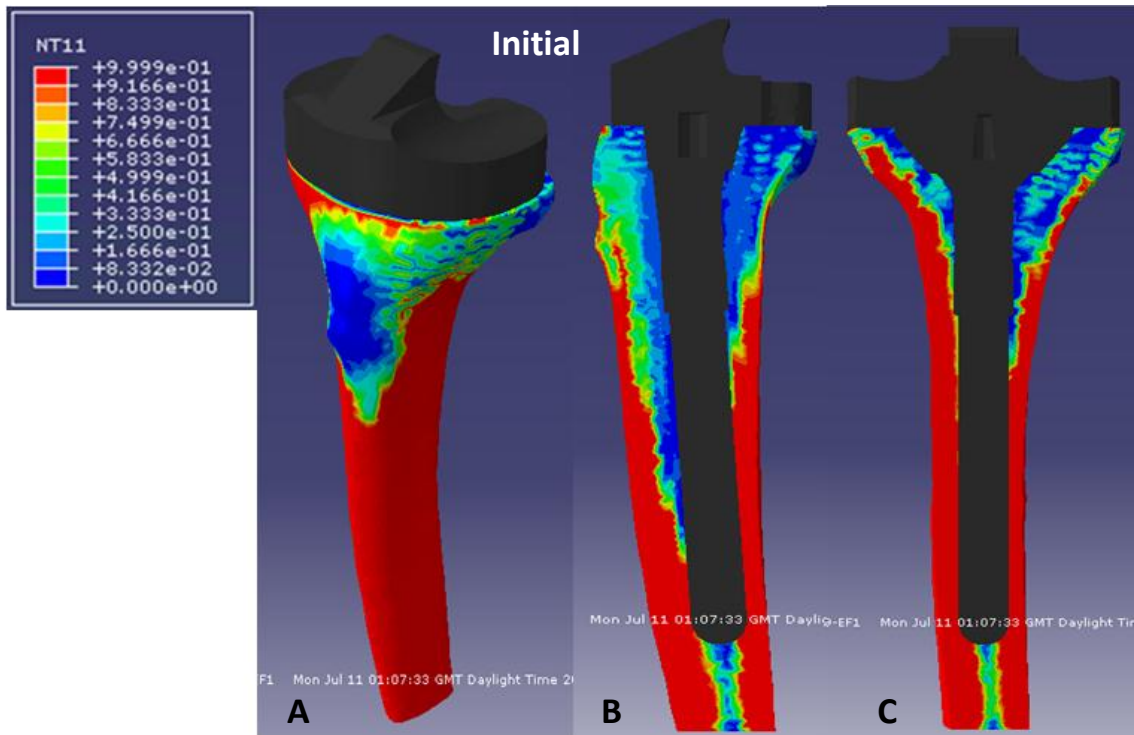


Figure 4.7 – Initial and final density distribution resulting from the model of bone remodeling for the implanted bone with press-fit prosthesis (interface implant-cement bonded). Relative densities,  $\mu$ , are represented in a color scale: red=cortical bone ( $\mu \approx 1$ ) and the remaining=trabecular bone. A – Global view; B – Lateral section, right sagittal view; C – Frontal section, anterior view.

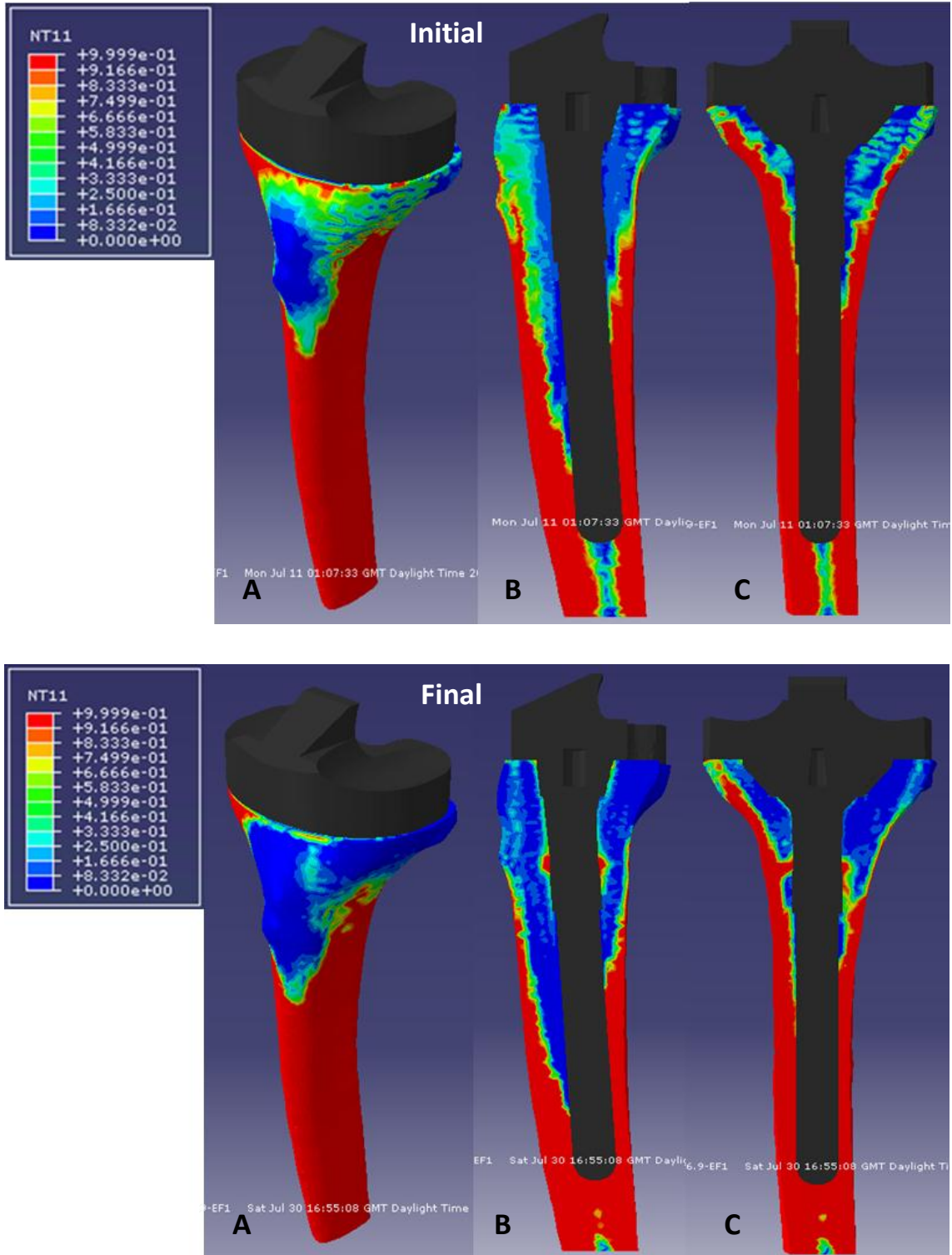


Figure 4.8 – Initial and final density distribution resulting from the model of bone remodeling for the implanted bone with press-fit prosthesis (interface implant-cement with friction). Relative densities,  $\mu$ , are represented in a color scale: red=cortical bone ( $\mu \approx 1$ ) and the remaining=trabecular bone. A – Global view; B – Lateral section, right sagittal view; C – Frontal section, anterior view.

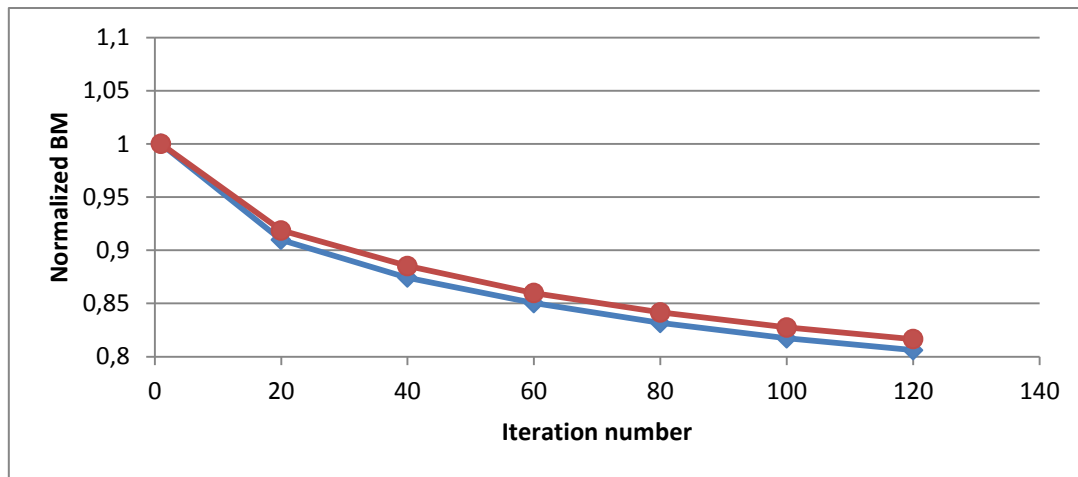


Figure 4.9 – Evolution of the total bone mass (BM) throughout the iterative process of bone remodeling, dimensionless by its initial mass, for the press-fit configuration considering interface implant-cement bonded (blue) and with friction coefficient of 0,3 (red).

Analyzing Table 4.3 it is verified for both cases an accentuated loss of BM for the regions 1 to 4, registering higher losses in the proximal area, about -40% for the case of bonded interface (region 1 and 2) and approximately -46% for the case with friction (region 1). As we move away from the proximal region the bone loss decreases, with a BM variation from about -40% to -10%, until reach region 5 where no change in BM is noticed (around 0%). In region 6 there is even an increase in BM of about 4%. All these BM losses are translated into a decrease in total BM, as seen in Figure 4.9. So, these results are consistent with those described above and are an indicative of the existence of an obvious effect of stress shielding in the press-fit configuration, i.e., this loss may reflect the bone response to altered mechanical loading conditions around the implant.

Table 4.3 – Bone mass variation for the regions 1 to 6 and for the whole bone, result of the bone remodeling process, for the press-fit prosthesis considering interface implant-cement bonded and with friction coefficient of 0,3.

	Bone mass variation (%)	
	Interface implant-cement Bonded	Interface implant-cement with friction
<b>Region 1</b>	-39,1660	-46,0414
<b>Region 2</b>	-42,2859	-30,6084
<b>Region 3</b>	-24,4517	-23,3520
<b>Region 4</b>	-9,0688	-8,4450
<b>Region 5</b>	0,0537	0,0955
<b>Region 6</b>	3,7382	3,7321
<b>Global</b>	-19,39	-18,35

#### 4.4 Stress analysis

To complement the bone remodeling analysis and compare the influence of the three different constructs of TKA on the stress distribution, the Von Mises stresses are also evaluated. The reason for choosing the Von Mises stresses to perform this comparison is because it combines the complex three-dimensional system of stresses, resulting from applied 3-D system of loads in the tibial numerical models, into a quantity called the equivalent stress, which can be compared to the yield stress of the material.

The registered Von Mises stresses for the FE models of intact and implanted proximal tibia are relative to the initial condition and to the third load case, which corresponds to physiological loading of the knee in the stance phase – 45% of the walking cycle – before toe-off (this load case as already been considered in stress analysis studies [22]). Nevertheless, an analysis of the remaining load cases would allow the same conclusions.

Regarding the consideration of two types of interface between implant-cement (bonded and with friction) in the numerical simulations, the bone remodeling model and stress analysis showed few differences in the results obtained for the cemented configuration, in particular in regions 1 and 2 and, subsequently in global BM, as it was seen in section 4.2. In Figure 4.10 the registered Von Mises stresses for the implanted proximal tibia with the two cemented configurations (bonded and with friction) are shown.

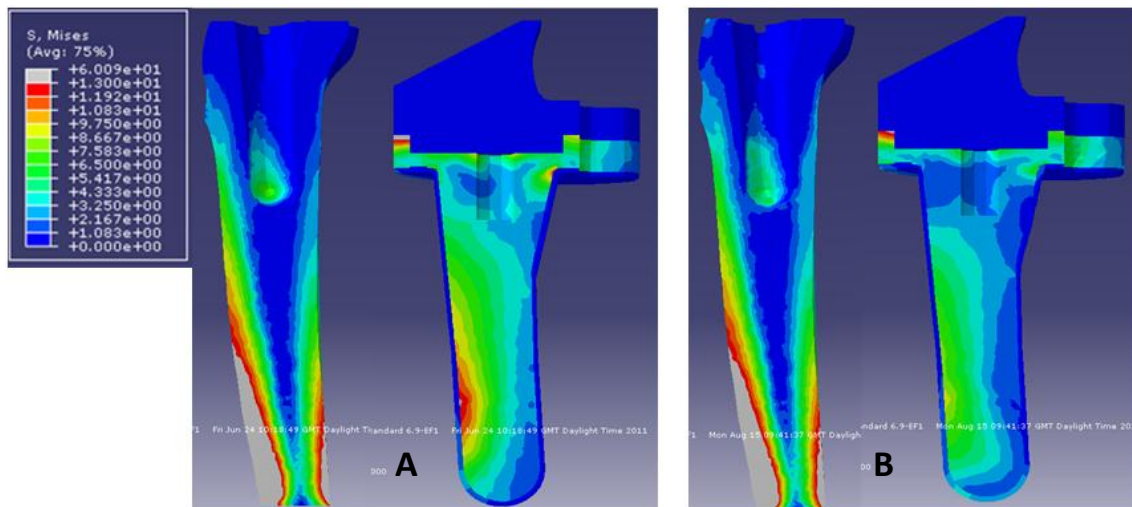


Figure 4.10 – Von Mises stresses for sagittal sections of bone and implant models for the cemented configuration, with interface implant-cement: A – bonded; B – with friction. Stresses represented in a color scale: grey=[13,60] MPa and the remaining=[0,13] MPa.

Comparing, in both cases, the Von Mises stresses (Figure 4.10) that the implant and bone are subjected; it is possible to notice for the model with bonded interface a greater demand of the stem and a lower solicitation of the bone in the proximal regions adjacent to the prosthesis. This result is consistent with the expected one, since being the implant bonded (completely linked) to the cement and, subsequently to the bone, the totality of the stresses of compression, tensile and shear are transmitted to each other [27]. This makes the stress-shielding effect of

the host bone to be increased. In other words, the mechanical loading is altered and the stresses pass and concentrate preferably on the tibial tray and stem attachment, which are stiffer materials, thereby shielding the bone and, causing the tibia to bear less stress. On the other hand, in the contact model with friction the shear stresses in the interface are partially transmitted and the tensile stresses are not transmitted between the cement and implant [27]. Thus, there is an inferior demand of the stem and a higher demand of bone, leading to an increase in bone densities (higher osteoblastic activity) adjacent to the prosthesis, especially in the interface nodes, for the friction interface case. The bone remodeling results corroborate these findings of stress analysis, with a significant decrease of bone mass in region 1 and 2 for bonded interface case. For the friction interface case there is a decrease not so significant in region 2 and in region 1 there is even an increase, i.e., this latter, cause less bone loss and justifies the fact that it presents a higher global bone mass than the bonded interface. Summarizing, in both cases there is stress shielding effect in bone, but it is more pronounced in the case of bonded contact between implant and cement.

The same results can be depicted for standard and press-fit designs for each of the contact definitions, but the differences between their bone remodeling results and stress patterns results are very little, which can be explained by the small contribution of the implant-cement interface, since there is a small area of contact between implant and cement. For this reason, only the stress results of the bonded interface are depicted next for all the three constructs of TKA. This allows analyzing the influence of the stem configuration (size of the stem) and mode of fixation (cemented/ cementless) in the existing bone loss due to the presence of implant.

The results for the stemless (standard) and stemmed tibias (cemented and press-fit) are presented in Figure 4.11 and allow one to visually compare the stresses to which the bone and implant are subjected for each of the considered configurations.

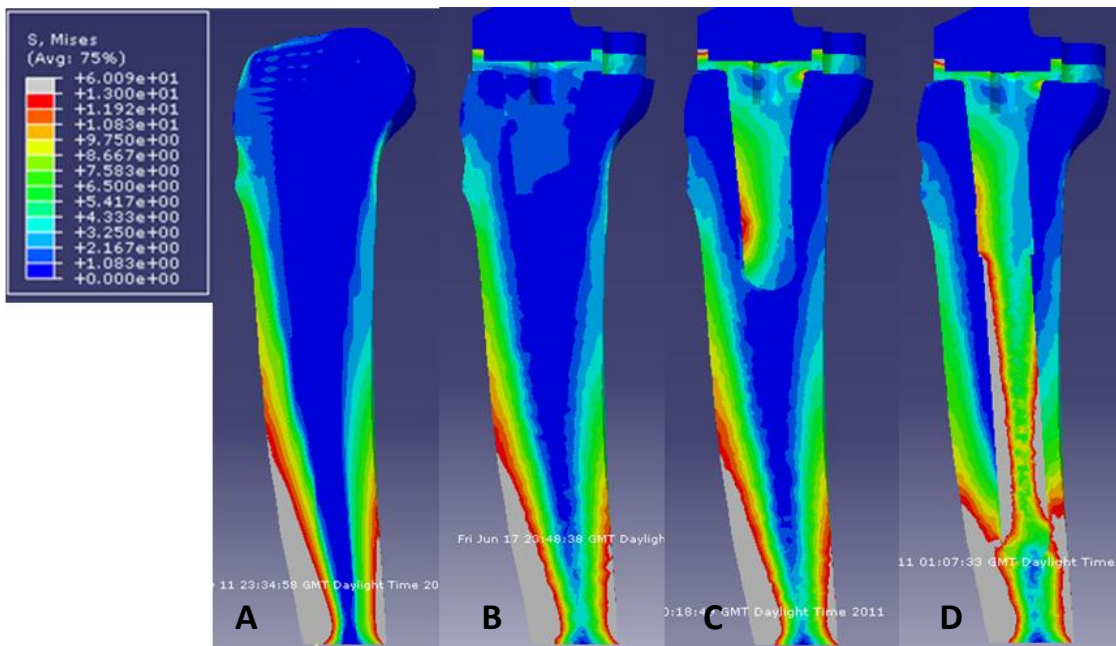


Figure 4.11 – Von Mises stresses for sagittal sections of bone and implant models with interface implant-cement bonded: A – Intact tibia; B – Standard configuration; C – Cemented configuration; D – Press-fit configuration. Stresses represented in a color scale: grey=[13,60] MPa and the remaining=[0,13] MPa.

Comparing the stresses differences between the implanted and the intact tibia it is possible to notice a significant stress shielding effect (reduction of stresses relatively to intact tibia) in the proximal bone region close to tibial tray (region 1 and 2) in the stemmed tibias (Figure 4.11 C and D). The press-fit model presented this effect a bit more extensively along the stem and until about half of it, as it can be seen in anterior and posterior regions of the middle diaphysis. In addition, it is possible to denote a progressive increase of the stresses from the keel to the stem's end. This stress shielding effect occurs because the normal bone stresses are reduced and redistributed by the implant. This means the stresses concentrate on the tibial tray and stem attachment, which are made of stiffer materials, so the strength that should originally be borne by bone is therefore undertaken and shared by the implant, causing the tibia to bear less stress (shielding bone from physiologic stress) and to have a different distribution with respect to the preoperative situation, leading to changes in bone remodeling.

This redistribution of stresses at the proximal level suggests a potential effect of bone resorption around the implant, due to osteoclastic activity in a physiological environment for the cemented and press-fit configuration. It also helps to explain the result previously obtained with the bone remodeling model, in which was verified a decrease of bone mass in the proximal region adjacent to the prosthesis (see sections 4.2 and 4.3). These numerical findings corroborate the ones published by Lonner et al. [25] that used DEXA (dual energy X-ray) to determine bone density in the proximal region of tibias after TKA and confirmed that bone density was less at the regions under the tibial tray relative to the intact bone. They also are in agreement with the experimental studies of Completo et al. [54, 62] and with the work of Nyman et al. [84] who claim that the use of tibial components with long stems (120 mm press-fit stem) provoke greater bone loss until about half of the stem, which is in accordance with the levels of stress shielding found in this study.

This proximal bone resorption after TKA is considered to occur mainly as a result of the phenomena of stress shielding of the bone by the prosthesis. This can cause a mechanical failure of the arthroplasty at long-term, with detachment of implants from bone support (tibial component loosening), which is a major and possibly increasing failure mechanism of TKR [24, 25], thereby requiring the implantation of a new prosthesis [47]. Thus, this bone loss may compromise the quality and outcome of a TKA revision.

In contrast to the stemmed tibias, Figure 4.11 B shows that the standard stem configuration evidenced a tendency for maintaining the stresses experienced by the bone, which can promote a physiological bone remodeling process of the host bone. This result is consistent with the one previously obtained by the bone remodeling model (section 4.1), where no bone mass loss was recorded for both of standard configurations (except for the region 1 of the bonded interface). These results also demonstrate a minor or absent effect of stress shielding with short stems relatively to the long stems for the cementless fixation mode, which is consistent with the study of Completo et al. [62]. So, one can conclude that apparently the length of stem is a major concern to proximally stress shielding effect. The increases on stem lengths, increase stiffness

differences and, consequently, there are more significant changes in bone quality (loss of bone density).

In addition to the effect of stress shielding, also stress concentrations (increase of stress relatively to intact tibia) were assessed through FE analyses closely to the distal tip of cemented and press-fit tibial stem designs. The first can be explained by the load transfer capacity of the cemented stem to the distal region, which is the result of the rigid bond between the cemented stem, cement mantle and diaphyseal bone around the stem, as explained above [73]. The latter is more evident and does not have the same cause of the cemented stem. The press-fit stem does not have a great load sharing capacity because this stem is only in contact with friction with bone without interference (diameter of stem = diameter of reamed bone). So, this localized increase of stresses in press-fit stem tip can be related with the tip stem fulcrum effect on the bone. In other words, this happens due to the bending moment generated in the condylar surface, in which the force moment pushes the tip of stem against the bone and provokes stress concentration around the tip region [54]. This can explain the stress shielding effect of the press-fit configuration, since the bending moment generated in the condylar surfaces is partially supported by the press-fit stem, originating a reduction of the bending moment through the bone along the stem length, and consequently, reduce bone stresses in these areas. In addition, this increased bending and torsional loads acting on the implant may jeopardize the fixation of the tibial tray at revision TKA (Albrektsson et al., 1990; Sharkey et al., 2002) [22].

The localized increase of stresses observed in bone near the stem's end, for stemmed tibias, can partially explain the clinical finding of the pain, at the distal end of stem after revision TKA, especially for the long stem where the stress values increase more relative to the intact tibia (Barrack et al., 1999, 2004; Haas et al., 1995). Barrack et al. (1999) reported 14% of patients with localized pain in tibia with press-fit stems. Similarly, Haas et al. [70] described that 20% of patients with long stems had pain. Moreover, this augments of stress at stem tip can increase the risk of tibial fracture at this region and can induce hypertrophy of the cortical bone, i.e., the increase in loads on the bone stimulates osteoblastic activity locally (Peters et al., 2005), and may lead to localized pain [54, 62]. The study of Completo et al. [62] presents the same findings (see Figure 4.12), where a scintigraphy of a painful implanted knee showed local osteoblastic activity (metabolic alterations) and radiographs evidence bone ossification (increase of density locally) at the distal tip of the stem due the stress concentration. This stemmed revision implant was a press-fit stem with 115 mm of length in titanium material, identical to the model studied here.

This same finding was captured in the density distribution resulting from the model of bone remodeling for the implanted bone with press-fit design (Figure 4.7 and Figure 4.8) and, not so pronounced, with cemented prosthesis (Figure 4.4 and Figure 4.5), where an increase of bone mass is shown in the area surrounding the stem tip. Thus, the increase of bone stresses at tip region stimulates locally osteoblastic activity and it is plausible an increase of locally bone density (ossification). These results are once again in agreement with the results obtained at the

University of Aveiro by Completo et al. [62] who studied the stress shielding through the FE analyses of different tibial stem designs. This work also contributes to corroborate the results obtained through the present study.

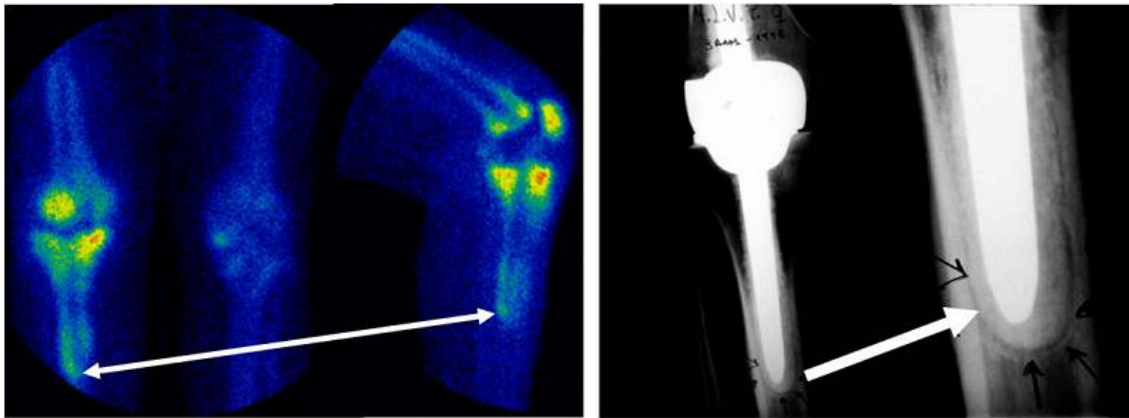


Figure 4.12 – Pictures of painful implanted knee prosthesis with a press-fit stem with 115 mm, identical to the model used in this study: scintigraphy (left) and radiography (right) [62].

Currently, there is a debate about the optimal design of the implant used in TKA procedure, in particular with respect to the configuration (stem length) and mode of fixation of the stem [85]. The reported alterations of proximal stress shielding and stress concentrations close to the distal tip, together with the consequent changes in bone adaptation, resulting from stemmed prosthetic implantation have become a clinical problem, compromising the stability of the implant and may contribute to prosthesis failure. The results of this study suggest that these problems are largely related with the use of stemmed tibial component (cemented and press-fit stem), in which a greater degree of bone loss is obtained compared to the un-stemmed design (standard), due to decreased proximal loading. This fact may explain the excellent long-term results generally achieved with standard configuration in primary TKA and makes this design the most advisable when carrying out TKA. However, this is only possible when the bone quality allows fixing the prosthesis, which is generally not the case when performing a revision TKA surgery, where the limited bone stock remaining requires the stemmed augments to improve fixation, alignment and stabilize the implant, enhancing the resistance to lift-off and shear [85].

Several clinical follow up studies have evaluated the differences of stemmed implants used in revision TKAs, but unfortunately, consensus has not emerged on which is the optimum method of fixation of the prosthetic components to bone [15]. Whiteside and Pafford [86] evaluated the load-bearing capacity of 2 stemmed implants, 1 shorter cemented and 1 press-fit of extended-length, and found proximal stress shielding of an equal magnitude with each design. More recently Fehring et al. reported a higher rate of loosening with press-fit stems compared to cemented stems [87]. In the end, 93% of cemented stems (100 of 107) were considered stable radiographically compared to only 71% (67 of 95) of the cementless stems. These authors urged caution in using cementless stems for fixation in revision TKA. Nowadays, the use of cement for fixation of at least a portion of the tibial component is well accepted in

most total knee procedures; however, when evaluating whether the stemmed portion should be cemented or press-fit, there is not a simple answer because there are clear advantages and disadvantages of each approach [60].

The cemented stem provides superior fixation to the contiguous bone, being a good option in the short term and is ideal for large diaphyses. It is also suitable for elderly or infirm patients, where damaged or sclerotic (bone deficiency) metaphyseal bone requires extension of cement into the canal to provide adequate fixation [23, 60, 85]. However, cement suffers several drawbacks, such as potential thermal necrosis during polymerization, cement fatigue failure because of cyclic loading, and difficulty in removing cemented components if further revision is required. It also has three 'weak-link zones' (the cement-implant interface, the cement-bone interface, and the cement mantle itself), which are potential sites for the initiation of loosening [23]. These findings have encouraged the development of cementless alternatives.

Despite, the absence of cement around the press-fit stem, it achieves a sufficient stability similar to a smaller cemented stem and are easy to remove, avoiding a major loss of bone if the implant has to be removed in re-revision case [70]. Nevertheless, a greater incidence of end-of-stem pain and an increase in stem-to-bone stiffness ratio has been positively correlated with stress shielding sense in the cementless configuration [23].

In the present study the cemented configuration was the one who provoked less bone resorption in the metaphysis and proximal diaphysis of the bone, when compared to the press-fit stem which had the biggest loss of global bone mass, due to a bit more extensive stress-shielding effect along the stem. This may be explained by the difference in the stems length and not only on the fixation mode difference. To study the influence of fixation mode in the bone resorption some tests should be performed with stems of the same length.

However, as it was seen, the choice between the use of cemented and uncemented stems (mode of fixation), as well as, the length of the stem remains controversial [60]. There is continuing debate regarding the best strategy for stem. Radnay and Scudery [88] advised that the length of the stem should be determined by the integrity of the residual bone and the diameter of the intramedullary canal. As the size of defect increases or the degree of support decreases, a longer stem should be used. They suggested a short cemented stem for host bone of poor quality, and a long press-fit stem engaging the diaphysis for patients with bone of higher quality. In general, cementless stems are indicated when there is both good diaphyseal bone of appropriate geometry to allow an adequate press-fit and adequate metaphyseal bone to allow for a good condylar cement interface [60].

Finally, the clinical stem choice is not firstly guided by the mechanical bone effect of stem, but many times by clinical reasons like the age and level of activity of the patient, the extent and distribution of bone loss, bone geometry, the quality of the remaining bone, the experience of the surgeon, implant design and technical surgery procedure [62, 85].

In summary, knee prosthesis is a device that still lacks of adequate design solutions. The obtained stress shielding and stress concentrations, and subsequent bone adaptation due to

the insertion of tibial component are frequent numerical and clinical evidences, which are intimately related to the design of the prosthesis and the stems used in revision TKA [62]. These bone adaptation alterations due to the insertion of tibial component can play an important role on the longevity of present TKA designs and are a key factor in their failure. Thus, the previously reported knowledge of the mechanical behavior of the implant-bone set is very important to predict the performance of the prosthesis and can be a useful adjunct for the design of future implants, possibly providing better conditions for longevity of the tibial component.

## 5. Conclusion and future developments

This work analyzed the bone remodeling of the tibia after a TKA, using the FEM and the bone remodeling model developed in IST [40, 43, 58, 63]. The results were compared with experimental results of Completo et al. from the University of Aveiro [54, 62]. The main aim was to evaluate the influence of stem configuration and fixation mode of the tibial component in the existent bone resorption due to the presence of the implant.

Initially, the work involved the geometric and FE modeling of the tibia and tibial component of knee prosthesis. The three-dimensional model of the proximal tibia was obtained using CT scans of the human body, which allowed assigning more realistic bone properties. The models of the different tibial components of TKA prostheses were developed based on the real models and with the support of Depuy Technical Monograph.

In a second phase the bone remodeling model was used to obtain the bone density distribution for the intact tibia. In this test the model converged to a solution with high similarity to the morphology of the real tibia. For a better reproduction of reality, the densities obtained in the model of intact bone were used as the initial density distribution for models with implant. Then, the model was applied to implanted tibia with three different tibial stem configurations (standard, cemented and press-fit), in order to observe the bone remodeling when loads are redistributed due to the insertion of implant.

This study showed that the mechanical behavior and, subsequently, the density distribution of bone around tibial tray and stem in revision TKA are dependent of the stem configuration (length) and fixation mode. Through FE analyses it was discovered that the use of tibial components with long stems (cemented and press-fit) is accompanied by a clear stress shielding of the proximal tibia and over the length of the stem until about half of it. This reduction of stresses, results in a significantly density reduction of bone with a consequently decrease in bone mass in regions adjacent to the prosthesis. This proximal bone resorption may contribute to the persistence of tibial component loosening as a major threat to survivorship. Results in long stems also showed a strong negative effect of stress concentrations close to the distal tip of the stem and a respective increase in bone mass in the tip region. This means that, although the use of a stem provides excellent resistance to lift-off and shear, it comes at a price. For the standard configuration (short stem) a tendency for maintaining the stresses experienced by the bone was noticed, which can promote a physiological bone remodeling process of the host bone, and can induce the short stems like the best option. Thus, consideration should be given to using shorter tibial stems, less cement, or alternative designs that avoid long-stem fixation, for increasing the probability of successful TKA procedure and injury prevention.

The results of this study support that short stems produce a minor effect in bone in comparison with long stems in terms of stress shielding and stress concentration. However, the clinical stem choice is not firstly guided by the mechanical bone effect of stem, but many times by clinical reasons like the age and level of activity of the patient, the extent and distribution of

bone loss, bone geometry, the quality of the remaining bone, the experience of the surgeon, implant design and technical surgery procedure.

To conclude, an overall analysis of both stress and bone remodeling results from the FE analyses of this study, allows concluding that they were consistent with each other and, with various clinical and numerical studies presented in the literature, which were shown here.

Some of the limitations of this study are related to the loads applied as input in the computational model of bone remodeling. The results were obtained using a multiple load formulation with six load cases, which correspond to the most significant loads on the tibia. However, a large number of loads should be considered for a better accuracy of the results. The number of load cases is a compromise with computational cost. Furthermore, these physiologic loads obtained by instrumented prosthesis were a simplification in terms of the total loads applied to the tibia, since forces associated to the structural links (tendons, ligaments and other soft tissues) between femur and tibia were not considered. Additionally, it needs to be mentioned that they were only referring to a single subject with a specific implant design. In the future determining all biological loads applied in the tibia and including them in the bone remodeling model is essential to accomplish these load dependent biomechanical studies which may yield even more reliable results. Thus, improved implant design could emerge from detailed knowledge of *in vivo* loading during a variety of activities.

To complement this work, some additional parameters should be considered in future studies. In particular, stem's augments with different lengths, mode of fixation and materials, and different designs of tibial trays should be analyzed. These complementary studies should help to understand what implant is closer to optimum (stress levels close to physiological ones, less alterations in bone quantity and quality) and what is the parameter that has a more pronounced effect in bone. For example, to reduce the proximal stress shielding effect, it has been suggested to use an implant with a material with elastic properties identical to those of natural bone that surrounds it [24]. Another attempt that could be a viable alternative to more common fixation techniques of long stems is the use of distal screws which improve the load transfer from implant to bone and help to dissipate the stresses concentrations at the stem tip that causes bone hypertrophy. This way, they provide means of fixing a small diameter stem, which helps to minimize stress shielding, and avoids the multiple problems associated with fully cementing prosthesis [23]. Finding a good balance between these designs parameters and mechanical bone effect is very challenging and can be a key factor to enhance the longevity of the tibial component.

Finally, this work is the result of a wider co-operation between medical doctors and engineers. The aim of this collaboration is to develop and improve techniques to choose the appropriate implant for the patient condition. This will allow reduction of risks related to operations and improvement of post-operation outcomes.

## REFERENCES

- [1] Palastanga, N. and Field D., *Anatomy and human movement structure and function*. 4<sup>th</sup> ed. 2002: Butterworth-Heinemann.
- [2] Kutzner, I., Heinlein, B., F. Graichen, A. Bender, A. Rohlmann, A.M. Halder, A. Beier, and G. Bergmann, *Loading of the knee joint during activities of daily living measured in vivo in five subjects*. J Biomech. 2010 Aug 10;43(11):2164-73.
- [3] Taylor, R., Heller, O., Bergmann, G., Duda, N., *Tibio-femoral loading during human gait and stair climbing*. Journal of Orthopaedic Research 22 (2004) 625-632.
- [4] Tortora, G. and Derrickson, B., *Principles of anatomy and physiology*. 12th ed. 2009: John Wiley & Sons, Inc.
- [5] Darrow, M., *The Knee Sourcebook*. 1st ed. 2002: McGraw-Hill.
- [6] Bei, Y., *Dynamic simulation of knee joint contact during human movement*. Dissertation for the doctor degree, University of Florida, 2003.
- [7] Carvalho, F., *Tratamento da gonartrose numa abordagem cirúrgica*, Dissertation for the master degree, Universidade da Beira Interior, 2010.
- [8] NIH Consensus Statement on total knee replacement. NIH Consens State Sci Statements 2003 Dec 8-10;20(1):1-34.
- [9] Shetty, A.A., A. Tindall, P. Ting, and F.W. Heatley, *The evolution of total knee arthroplasty. Part I: introduction and first steps*. Current Orthopaedics, 2003. 17: p. 322-325.
- [10] Wyld, V., Dieppe, P., Hewlett, S., Learmonth, I.D., *Total knee replacement: Is it really an effective procedure for all?*. The Knee 14 (2007) 417–423.
- [11] Pryde, A., *Physical Rehabilitation*, 2007, Pages 219-250.
- [12] Lonner, H., Frank, Pedlow, Siliski, *Total Knee Arthroplasty for Post-Traumatic Arthritis*. The Journal of Arthroplasty Vol.14 No. 8 1999.
- [13] Yercan, H., Selmi, T., Sugun, T., Neyret, P., *Tibiofemoral instability in primary total knee replacement: A review, Part 1: Basic principles and classification*. The Knee 12 (2005) 257–266.
- [14] Lombardi, A., Berasi, C., Keith, Berend, R., *Evolution of Tibial Fixation in Total Knee Arthroplasty*. The Journal of Arthroplasty Vol.22 No.4 Suppl.1 2007.
- [15] Peters, L., Erickson, J., Kloepper, G., Mohr, A., *Revision Total Knee Arthroplasty With Modular Components Inserted With Metaphyseal Cement and Stems Without Cement*. The Journal of Arthroplasty Vol. 20 No. 3 2005.
- [16] Delaunay, C., Blatter, G., Canciani, J., Jones, D., Laffargue, P., *Survival analysis of an asymmetric primary total knee replacement: A European multicenter prospective study*. Orthopaedics & Traumatology: Surgery & Research (2010) 96, 769-776.
- [17] Kurtz, S., Ong, K., Lau, E., Widmer, M., Maravic, M., *International survey of primary and revision total knee replacement*. International Orthopaedics (SICOT) DOI 10.1007/s00264-011-1235-5, (2011).
- [18] Heinlein, B., I. Kutzner, F. Graichen, A. Bender, A. Rohlmann, A.M. Halder, A. Beier, and G. Bergmann, *ESB Clinical Biomechanics Award 2008: Complete data of total knee replacement*

loading for level walking and stair climbing measured in vivo with a follow-up of 6-10 months. Clin Biomech (Bristol, Avon), 2009. 24(4): p. 315-326.

[19] Kennedy, L., Newman, J., Ackroyd, C., Dieppe, P., *When should we do knee replacements?*. The Knee 10 (2003) 161–166.

[20] Kane RL, Saleh KJ, Wilt TJ, Bershadsky, B, MacDonald RM, *Total Knee Replacement. Evidence Report/Technology Assessment*. No. 86 (Prepared by Minnesota Evidence-based Practice Center, Minneapolis, Minnesota). AHRQ Publication No.04-E006-1. Rockville, MD: Agency for Healthcare Research and Quality. November 2003.

[21] Singh, J., *Epidemiology of Knee and Hip Arthroplasty: A Systematic Review*. The Open Orthopaedics Journal, 2011, 5, 80-85.

[22] Completo, A., Rego, A., F. Fonseca, A. Ramos, C. Relvas, J.A. Simões, *Biomechanical evaluation of proximal tibia behaviour with the use of femoral stems in revision TKA: An in vitro and finite element analysis*. Clinical Biomechanics 25 (2010) 159–165.

[23] Nyman, J., Hazelwood, S., Rodrigo, J., *Long Stemmed Total Knee Arthroplasty With Interlocking Screws: A Computational Bone Adaptation Study*. University of California (2004).

[24] Anthony, G., Raso, V., Liggins, A., Amirfazli, A., *Contribution of loading conditions and material properties to stress shielding near the tibial component of total knee replacements*. Journal of Biomechanics 40 (2007) 1410–1416.

[25] Lonner JH, Klotz M, Levitz C, Lotke PA. *Changes in bone density after cemented total knee arthroplasty: influence of stem design*. J Arthroplasty 2001;16(1):107–11.

[26] Sierra, R.J., Pagnano, M.W., Trousdale, R.T., *Reoperations after 3200 revision total knee replacements: rate, etiology, and lessons learned*. In: Proceedings of the 70th Annual Meeting of the AAOS. New Orleans, (2003) p. 40.

[27] Completo, A., Rego, A., F. Fonseca, J.A. Simões, *Modelo numérico e experimental da tibia intacta e com componente tibial da prótese do joelho*. Universidade de Aveiro.

[28] Levangie, P.K. and C.C. Norkin, *Joint Structure and Function - A comprehensive analysis*. 4th ed. 2005, Philadelphia: F. A. Davis Company.

[29] L. Drake, Vogl W., Mitchell, A., *Gray's Anatomy for students*. Elsevier/Churchill Livingstone, 2007.

[30] Darwish, S.M. and A. Al-Samhan, *The effect of cement stiffness and tibia tray material on the stresses developed in artificial knee*. International Journal of Adhesion & Adhesives, 2008. 28: p. 120-125.

[31] Rauch, F., Travers, R., Glorieux, F., *Intracortical remodeling during human bone development - A histomorphometric study*. Bone 40 (2007) 274–280.

[32] Peterson, M., Riggs, M., *A physiologically based mathematical model of integrated calcium homeostasis and bone remodeling*. Bone 46 (2010) 49–63.

[33] Proff, P., Romer, P., *The molecular mechanism behind bone remodelling: a review*. Clin Oral Invest (2009) 13:355–362, DOI 10.1007/s00784-009-0268-2.

[34] Zumsande, M., Stiefs, D., Siegmund, S., *General analysis of mathematical models for bone remodeling*. Bone 48 (2011) 910–917.

- [35] Sims, N., Gooi, J., *Bone remodeling: Multiple cellular interactions required for coupling of bone formation and resorption*. *Seminars in Cell & Developmental Biology* 19 (2008) 444–451.
- [36] Pivonka, P., Zimak, J., Smith, D., *Model structure and control of bone remodeling: A theoretical study*. *Bone* 43 (2008) 249–263.
- [37] Robling, A., Castillo, A., Turner, C., *Biomechanical and Molecular Regulation of Bone Remodeling*. *Annual Rev. Biomed. Eng.* 2006. 8:455–98.
- [38] Ronald, R., *Modeling and remodeling in bone tissue*. Eindhoven: Technische Universiteit Eindhoven, 2005. Proefschrift. - ISBN 90-386-2856-0.
- [39] Hadjidakis DJ, Androulakis, *Bone remodeling*. *Ann N Y Acad Sci.* 2006 Dec;1092:385-96.
- [40] Fernandes, P., Rodrigues, H., Jacobs, C., *A model of bone adaptation using a global optimisation criterion based on the trajectorial theory of Wolff*. *Comput Methods Biomech Biomed Engin.* 1999;2(2):125-138.
- [41] Huiskes, R., Weinans, H., Grootenboer, H.J., *Adaptive bone-remodeling theory applied to prosthetic-design analysis*. *Journal of Biomechanics* 20 (1987), 1135-1150.
- [42] Pearson, O., Lieberman, D., *The Aging of Wolff's "Law": Ontogeny and Responses to Mechanical Loading in Cortical Bone*. *Yearbook of physical anthropology* 47:63–99 (2004).
- [43] Fernandes, P., Rodrigues, H., *A material optimization model for bone remodeling around cementless hip stems*. *ECCM'99* (1999).
- [44] Creaby, M., Wang, Y., *Dynamic knee loading is related to cartilage defects and tibial plateau bone area in medial knee osteoarthritis*. *Osteoarthritis and Cartilage* 18 (2010) 1380-1385.
- [45] Toronto Arthroplasty Research Group Writing Committee, *Variability in Physician Opinions About the Indications for Knee Arthroplasty*. *The Journal of Arthroplasty* Vol. 26 No. 4 2011.
- [46] Lima, D., Patil, S., *In vivo knee moments and shear after total knee arthroplasty*. *Journal of Biomechanics* 40 (2007) S11–S17.
- [47] Judas, F., Costa, P., Teixeira, L., *Procedimentos cirúrgicos do joelho na artrite reumatóide*. *Acta Reum. Port.* 2007;32:333-339.
- [48] Chou, D., Swamy, G., *Revision of failed unicompartmental knee replacement to total knee replacement*. Article in press (2011).
- [49] *Unicondylar Knee Replacement Options for Osteoarthritis of the Knee* [cited July, 2011] [http://www.hss.edu/conditions\\_partial-knee-replacement.asp](http://www.hss.edu/conditions_partial-knee-replacement.asp).
- [50] *P.F.C Sigma Knee System: Technical Monograph*. 2000, England: DePuy International Ltd.
- [51] *P.F.C. Sigma Knee System: Primary cruciate-retaining and cruciate-substituting procedures*. 2000, England: DePuy International Ltd.
- [52] *Knee replacement* [cited June 2011] [http://www.kneeclinic.info/problems\\_total\\_replacement.php](http://www.kneeclinic.info/problems_total_replacement.php)
- [53] Gamelas J., *Artroplastias totais do joelho. Estudo comparativo de dois métodos de alinhamento no posicionamento do componente tibial*. Tese de Doutoramento, FCMUNL, Lisboa, 2006.

- [54] Completo, A., Rego, A., F. Fonseca, J.A. Simões, *Strain shielding in proximal tibia of stemmed knee prosthesis: Experimental study*. Journal of Biomechanics (2007), doi:10.1016/j.jbiomech.2007.10.006.
- [55] Knee: Total Knee Arthroplasty Procedure Overview [cited July 2011] <http://www.weberorthopedics.com/knee/knee-procedure.php>.
- [56] Bellemans, J., M.D. Ries, and J. Victor, *Total knee arthroplasty: a guide to get better performance*, 2005, Germany: Springer.
- [57] Li, M., Nilsson, K., *The Effect of the Preoperative Bone Quality on the Fixation of the Tibial Component in Total Knee Arthroplasty*. The Journal of Arthroplasty Vol. 15 No. 6 2000.
- [58] Fernandes P. R., Folgado J., Jacobs C and Pellegrini V., *A contact model with ingrowth control for bone remodelling around cementless stems*. Journal of Biomechanics 35(2) (2002) pp. 167-176.
- [59] Sparmann, M., Wolke, B., Czupalla, *Positioning of total knee arthroplasty with and without navigation support*. J Bone Joint Surg [Br] 2003;85-B:830-5.
- [60] Mabry, T., Hanssen, A., *The Role of Stems and Augments for Bone Loss in Revision Knee Arthroplasty*. The Journal of Arthroplasty Vol. 22 No. 4 Suppl. 1 June 2007.
- [61] Bozic KJ, Kurtz SM, Lau E, *The epidemiology of revision total knee arthroplasty in the United States*. Clin Orthop Relat Res. 2010 Jan;468(1):45-51.
- [62] Completo, P., Talaia, A., F. Fonseca, J.A. Simões, *Relationship of design features of stemmed tibial knee prosthesis with stress shielding and end-of-stem pain*. Materials and Design 30 (2009) 1391–1397.
- [63] Fernandes, P., Rodrigues, H., *Optimization models in the simulation of the bone adaptation process*, “Computational Bioengineering Current trends and applications”, M. Cerrola, M. Dobalré, G. Martínez, B. Calvo, Imperial college press (2004).
- [64] Cartraud, P., Messenger, T., *Computational homogenization of periodic beam-like structures*. International Journal of Solids and Structures 43 (2006) 686–696.
- [65] Guedes, J., Kikuchi, N., *Preprocessing and postprocessing for materials based on the homogenization method with adaptive finite element methods*. Computer methods in applied mechanics and engineering (Elsevier Science Publishers) 83 (1990): 143-198.
- [66] Folgado, J., Fernandes, P., Rodrigues, H., *Topology Optimization of Three-Dimensional Structures under Contact Conditions*. IDMEC – IST, Portugal.
- [67] Ribeiro, N., Fernandes, PC, Lopes, DS, *3-D solid and finite element modeling of biomechanical structures – A software pipeline*. 7th EUROMECH Solid Mech. Conference (2009).
- [68] Lopes, D., *Geometric Modeling of Human Structures Based on CT Data – a Software pipeline*. IDMEC – IST, Portugal (2006).
- [69] Chan, A., *Biomechanical analysis of the tibial tray design in TKA: comparison between modular and offset tibial trays*. IDMEC – IST, Portugal (2009).
- [70] Haas SB, Insall JN, Montgomery W, Windsor RE. *Revision total knee arthroplasty with use of modular components with stems inserted without cement*. J Bone Joint Surg Am 1995;77:1700–7.

- [71] Reddy, J.N., *An Introduction to the Finite Element Method*. 3rd ed. 2006, New York: McGraw-Hill.
- [72] Orias, A., Deurling, J., Landrigan, M., *Anatomic variation in the elastic anisotropy of cortical bone tissue in the human femur*. *Journal of the mechanical behavior of biomedical materials* (2009) 255-263.
- [73] Completo, A., J.A. Simões, F. Fonseca, *The influence of different tibial stem designs in load sharing and stability at the cement-bone interface in revision TKA*. *The Knee* 2008.15:p.227-232
- [74] Mann, K., Bartel, D., Wright, T., *Coulomb frictional interfaces in modeling cemented total hip replacements: a more realistic model*. *J. Biomechanics*. Vol. 28.No.9.1067-1078.(1995).
- [75] Viceconti, M., Muccini, R., *Large-sliding contact elements accurately predict levels of bone implant micromotion relevant to osseointegration*.*Journal of Biomechanics* 33 (2000) 1611 1618
- [76] Jeffers, J., Browne, M., *Cement mantle fatigue failure in total hip replacement: Experimental and computational testing*. *Journal of Biomechanics* 40 (2007) 1525–1533.
- [77] Huiskes, R., Verdonschot, N., *The effects of cement-stem debonding in THA on the long-term failure probability of cement*. *J. Biomechanics* Vol.30 No.8, pp. 795-802, 1997.
- [78] *Abaqus - Theory Manual*, Version 6.8. 2008: Dassault Systemes.
- [79] *Orthoload: Loading of orthopaedic implants*. [cited May, 2011]; Available from: <http://www.orthoload.com/main.php>.
- [80] Winby, CR, Lloyd, DG, *Muscle and external load contribution to knee joint contact loads during normal gait*. *Journal of Biomechanics* 42 (2009) 2294–2300.
- [81] Lima, D., Christopher, P., *An implantable telemetry device to measure intra-articular tibial forces*. *Journal of Biomechanics* 38 (2005) 299–304.
- [82] Hurwitz, D., Sumner, D., *Dynamic knee loads during gait predict proximal tibial bone distribution*.*Journal of Biomechanics* 31 (1998) 423-430.
- [83] Viceconti, M., L. Bellingeri, L. Cristofolini, and A. Toni, *A comparative study on different methods of automatic mesh generation of human femurs*. *Med Eng Phys*, 1998. 20(1): p.1-10.
- [84] Nyman JF, Hazelwood SJ, Rodrigo JJ, *Long stemmed total knee arthroplasty with interlocking screws: a computational bone adaptation study*. *J Orthop Res* 2004;22:51–8.
- [85] Whittaker, J., Dharmarajan, R., *The management of bone loss in revision total knee replacement*.*J Bone Joint Surg [Br]* 2008;90-B:981-7.
- [86] Whiteside LA, Pafford J, *Load transfer characteristics of a noncemented total knee arthroplasty*. *Clin Orthop* 239:168, 1989.
- [87] Barrack R., Stanley, T., Burt, M., *The Effect of Stem Design on End-of-Stem Pain in Revision Total Knee Arthroplasty*. *The Journal of Arthroplasty* Vol. 19 No. 7 Suppl. 2 2004.
- [88] Radnay CS, Scuderi GR. *Management of bone loss: augments, cones, offset stems*. *Clin Orthop* 2006;446:83-92.

## Annex A

### Algorithm for transition of densities from the intact bone to the implanted bone

The algorithm starts by reading all the nodes of the intact bone mesh (initial mesh), saving the information about their spatial coordinates and densities for each node. It also reads all the nodes of the implanted bone mesh (final mesh) saving the respective spatial coordinates. Then, goes node to node through the mesh for which we want to transit the densities (final mesh) and calculates what are the spatially closest nodes of the initial mesh. If it finds only one node (closest node) its density is attributed to the final mesh node, i.e., the final mesh node will present the properties of that node. If there is more than one initial mesh node at minimum distance of the node of the final mesh, it is then made the weighted average of densities of the initial mesh nodes and, at the end, it is attributed to the node of the final mesh. The Figure A.1 illustrates the application of this algorithm for the standard configuration.

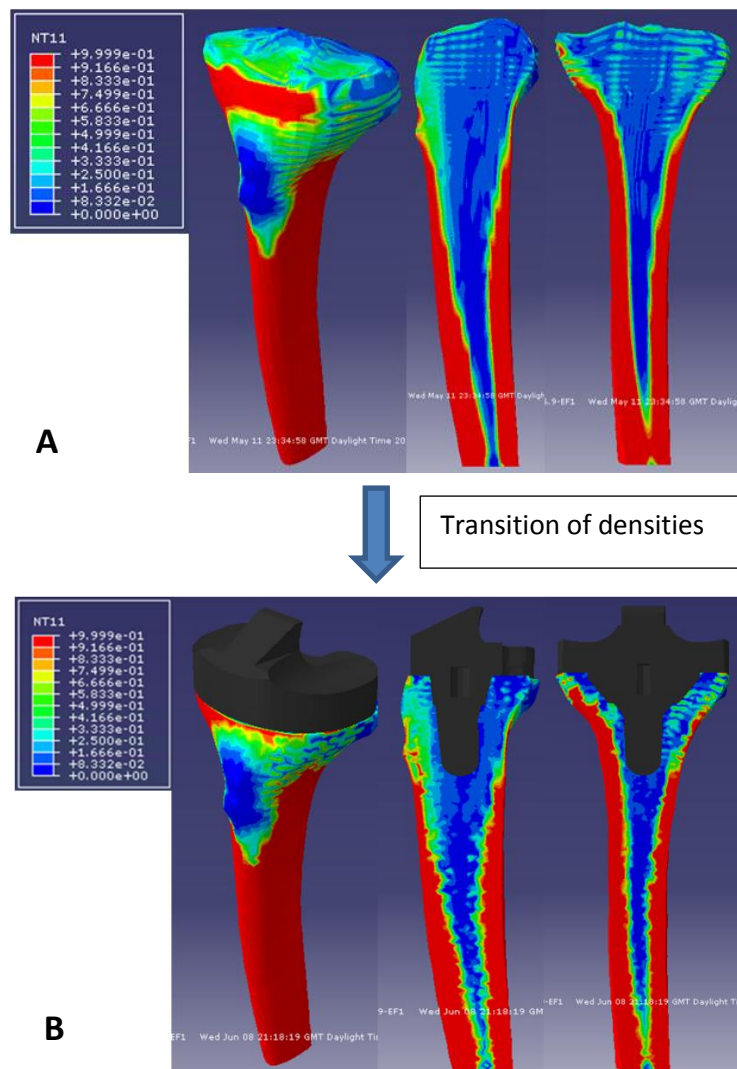


Figure A.1 – Illustrates the application of the transition of densities algorithm for the standard configuration: A - Density distribution resulting from the model of bone remodeling for the initial non-homogeneous input of the Figure 3.31 with  $k=0,003 \text{ N/mm}^2$ , step = 5 and 200 iterations; B – Similar density distribution of A, with standard prosthesis. Relative densities,  $\mu$ , are represented in a color scale: red=cortical bone ( $\mu \approx 1$ ) and the remaining=trabecular.